DEVELOPMENT OF POLY(LACTIC ACID) BIO-COMPOSITE FILAMENTS BY USING LIGNIN MODIFIED BY ALCOHOLIZED PLA FOR 3D-PRINTING APPLICATIONS

By

Mr. Wikoramet TEEKA

A Thesis Submitted in Partial Fulfillment of the Requirements

for Master of Engineering CHEMICAL ENGINEERING

Department of CHEMICAL ENGINEERING

Silpakorn University

Academic Year 2025

การพัฒนาเส้นใยชีวภาพพอลิแลคติกแอซิดคอมโพสิตโดยใช้ลิกนินดัดแปลงโครงสร้างด้วยแอลกอฮอไลซ์พอลิแลคติกแอซิดสำหรับการใช้งานการพิมพ์ 3 มิติ

โดย
นายวิกรเมศวร์ ฑีฆะ

วิทยานิพนธ์นี้เป็นส่วนหนึ่งของการศึกษาตามหลักสูตรวิศวกรรมศาสตรมหาบัณฑิต
สาขาวิชาวิศวกรรมเคมี แผน ก แบบ ก 2
ภาควิชาวิศวกรรมเคมี
มหาวิทยาลัยศิลปากร
ปีการศึกษา 2568

DEVELOPMENT OF POLY(LACTIC ACID) BIO-COMPOSITE FILAMENTS BY USING LIGNIN MODIFIED BY ALCOHOLIZED PLA FOR 3D-PRINTING APPLICATIONS

By

Mr. Wikoramet TEEKA

A Thesis Submitted in Partial Fulfillment of the Requirements

for Master of Engineering CHEMICAL ENGINEERING

Department of CHEMICAL ENGINEERING

Academic Year 2025

Title	Development of Poly(lactic acid) Bio-composite Filaments by Using Lignin Modified by Alcoholized PLA for 3D-Printing Applications
By	Mr. Wikoramet TEEKA
Field of Study	CHEMICAL ENGINEERING
Advisor	Associate Professor Sirirat Wacharawichanant
Co advisor	Associate Professor Pakorn Opaprakasit

Faculty of Engineering and Industrial Technology, Silpakorn University in Partial Fulfillment of the Requirements for the Master of Engineering

.....Dean of Faculty of Engineering and Industrial Technology
(Assistant Professor Arunsri Leejeerajumnean)

Approved by

.....Chair person
(Associate Professor Prakorn Ramakul)

.....Advisor
(Associate Professor Sirirat Wacharawichanant)

.....Co advisor
(Associate Professor Pakorn Opaprakasit)

.....Committee
(Associate Professor Okorn Mekasuwandumrong)

.....External Examiner
(Associate Professor Sunan Tiptipakorn)

660920018 : Major CHEMICAL ENGINEERING

Keyword : Poly(lactic acid) : PLA, Lignin, Alcoholysis, Chemical modified, 3D-printing filament

Mr. Wikoramet TEEKA : Development of Poly(lactic acid) Bio-composite Filaments by Using Lignin Modified by Alcoholized PLA for 3D-Printing Applications

Thesis advisor : Associate Professor Sirirat Wacharawichanant

The aim of this research is to develop 3D printing filament materials from biodegradable polymers, based on the chemical integration and chemical recycling concepts of PLA and lignin extracted from black liquor waste by acidification under appropriate conditions. Under optimal conditions, lower pH adjustment improves the precipitation efficiency of lignin in inorganic acid solution, giving better yield, and lignin has amorphous fraction. and has the crystalline form of $Ca(OH)_2$ and $CaCO_3$, which is consistent with the results of SEM-EDS and XRD analysis. In the chemical recycling of PLA by alcoholysis reaction, the effects of methylene chain length and the structural conformation of hydroxyl groups of both primary and secondary alcohols on the reaction were studied. From the results of FTIR and ^{1}H-NMR analysis, it shows the transesterification change. This shortens the chain structure of PLA. The use of ethylene glycol (EG) provides higher reaction efficiency and controls the structure of the resulting oligomer with the PLA:diol ratio. The obtained lignin was chemically modified with maleic anhydride (MA) and alcoholyzed PLA using various pre-treatment and non-pre-treatment methods. It was found that the second pre-treatment, a separate step after alcoholysis of PLA, provided the best phase compatibility and the formation of ester bonds and hydrogen bonds between anhydride groups and hydroxyl groups of lignin and alcoholyzed PLA, and for PLA resin/A-PLA-cured lignin-M composites, the mechanical properties were significantly improved with higher strength and rigidity. Adjusting the ratio of alcoholyzed PLA from 3:1 to 9:1 improved both the material strength and flexibility by approximately 10-35%, indicating a balance between flexibility and material strength, as well as improved interphase bonding due to the blending behavior of the increased torque values. In addition, the resulting composite materials are shaped into filaments for extruders to produce 3D printing filaments, with printing behaviors tested in different axes, namely XY (Flat), XZ (Horizontal), and ZX (Vertical), to study the relationship between printing direction and mechanical properties of the workpieces. The results of the study showed that printing in the XY (Flat) direction provided good adhesion between layers and material loading direction. This information can be used as a guideline for adjusting printing conditions to obtain materials with the highest efficiency.

ACKNOWLEDGEMENTS

Firstly, I would like to be gratitude to my advisor, Associate Professor Dr. Sirirat Wacharawichanant and Associate Professor Dr. Pakorn Opaprakasit for their support, stimulating, useful discussions throughout this research and devotion to revising this thesis otherwise it cannot be completed. In addition, the author would like to gratefully acknowledge Associate Professor Dr. Prakorn Ramakul, as the chairman of the chairman of the committee, Associate Professor Dr. Okorn Mekasuwandumrong as the members of thesis committee and Associate Professor Dr. Sunan Tiptipakorn as the members of thesis external examiner for their kind evaluation of work and valuable suggestions that could be beneficially used to improve working behavior. Special thanks for the kind suggestions and useful help to members of Polymer Innovation Laboratory, including Center of Excellence in Functional Advance Materials Engineering (CoE FAME), Thammasat University, and members of the research zone for their assistance. The author would like to be acknowledged by Professor Dr. Piyasan Praserthdam, Center of Excellence on Catalysis and Catalytic Reaction Engineering, Chulalongkorn University for analysis and measurement tools. This research is financially supported by Thailand Science Research and Innovation (TSRI) National Science, Research and Innovation Fund (NSRF) (Fiscal Year 2024)

Moreover, I sincerely thank my family and for their continuous support and encouragement over the years.

Wikoramet TEEKA

TABLE OF CONTENTS

Page

LIST OF TABLES

Page

LIST OF FIGURES

Page

มหาวิทยาลัยศิลปากร

CHAPTER I

INTRODUCTION

1.1 Motivation

Plastic pollution in natural environments is a significant concern, garnering attention from researchers and the public. Plastic waste threatens ecosystems as organisms can ingest it or become entangled [1]. Cheap and durable, plastics degrade into smaller pieces over time, but the timeframe for complete degradation remains to be determined. The production of disposable plastic has skyrocketed, with common polymers like HDPE, LDPE, PVC, PS, PP, and PET dominating production and pollution [2]. Due to their durability, plastics persist in the environment, with microplastics and microplastics causing particular concern. Microplastics, less than 5 mm in size, are especially problematic as they can be ingested by marine life and act as vectors for pollutants. [3] In this regard, PLA is considered a potential bioplastic and has emerged as a popular alternative to petroleum-based polymers in many applications [4].

Therefore, this research aims to study or develop biodegradable plastics that can be degraded naturally as a substitute for petroleum-based plastics. Biodegradable polymers are environmentally friendly and come from renewable sources like polysaccharides or plant /microbial. [5]. These materials can also be synthesized from renewable resources such as bio-derived monomers [6]. Biodegradable polymers break down into simpler components during biodegradation, contributing to elemental cycles such as carbon and nitrogen [7]. Poly(lactic acid) (PLA) is a famous that takes approximately 180 days to decompose. Recycling is a good option for upcycling and adding value to the materials. The recovery of PET was studied using the Glycolysis method; PET is a polyester type similar to PLA.[8] The chemical recycling process converts PLA waste into value-added starting materials for other methods, such as alcoholysis reaction [9], which uses hydroxyl-containing substances, especially ethylene glycol (EG), to produce hydroxyl-capped PLA oligomers [10].

In agricultural and industrial processes, there are by-products or biomass that can be converted to valuable feedstocks, like lignocellulose, cellulose, and lignin [11, 12]. By combining ideas using the bio-circular green economy (BCG) principles, researchers are exploring the reuse of by-products, such as black liquor from the paper industry. Various cost-effective and environmentally friendly methods have been developed to modify lignin [11, 13] for used in multiple applications such

as additives, adhesives, and adsorbents [14]. Among these, using it as an additive for bioplastics is of interest for reinforcement [15].

Various processes have been developed to enhance bioplastic properties, including using additives or fillers, block copolymerization [16]. However, the added additives have little effect on improving efficiency. Therefore, various additives have been modified to be suitable as bioplastic fillers to improve composite dispersion efficiency. Acid anhydrides, such as maleic anhydride, have been employed to adjust their chemical structures through transesterification reactions to suit the additive and increase its compatibility [11, 14, 15]

The 3D printing process has been widely used and further developed. 3D printing benefits production concepts through fused deposition modeling (FDM) technology, commonly known as a research interest in 3D printing technology for non-laser applications. It is a low-cost model with high potential [17]. In this method, the fiber is the most commonly used commercially, such as acrylonitrile butadiene styrene (ABS), poly(lactic acid) (PLA), and various combinations [18]. Otherwise, 3D printing still needs to be studied in multiple parameters, such as the mechanical properties of filament, temperature, viscosity, and printing characteristics along various axes [19].

In this research, a process for converting black liquor, a by-product of the paper industry, into value-added feedstock was developed by extracting its lignin component for use as an additive in PLA bioplastic. The extraction parameters were optimized through an acidification process. The obtained lignin was subsequently modified to enhance its efficiency as an additive and to improve its compatibility with PLA. The next stage of the study involves the chemical recycling of poly(lactic acid) (PLA) to produce alcoholyzed PLA (A-PLA) products, which serve as starting materials. The alcoholysis parameters—such as the PLA-to-alcohol ratio, reaction temperature, and time—are optimized to obtain products with desirable properties for fabricating high-quality PLA filaments. For 3D printing applications, the factors influencing printing performance and the mechanical properties of the printed products are systematically evaluated.

1.2 Objective

The objective of this study is to develop an integrated process for upcycling industrial and bioplastic wastes into value-added materials. Specifically, the work aims to extract and modify lignin from black liquor, a by-product of the paper industry, for use as a functional additive in PLA bioplastics, and to chemically recycle poly(lactic acid) (PLA) into alcoholyzed PLA (A-PLA)

precursors for filament fabrication. The combined approach seeks to optimize processing parameters and improve material compatibility, mechanical performance, and 3D printing quality—contributing to sustainable material utilization and circular bioeconomy development.

1.3 Scope of Research

The research investigates optimizing the performance of filament materials by using lignin recovered from black liquor in stable conditions and chemically modifying it as an additive. The chemical recycling of PLA by Alcoholysis reaction has the potential for 3D printing filament. The scope of this research is as follows:

1.3.1 Develop a lignin recovery process from black liquor by acidification process under optimum conditions by varying acidity and alkalinity, types of acid (organic and inorganic), and purity.

1.3.2 Develop a chemical recycling process for poly(lactic acid) (PLA) by alcoholysis reaction using ethylene glycol (EG) and glycerol in the appropriate ratio and time to be used as a starting material.

1.3.3 Develop a chemical structure modification process for lignin for use as additives in producing high-performance lignin/maleic anhydride/alcoholysis PLA filaments.

1.3.4 Develop chemically modified bioplastic materials containing A-PLA additives, cured lignin-M composites in PLA matrix for efficient 3D printing filaments.

1.3.5 Study factors affecting 3D printing performance and properties of the printed products.

1.4 Signification of the research

This research provides important information on a new approach to efficiently recover lignin from black liquor through acidification. Applying the concept of the bio-circular green economy (BCG) model and developing additives that have even better abilities to improve the properties of biodegradable plastics, including PLA chemical recycling, and finally providing information on effective 3D printing methods, to be used in research, industries, and provide benefits to a friendly environment.

1.4.1 Research Community

The results from this work can be used as a guideline for further interesting developments in lignin extraction. Chemical recycling of PLA develops the processes for other applications. Including the ability of additives to improve the properties of polymers in various aspects, this work also provides guidelines for developing 3D printing for multiple parameters that affect molding. The research community gains knowledge about the development of lignin extraction processes and production using efficient 3D printing technology that can be extended to the industrial level to save production time and reduce costs.

1.4.2 Industrial sector

The industry can apply the guidelines for creating new material products in 3D printing by using resources efficiently, reducing costs, saving time, and having good printing efficiency in production.

1.4.3 Environment

The bio-circular green economy (BCG) model uses by-products or waste to develop value for money in various fields. To reduce the accumulation of garbage (bioplastic) and waste (such as by-products) so as not to affect the environment. It is an increase in the value of by-products for other uses, reducing waste in the system and reducing the problem of toxic contamination in the aquatic ecosystem.

CHAPTER II

BACKGROUND AND THEORY

2.1 Poly(lactic acid) (PLA)

Poly(lactic acid), or PLA, is a biodegradable polymer made from lactic acid. The monomer is typically produced through the fermentation of plant starches such as corn, cassava, sugarcane, or sugar beet pulp. Figure 1 depicts two enantiomeric isomers: poly(L-lactic acid) (PLLA) and poly(D-lactic acid) (PDLA) [20].

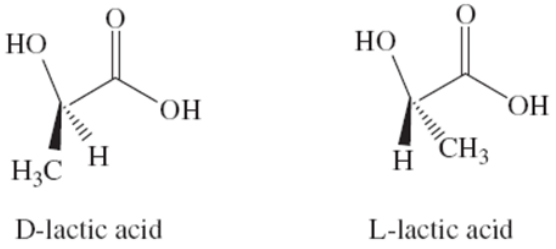

Figure 1 Stereoisomers of lactic acid [20].

PLA is produced either by ring-opening polymerization (ROP) of lactides or by condensation polymerization of the lactic acid monomers at temperatures above 100 ºC, as shown in Figure 2.

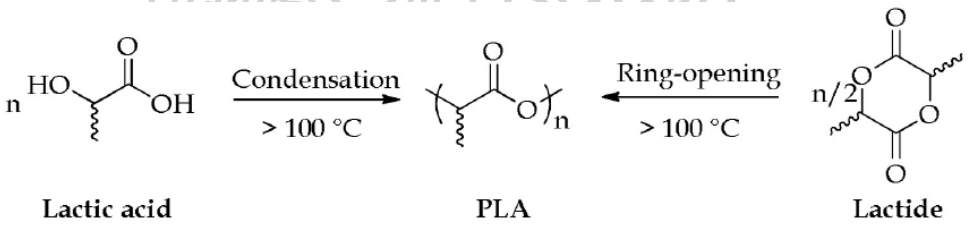

Figure 2 Polymerization reaction of lactic acid [20].

PLA is biodegradable, compostable, derived from renewable resources, and nontoxic to humans and the environment. However, its shortcomings include low thermal resistance and intrinsic brittleness [20].

2.2 Black Liquor

Black liquor is a significant by-product from the paper industry, which contains some components that can be converted to value-added products. The composition of black liquor varies based on the raw material (softwoods, hardwoods, or fibrous plants) and pulping conditions. It is a complex aqueous solution containing organic materials (lignin, polysaccharides, low molecular

weight resinous compounds) and inorganic compounds (mostly soluble salt ions). These constituents influence its properties, particularly its behavior in the recovery unit (Figure 3) [21].

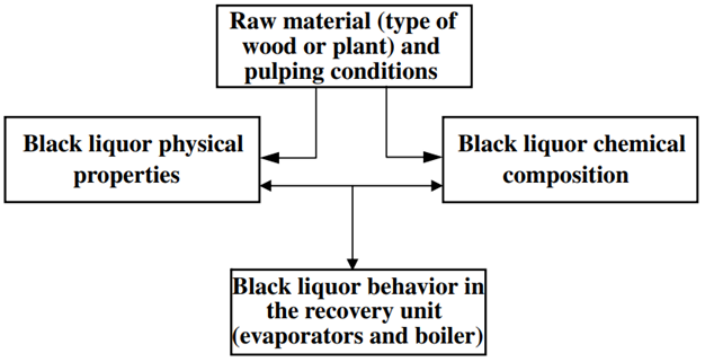

Figure 3 Origin of the black liquor in the industrial recovery unit [21].

Figure 4 illustrates the chemical structures and compositions of black liquor, which contains lignin and polysaccharide clusters, salt ions, and water. Lignin, the bonding agent in wood or fibrous plant fibers, forms a polymer with phenyl-propane structures. During pulping, lignin fragments and carbohydrates dissolve into low molecular weight acids. However, the Xylan fraction, a main hemicellulose in hardwoods, remains undegraded and contributes to the composition of black liquor [21].

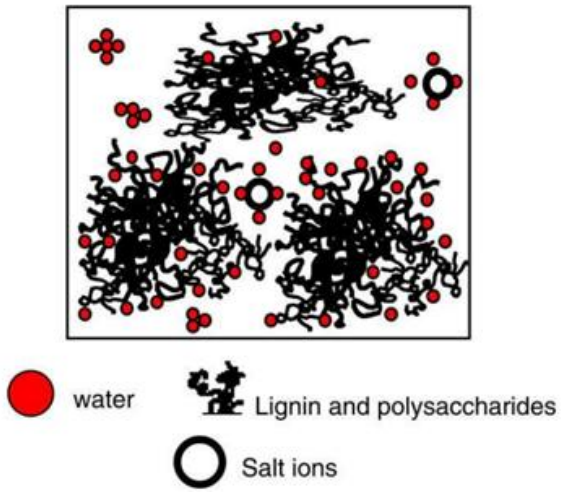

Figure 4 Simplified schematic representation of the black liquor structure [22].

2.3 Lignin

Figure 5 depicts lignin, a biological component present in ordinary wood, one of the most essential raw materials in industry. This describes the structures of the cell wall, which includes lignin, cellulose, and hemicellulose. As a result, the pulp boiling process requires wood to remove

lignin from the pulp. Lignin causes the paper to turn yellow when exposed to light. The eliminated lignin will be contaminated with water, known as black liquor. Black liquor is waste from the pulp industry. Wood is made up of cells, and the cell wall consists primarily of 3 organic components: cellulose (40-60 wt%), hemicelluloses (25-35 wt%), and lignin (15-30 wt%) [23].

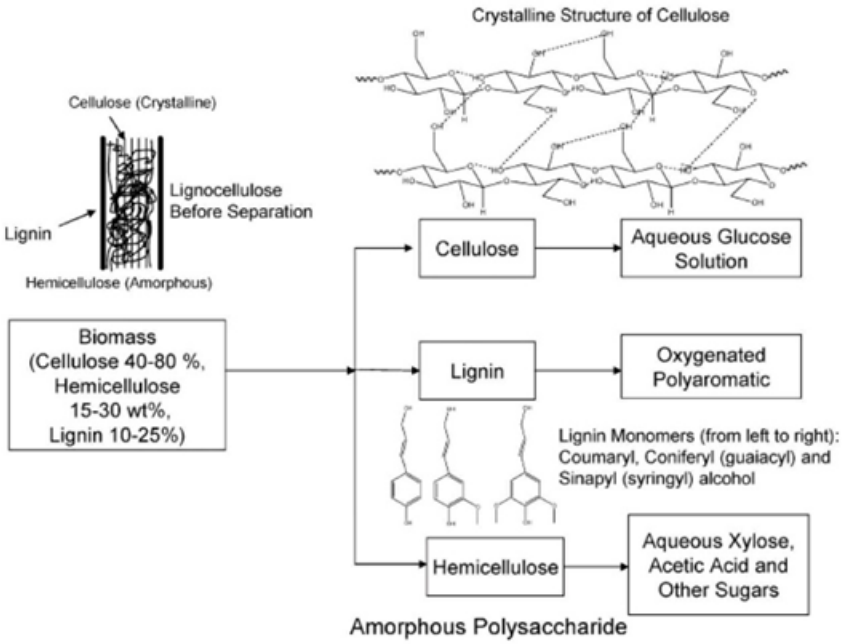

Figure 5 Schematic structures of cell walls [24].

The lignin structure is asymmetrical and amorphous and contains the highly complex chemical nature of 3 distinct phenylpropane monomers (Figure 6). For the above reasons, lignin is not a regular structure like cellulose but a physically and chemically heterogeneous material. However, the specific chemical structure still needs to be clarified [25].

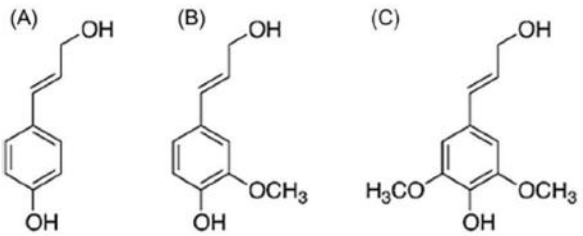

Figure 6 Three different phenyl propane monomers (A) p-coumaryl alcohol, (B) coniferyl alcohol, (C) sinapyl alcohol [26].

2.4 Transesterification Process

Transesterification, a crucial organic reaction, involves the conversion of an ester into another through alkoxy moiety interchange. When the reaction involves an ester and an alcohol, it is termed alcoholysis. In this context, transesterification is synonymous with alcoholysis of carboxylic esters (Figure 7). Typically, in an equilibrium reaction, catalysts, often strong acids or bases, notably accelerate transesterification's equilibrium adjustment. Excess alcohol is required to achieve a high yield of the ester [27, 28].

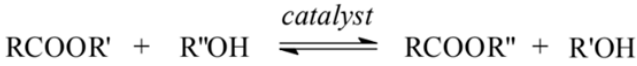

Figure 7 General equation for a transesterification reaction [28].

Transesterification finds wide industrial applications beyond laboratory settings. Various industrial processes utilize this reaction to produce different compounds [27]. For instance, PET (polyethylene terephthalate) production involves transesterification of dimethyl terephthalate with ethylene glycol, using zinc acetate as a catalyst (Figure 8) [29]. Numerous acrylic acid derivatives are also generated by trans-esterifying methyl acrylate with diverse alcohols, employing acid catalysts.

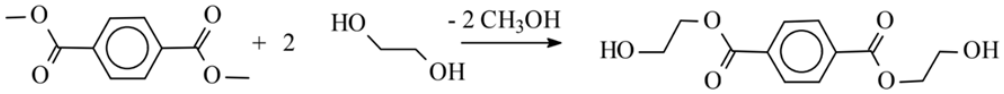

Figure 8 Transesterification of dimethylterephthalate with ethylene glycol [29].

2.5 Esterification Process

Esters, widely used in industrial processes, face conversion and reaction time limitations due to equilibrium establishment in Fischer esterification. Ester hydrolysis, the reverse reaction, starts with a water supply. Various approaches have been developed to improve conversion and reaction rates [30].

Esterification is a key reaction in organic synthesis, with esters prevalent in natural and synthetic organic compounds.[31] In Fisher esterification, carboxylic acids and excess alcohols are heated with a catalyst to reach equilibrium over time (Figure 9), governed by kinetics and thermodynamics. Shifting the equilibrium forward typically requires excess alcohol or continuous

water removal. However, the reaction often does not need to be complete, affecting the product yield [30].

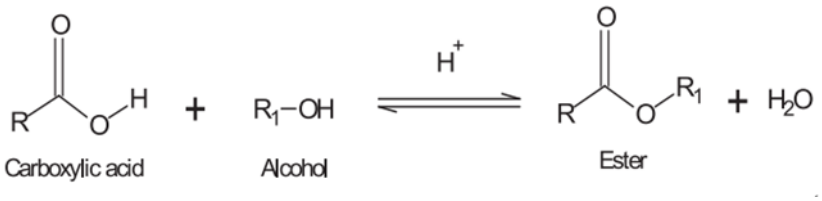

Figure 9 General equation for an esterification reaction [30].

2.6 Internal Mixer

An internal mixer typically comprises two rotors within a mixing chamber. The Banbury Mixer is a commonly used design (Figure 10), where the rotors (1) rotate towards each other at slightly different speeds. Each rotor has a spiral-shaped blade and can be cooled or heated through water or a suitable heating agent passage [32].

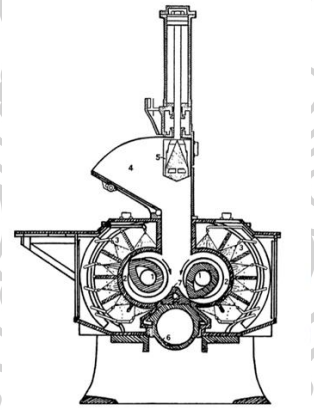

Figure 10 Schematic drawing of a Banbury Mixer [32].

Sprays (3) can chill or heat the mixing chamber (2). The ingredients to be blended enter the mixing chamber via the feed hopper (4). A floating weight (5) is powered by compressed air and rests on the feed, confining the material to the mixing space and applying pressure. As seen in this picture, the mixed material is discharged using the slide discharge mechanism (6). The saddle (7) sits between the rotors [32].

2.7 Extruders

Single-screw extruders are commonly employed in polymer extrusion due to their cost-effectiveness, simplicity, durability, and favorable performance-to-cost ratio despite their limited

mixing capabilities. Many compounding operations include at least one of these machines [33]. A single-screw extruder is a drag pump for highly viscous fluids such as polymeric melts. Its usual screw configuration consists of 20 or more spins with a pitch close to the diameter, resulting in a long, slender machine capable of maintaining and managing significant longitudinal temperature gradients. Furthermore, large shear pressures during aircraft landings promote dispersive mixing, breaking apart agglomerates like pigments and waxes. Figure 11 shows a conventional single-screw extruder [34].

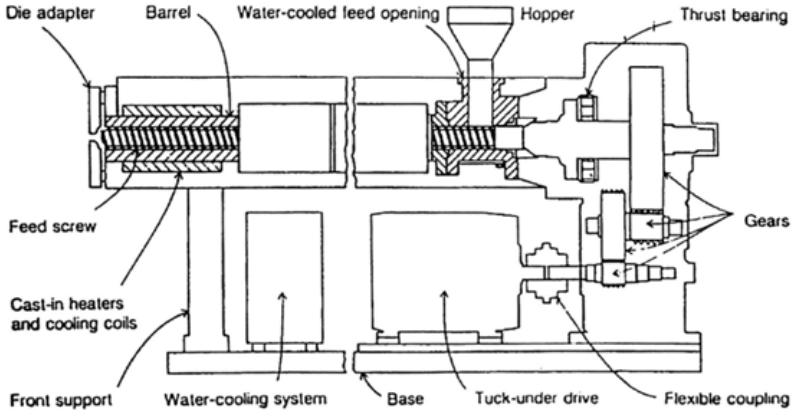

Figure 11 Typical single-screw extruder [32].

The extruder's function is to heat plastic material uniformly, melt it, and force it through the extrusion die. This continuous procedure necessitates consistent output from the melt preparation apparatus. Because of the limited thermal conductivity, high specific heat, and viscosity of thermoplastics, melting is primarily reliant on a revolving screw. The issue of achieving homogeneous melt preparation and consistent delivery at suitable pressure has resulted in several extruder designs [32].

The two basic types of extruders are single-screw and twin-screw. The single-screw extruder is the most widely used (as illustrated in Figure 12). Twin-screw extruders can feature parallel or conical screws that can rotate in the same direction (co-rotating) or in opposite directions (counter-rotating), as illustrated in Figure 13 [32].

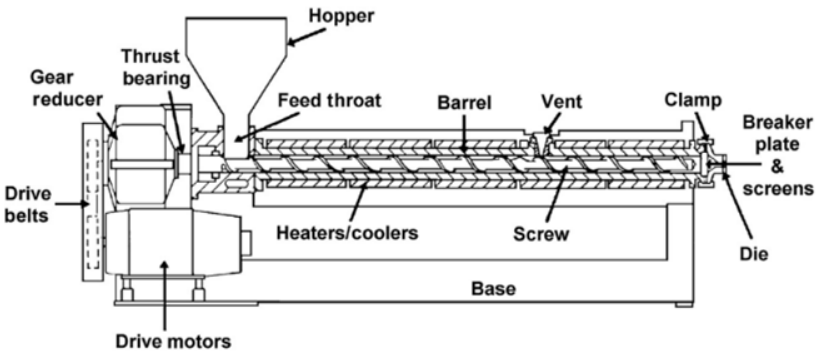

Figure 12 Typical single-screw extruder with a vented barrel [32].

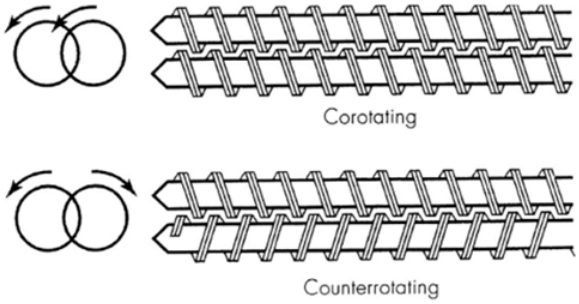

Figure 13 Co-rotating and counter-rotating twin screws [32].

2.8 Compression Molding Machine

Compression molding, one of the oldest plastics forming methods (Figure 14), usually consists of four steps [32]:

- Pre-formed blanks, powders, or pellets are placed in the lower area of a heated mold or die.

- The mold's second half is lowered, creating pressure.

- Under heat and pressure, the material softens and flows into the mold, with any extra material pushed out. Thermoset plastics cross-link in the mold, while thermoplastics solidify after cooling under pressure.

- The mold is opened, and the portion is removed.

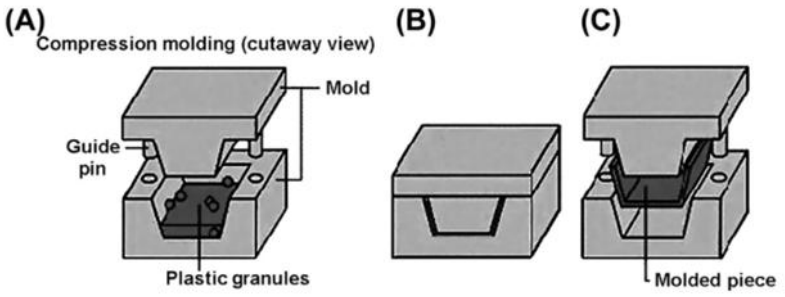

Figure 14 Schematic drawing of the stages of the compression molding process. (A) Filling the mold; (B) heating the closed mold; (C) opening the mold and removal of the molded part [32].

Compression molding involves heating and compressing molding powder or pellets to create a specified shape. Rapid melting of thermoset materials is required to ensure that the mold is filled before solidification occurs. Commercial machines use high pressure and temperatures to shorten cycle times. When the mold opens, the ejector pins automatically force the molded product out. Figure 15 shows a schematic diagram of a compression molding press and its components [32].

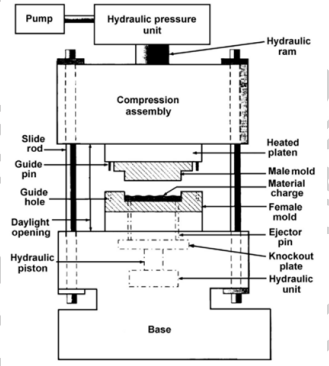

Figure 15 Schematic drawing of compression molding press and its components [32].

2.9 3D Printing

3D bioprinting, a cutting-edge technology, is widely utilized in various applications, e.g., packaging, tissue engineering, and regenerative medicine, to build complex tissue architectures that resemble original organs. This method entails depositing layers of cell-laden biomaterials in a specified architecture and combining biomaterials, live cells, and precise motor systems to achieve more control over structure growth. As a result, it enables the creation of complex structures, such as tissue engineering scaffolds with regulated properties and biomedical devices, transforming tissue modeling and production [35]. Computer-aided design (CAD) allows for complicated 3D tissue structures by employing detailed geometrical data from medical imaging modalities such as X-ray,

MRI, and μ-CT scans. The advantages of using 3D bioprinting in the biomedical area include the capacity to create individualized patient-specific designs with great precision at a low cost and the rapid construction of complicated structures as needed [35]. Fused deposition modeling (fdm), direct ink writing (diw), inkjet bioprinting, selective laser sintering (sls), stereolithography (sla), and laser-induced forward transfer (lift) are some of the most popular 3d printing processes for printing live cells [35].

2.10 Fused Deposition Modeling (FDM)

Fused deposition modeling (FDM) is a popular process in 3D printing that falls under additive manufacturing engineering. It is gaining popularity in research and industry because of its capacity to build complicated structures effectively, resulting in less material waste than traditional manufacturing processes. FDM, similar to injection molding, enables mass customization by making bespoke objects without the need for expensive molds or tools, resulting in low prices despite individualized output [36, 37].

The FDM machine heats the filament to a semi-liquid condition at the nozzle before extruding it onto a previously printed plate or layer. Polymer filaments are thermoplastic, which allows them to fuse during printing and harden at room temperature afterward. Despite its apparent simplicity, FDM printing requires complicated processes with interconnected parameters determining product quality and material qualities, making it difficult to grasp. Different 3D printing items demand different levels of quality and material attributes. The combination of print settings on the FDM machine is dependent on filament type and size, emphasizing the need to investigate the impact of mechanical performance parameters [37].

The primary parameters of the FDM printing process, as shown in Figure 16a, depict the build orientation as determined by the step in which the part is orientated toward the X, Y, and Z axes on the build platform. The layer thickness depicted in Figure 16b represents the thickness of the layer deposited on the nozzle tip. The user's thickness value in each range is determined by the nozzle diameter and limited by the printer's precision. Figure 16c depicts the FDM tool path, which includes numerous parameters such as raster angle, width, contour width, number of contours, etc. [37, 38].

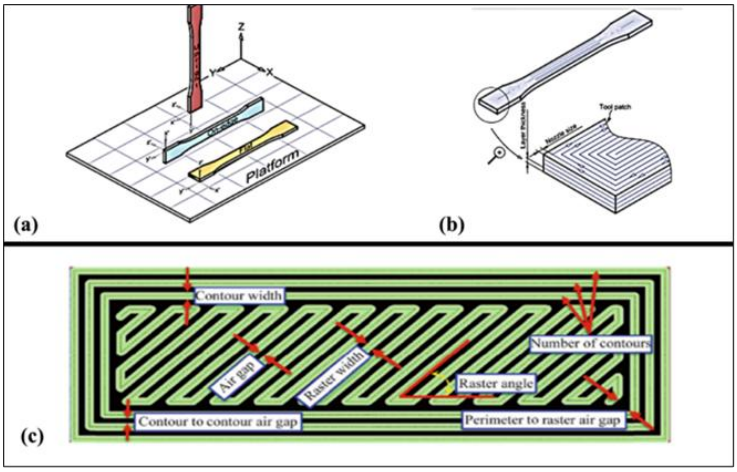

Figure 16 (a) Build orientations [38], (b) layer thickness [38], and (c) FDM tool path parameters [37].

The raster angle, which ranges from 0° to 90°, indicates the inclination of the raster pattern relative to the X-axis on the lowest layer. Precision in establishing this angle is critical, especially for parts with minor curves, to ensure the best results. Raster width refers to the width of the material droplets utilized in the raster, which varies depending on the nozzle tip size. A greater raster width results in a stronger interior for the part, but a smaller width reduces production time and material utilization [37].

2.11 Fabrication of Filament

The basic material used in FDM is filament, which is typically made of pure polymer with a low melting point. To increase strength, academics and enterprises have created polymer composites that combine the matrix with reinforcing components. It produces materials with superior structural qualities and functional benefits that are impossible with pure polymer alone. [37] Filaments manufactured from commercial pure polymers are often appropriate for direct processing in FDM. Composite filament manufacture, on the other hand, necessitates specific handling due to the diverse properties produced by each reinforcement added to the composite polymer [39].

Figure 17 depicts the processes of filament production, which include selecting the filament diameter, setting extrusion settings, introducing material pellets, and extruding through the nozzle die hole until it wraps around the roller machine. [40] Figure 18 depicts the working concept of extruder machines in general. It demonstrates how pellets are converted into filaments, beginning with their insertion into the hopper and progressing via melting and extrusion [41].

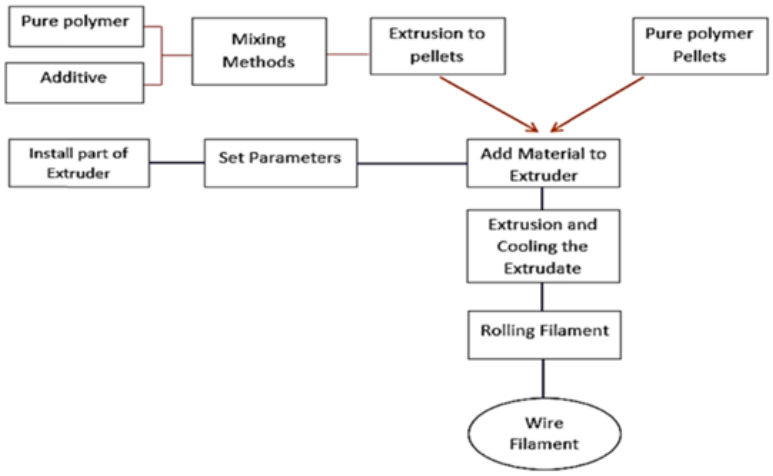

Figure 17 Filament workflow [37].

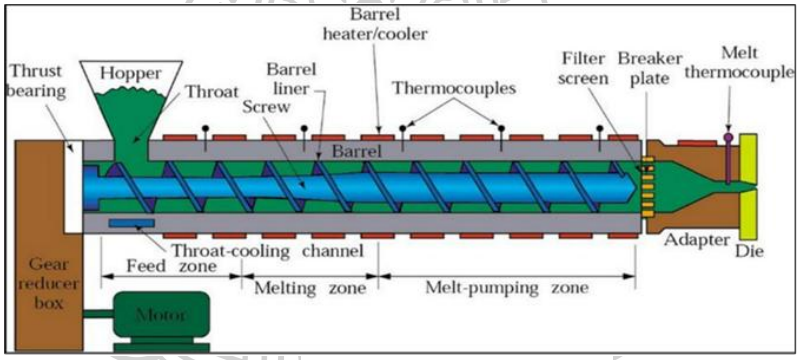

Figure 18 Extruder machine parts [42].

2.12 Universal Tensile Machine (UTM)

Universal testing devices, such as universal testers, measure materials under tension, compression, or bending and provide stress-strain curves. They are available in electromechanical or hydraulic configurations with varying load application methods. Electromechanical machines use a variable-speed electric motor, a gear reduction system, and one, two, or four screws to move the crosshead, which applies tension or compression on specimens. Crosshead speeds can be adjusted by changing the motor speed, and precision control is possible with a microprocessor-based closed-loop servo system. Hydraulic testing devices (Figure 19) use either a single or dual-acting piston to move the crosshead. Most static hydraulic testing machines have a single-acting piston, but manual operation requires setting a pressure-compensated needle valve for loading rate control. Closed-loop hydraulic servo systems achieve precise control by replacing the needle valve with an electrically driven servo valve [43].

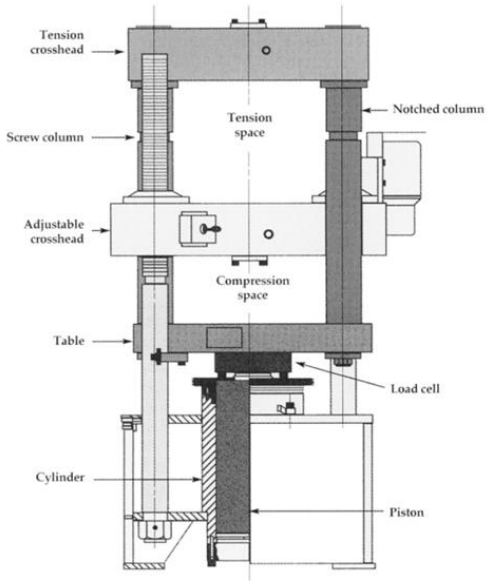

Figure 19 Schematic of a hydraulic universal testing machine [43].

2.13 Field Emission Scanning Electron Microscopy (FE-SEM)

The Scanning Electron Microscope (SEM) scans a sample with an electron beam, producing images with a high depth of field and spatial resolution due to its short wavelength. Figure 20 depicts the electron beam column, including an electron gun, condenser, and objective lens. When the electron beam interacts with atoms on the sample's surface, it produces signals that may be analyzed to provide data such as surface roughness, corrosion pit characterization, corrosion location, and the morphology of corrosion products such as oxides. These interactions are detected and converted into images, making SEM an effective tool for thorough study [44].

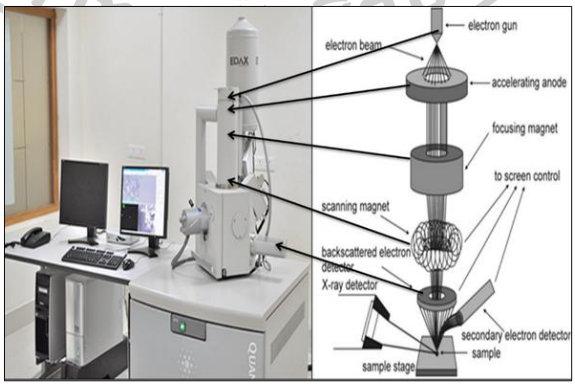

Figure 20 Schematic of Scanning Electron Microscopy (SEM) [44].

2.14 Fourier Transform Infrared Spectroscopy (FTIR)

The Fourier transform infrared (FTIR) spectrometer is an instrument for analyzing substances chemical structures and functional groups by measuring radiation absorption in the infrared range. It can examine samples of solids, liquids, and gases. Infrared radiation, while invisible, produces heat that can be felt. It is classified into three regions: near-infrared (12800-4000 cm^{-1}), mid-infrared (4000-200 cm^{-1}), and far infrared (200-10 cm^{-1}). The mid-IR region is especially valuable in chemical investigation because molecules absorb infrared radiation, causing molecular vibrations and changes. Each organic material has a unique oscillation frequency used to analyze organic structures. This analysis shows the link between wave number and transmittance, which make up the infrared spectrum (Figure 21) [45].

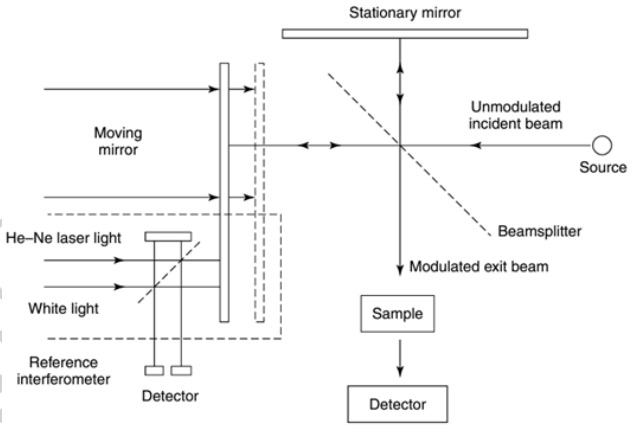

Figure 21 Schematic the main component of FTIR spectrophotometer [46].

2.16 Proton Nuclear Magnetic Resonance Spectroscopy (^{1}H-NMR)

Proton Nuclear Magnetic Resonance (^{1}H NMR) spectroscopy is a potent analytical method for examining the molecular structure of organic compounds. It operates on the principle of nuclear magnetic resonance, where protons within a sample absorb energy under a magnetic field and emit it as radiofrequency radiation upon returning to their initial state. In ^{1}H NMR spectroscopy, a sample's hydrogen atoms (protons) are exposed to a strong magnetic field and radiofrequency pulses. The protons absorb and emit energy during nuclear magnetic resonance, influenced by their chemical surroundings, like neighboring atoms and functional groups. Consequently, distinct signals, or resonances, appear in the NMR spectrum for each type of hydrogen atom in the molecule. The NMR spectrum is typically displayed as a plot of signal intensity (absorption or emission) against the

applied magnetic field strength or, more commonly, against the frequency of the radiofrequency radiation. By analyzing the positions (chemical shifts), intensities, and splitting patterns of the peaks in the NMR spectrum, chemists can determine the number and types of hydrogen atoms in the molecule, as well as their connectivity and stereochemistry. This information is invaluable for structural elucidation, identification of unknown compounds, and characterization of chemical reactions in organic chemistry, biochemistry, and related fields. (as shown in Figure 22) [47]

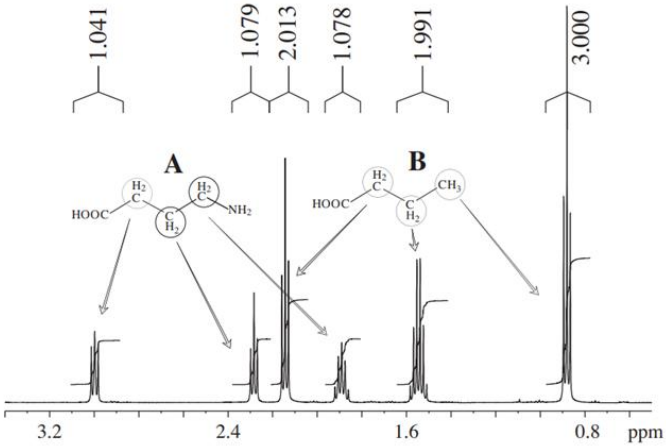

Figure 22 Example analysis results of Proton Nuclear Magnetic Resonance (^{1}H NMR) spectroscopy [47].

2.17 X-Ray Diffraction (XRD)

X-ray diffraction (XRD) is based on the interaction of X-rays with a material's crystal lattice. When X-rays hit a crystalline material, they are scattered by the atoms in the crystal lattice. X-rays' constructive and destructive interference causes this scattering pattern as they contact atoms in the crystal lattice. Bragg's law governs this interaction, $n\lambda = 2d\sin(\theta)$, where n represents the order of the diffraction, λ is the wavelength of the X-rays, d is the spacing between atomic planes in the crystal lattice, and θ is the angle of incidence of the X-rays concerning the crystal lattice planes. Measuring the angles and intensities of diffracted X-rays yields information about the crystal structure, including lattice parameters, atomic spacing, and crystal plane orientation. This information can be used to identify the crystalline phases in a sample, calculate its crystal structure, and examine its physical qualities. XRD is a strong technique used in materials science, mineralogy, chemistry, and other domains to analyze the structural properties of crystalline materials. (As seen in Figure 23) [48]

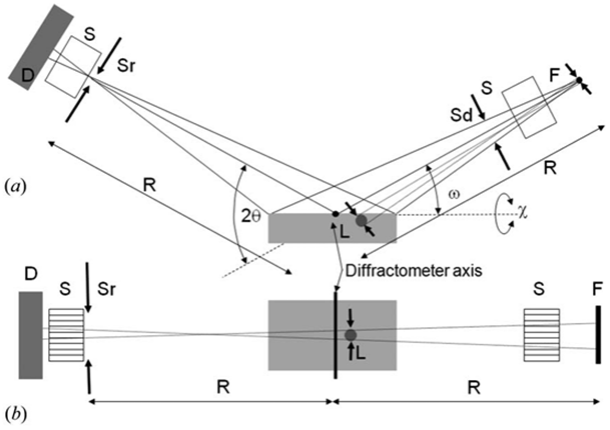

Figure 23 Schematic representation of the XRD machine. The Bragg–Brentano geometry with a sample including crystallites of diameter L, which experience an angular spread defined by L and the focus dimension F. (b) is the projection normal to (a) [48].

2.18 Thermogravimetric Analysis (TGA)

Thermogravimetric analysis (TGA) is a thermal analysis technique that examines a sample's mass changes as a function of temperature or time in a controlled environment. TGA involves steadily heating (or cooling) the sample while continually monitoring its mass. As the temperature rises, the sample can undergo various physical and chemical processes, including breakdown, dehydration, oxidation, and reduction. These processes cause changes in the sample's mass, which is measured by the TGA equipment. Researchers can learn much about a sample's composition, thermal stability, breakdown kinetics, and reaction processes by analyzing its mass loss or gain across a wide temperature range. TGA is widely used in materials science, chemistry, pharmaceuticals, and polymers to characterize and understand the thermal properties of various materials [49].

CHAPTER III

LITERATURE REVIEWS

3.1 Lignin Precipitation

Lignin is the most common natural polymer after cellulose, acting as a link between the molecules within the structure, making plants strong and durable [50]. Lignin is a significant component in black liquor, the by-products from the paper-making industry. The separation of lignin from black liquor has been developed, using 3 standard methods: 1. Acidification 2. Ultrafiltration and 3. Electrolysis. It was found that the extraction of lignin from black liquor by the Acidification method is an efficient and cost-effective method using the Kraft process to precipitate lignin under an acidic environment [11, 13, 51]. Preliminary studies have also found that adjusting the pH value to below 10 will cause lignin to precipitate more. The type of acid used, namely organic and inorganic, affects lignin extraction in terms of yield and environmental aspects. This is because, when using inorganic acid, the resulting product will have more sulfur and nitrogen remaining than if used with organic acid [11, 12]. The purity of the extracted lignin was also studied when impurities were separated from the process. The figure shows FTIR spectra of lignin samples. The spectral bands 1705 and 1600 cm^{-1} were observed as plant protein and water contaminants associated with lignin. It is the part that indicates the purity of lignin after extraction from the process [52].

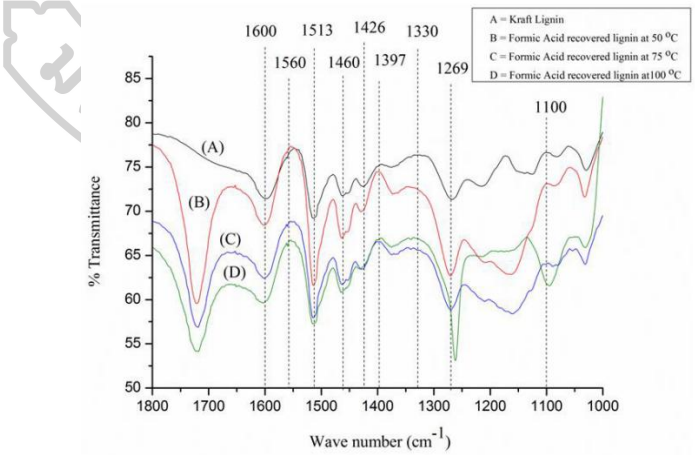

Figure 24 FTIR spectra of kraft lignin (A), Formic acid recovers lignin at different temperatures: 50ºC (B), 75ºC (C), and 100ºC (D) [53].

3.2 Glycolysis of PLA

Many studies have focused on recycling postconsumer PET and PLA, which are bio-polyesters, through transesterification. Figure 25 shows a diagram of the glycolysis depolymerization

of PET. [54] The glycolysis of PLA produces hydroxyl-capped low- to medium molecular-weight PLA oligomers from the transesterification process with various types of alcohol. The structures and properties of glycolyzed products of PLA using ethylene glycol (EG) have been investigated. [55] The study kept the reaction temperature at approximately 195ºC. The GlyPLA product was recovered by dissolving it in chloroform and precipitating it with methanol. From GPC analysis, molecular weight (M_n) and average molecular weight (Mw) were 3600 and 4800, respectively. The process took 30 min, the temperature was 170ºC, and the weight ratio was 1:2 (PLA: EG). It was found that increasing the amount of EG, reaction time, and temperature will cause the Mw value to decrease [10].

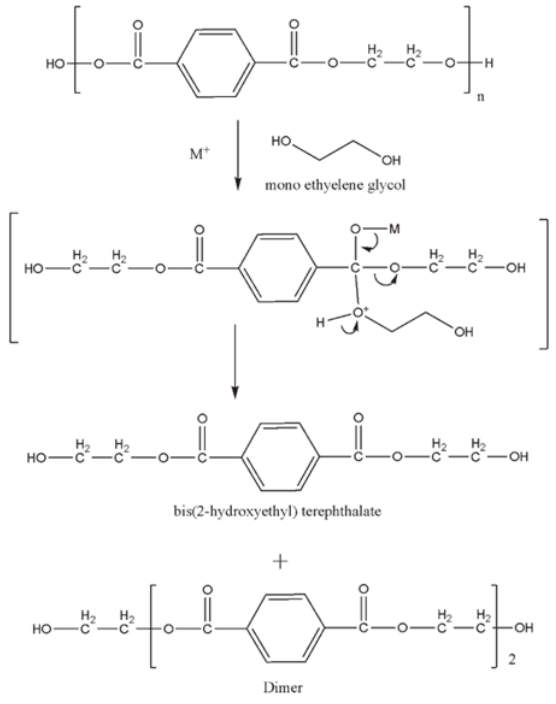

Figure 25 Diagram of glycolysis depolymerization of PET [10].

3.3 Conventional reflux for glycolysis reaction

The cosolvent method is a method for accelerating a chemical reaction or adding a solvent that can change the efficiency of the reaction. For example, in the alcoholysis reaction of vegetable oil, the efficiency will improve when water is added to the system [56]. Ionic liquids (ILs) have been studied as polymer degradation solvents due to their chemical stability characteristics or the ability to be a common solution. It can also be used as a single solvent or as a catalyst to increase the rate of a reaction [57]. Extensive research has been done on the hydrolysis of PET (or polyester) heated in a mixture of triol and glycol at approximately 260ºC. The process is carried out in a reflux condenser

(Figure 26.), and a transesterification catalyst is added to heat to about 250ºC, which will retain products with low M_w from decomposition [58].

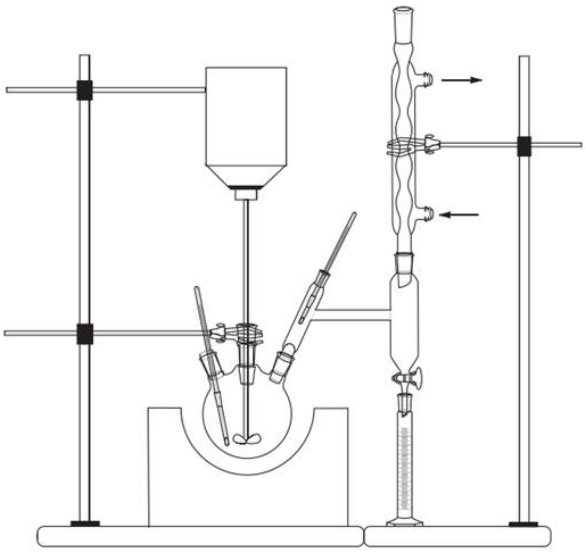

Figure 26 Diagram of the sample conventional reflux of alcoholysis process [58].

3.4 Chemically modification

3.4.1 Lignin modified (lignin-M)

Lignin is a natural aromatic polymer composed of the phenylpropanol structure. [59] Extensive research has been conducted on the main components of biomass. Lignin has a complex, unordered structure. The units are coumaryl, coniferyl, and sinapyl [60]. Figure 27 shows the Structures of monolignols: p-coumaryl alcohol (H), coniferyl alcohol (G), and sinapyl alcohol (S) that are connected by ethes or C-C bonds [61].

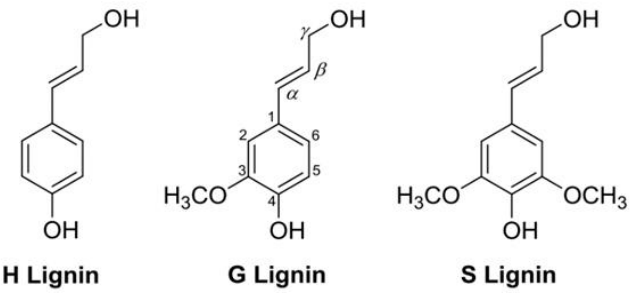

Figure 27 Structures of monolignols: p-coumaryl alcohol (H), coniferyl alcohol (G), and sinapyl alcohol (S) [61].

Therefore, the chemical modification of lignin has been studied for use as an additive in polymer modification. Because of the diversity of functional groups such as phenolic, carbonyl, etc.,

especially the aliphatic and phenolic hydroxyl (OH) groups are the parts which can be modified through the esterification process (or alkylation), resulting in some improved chemical properties due to structural complexity is an attractive filler material [14]. There have been studies of chemically modifying the lignin structure between the chemical structure of the phenolic hydroxyl groups of lignin and the anhydride groups of maleic anhydride (or some studies have used acetic anhydride) at a temperature and appropriate time [14], as shown in Figure 28. Diagram of the esterification process between an anhydride group and phenolic hydroxyl group.

FTIR spectrum analysis provides information about the structural changes. Figure 29 shows the FTIR spectrum; a wide peak band caused by aromatic and aliphatic hydroxyl in lignin can be seen at 3400-3500 cm^{-1}. After the chemical modification of lignin, two peaks appeared at 1722 cm^{-1} and 1127 cm^{-1}, indicating the formation of ester groups with C=O and C-O bonds. The adsorption bands of the vinyl group were observed at 1617 cm^{-1}, indicating that maleic anhydride can react with lignin and that esterification reactions can occur on the surface of lignin [14].

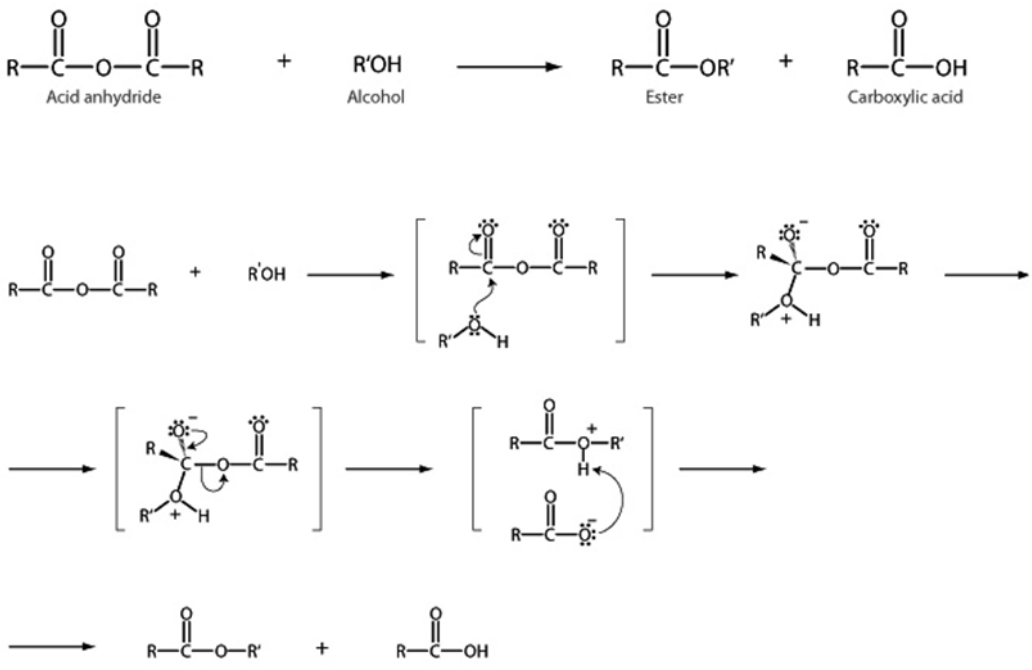

Figure 28 Diagram of the esterification process between an anhydride group and phenolic hydroxyl group.

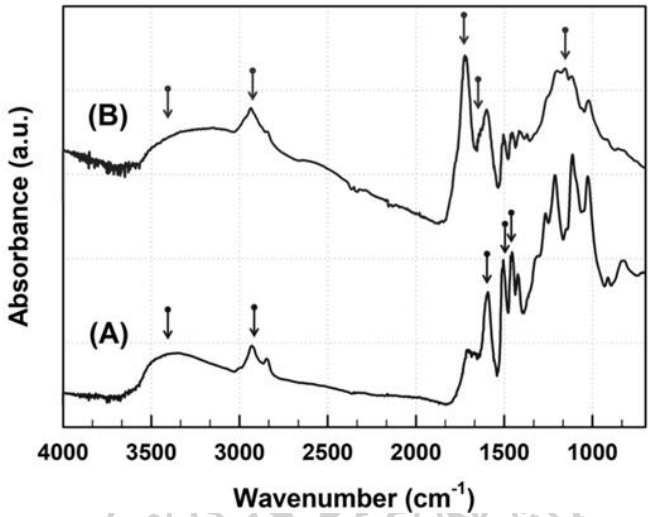

Figure 29 FTIR spectra of pristine lignin (A) and chemically modified lignin (B) [14].

3.4.2 GlyPLA-cured lignin-M

The OH-capped PLA oligomers have the potential to be used in a variety of chemical reactions. Lignin has a complex structure and various functional groups, especially carbonyl groups, that create grafting or crosslinking structures for GlyPLA-cured COOH-lignin.

3.4.2.1 Melt blending

A study was conducted on preparing a copolymer, an example of which was the preparation of GENR by mixing ENR20 and glycolysis PLA (GPLA) by melt mixing. The TGA thermograms showed a maximum decomposition temperature of 400ºC, with a decomposition temperature of 300ºC belonging to ENR. Therefore, the temperature between 350-400ºC belongs to the GENR network. The degradation of the lactate block sequence that acts as a crosslinker in ENR during the degradation at 450ºC may be due to crosslinking loss. The simulated structure is shown in Figure 30. The efficiency of GENR's curing process is examined in terms of compatibility. The solvent extraction values for grafting and crosslinking were 12 and 32 %wt, respectively. This indicates the crosslinking efficiency of GPLA with ENR. In terms of mechanical properties, it was found that the combination of GPLA and ENR Helps increase elongation at break, including tensile strength and modulus, as shown in Table 1 [62].

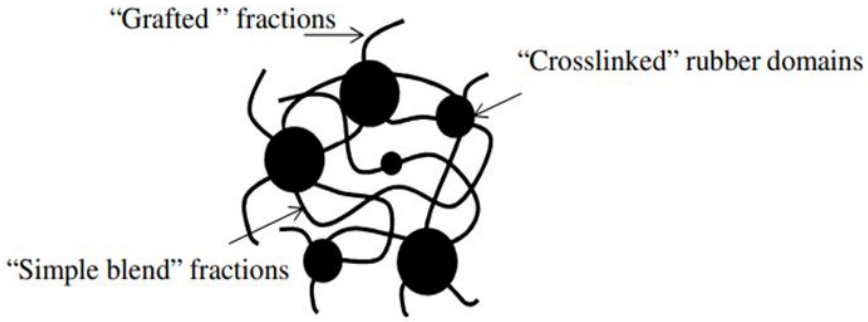

Figure 30 The simulated structure of GENR materials.

Table 1 Tensile and impact properties of neat PLA, GENR/PLA, and uncured ENR/PLA blends at various blend compositions.

Samples	Tensile strength (MPa)	Elongation at break (%)	Modulus (GPa)	Impact strength (GPa)
Neat PLA	36±5	2.2±0.5	2.1±0.10	2.4±0.04
GENR/PLA 5	42±1	2.5±0.2	2.1±0.10	2.7±0.08
GENR/PLA 10	30±1	3.0±0.1	1.9±0.05	2.8±0.04
GENR/PLA 15	31±1	3.5±0.1	1.8±0.08	2.7±0.03
Uncured ENR/PLA 5	31±1	2.4±0.1	2.1±0.05	2.1±0.05
Uncured ENR/PLA 10	20±2	1.3±0.1	1.9±0.08	2.8±0.09
Uncured ENR/PLA 15	14±1	1.1±0.1	1.7±0.10	0.6±0.10

3.5 Fabrication of 3D-printing filaments

Effect of temperature on extrusion as well as screw speed. A study was conducted using data on the diameter of the fibers obtained under various conditions, as shown in Table 2. When the screw speed was from 2 rpm to 6 rpm, the diameter of the fibers decreased. Moreover, the extrusion temperature increased. In short, the viscosity of a liquid decreases with increasing temperature. This improves the flow and does not affect the swelling of the die, as shown in the fiber example in Figure 31. In Table 2, it can be explained that the melt volume increases with the speed of the screw. This will cause the die to become noticeable and have a larger diameter [63].

Table 2 Filament diameter data were obtained under various extrusion temperatures and screw speeds [63].

	185°C	190°C	195°C	200°C
2rpm	1.756	1.680	1.620	1.448
3rpm	1.760	1.721	1.680	1.575
4rpm	-	1.791	1.727	1.665
5rpm	-	1.831	1.810	1.747
6rpm	-	1.946	1.888	1.857

*(-) No satisfied filaments obtained

(a) fabricated at 2 rpm (b) fabricated under 200ºC

Figure 31 Photography of filaments fabricated under constant extrusion speed (a), or constant extrusion temperature (b) [63].

3.6 Preparation of 3D-printing specimens

The effects of 3D printing along different axes were studied. It is explained that the orientation of printing is essential in determining the strength of the workpiece, such as impact resistance. Flat orientation (XY = 152.5 J/m), horizontal orientation (XZ = 113.2 J/m), and vertical orientation (ZX = 77.4 J/m) gave different results. Figure 32 (a) shows an example of printing along various axes. The purpose is to study the effects of printing on other layers. The ratio of shell/infill along the plate, as shown in Figure 3.10 and Figure 32 (b), shows the layer printing at different angles. Referring to Figure 33 (b), the initial and subsequent layers are positioned 90 degrees from the previous layer [19].

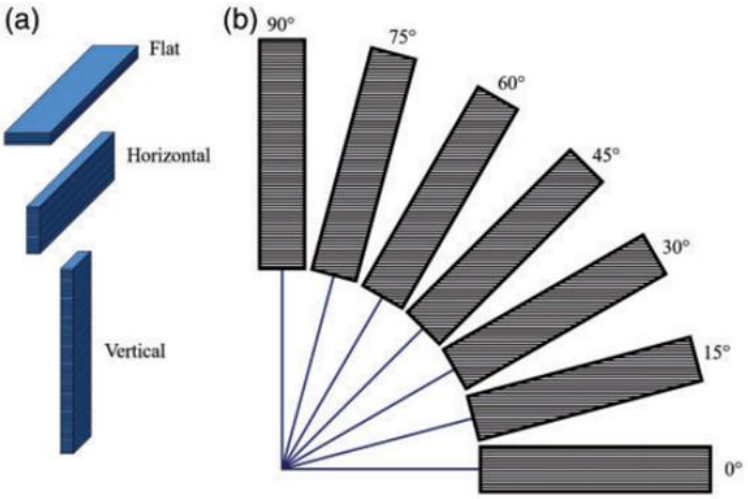

Figure 32 (a) Printing orientations and (b) raster angles [19].

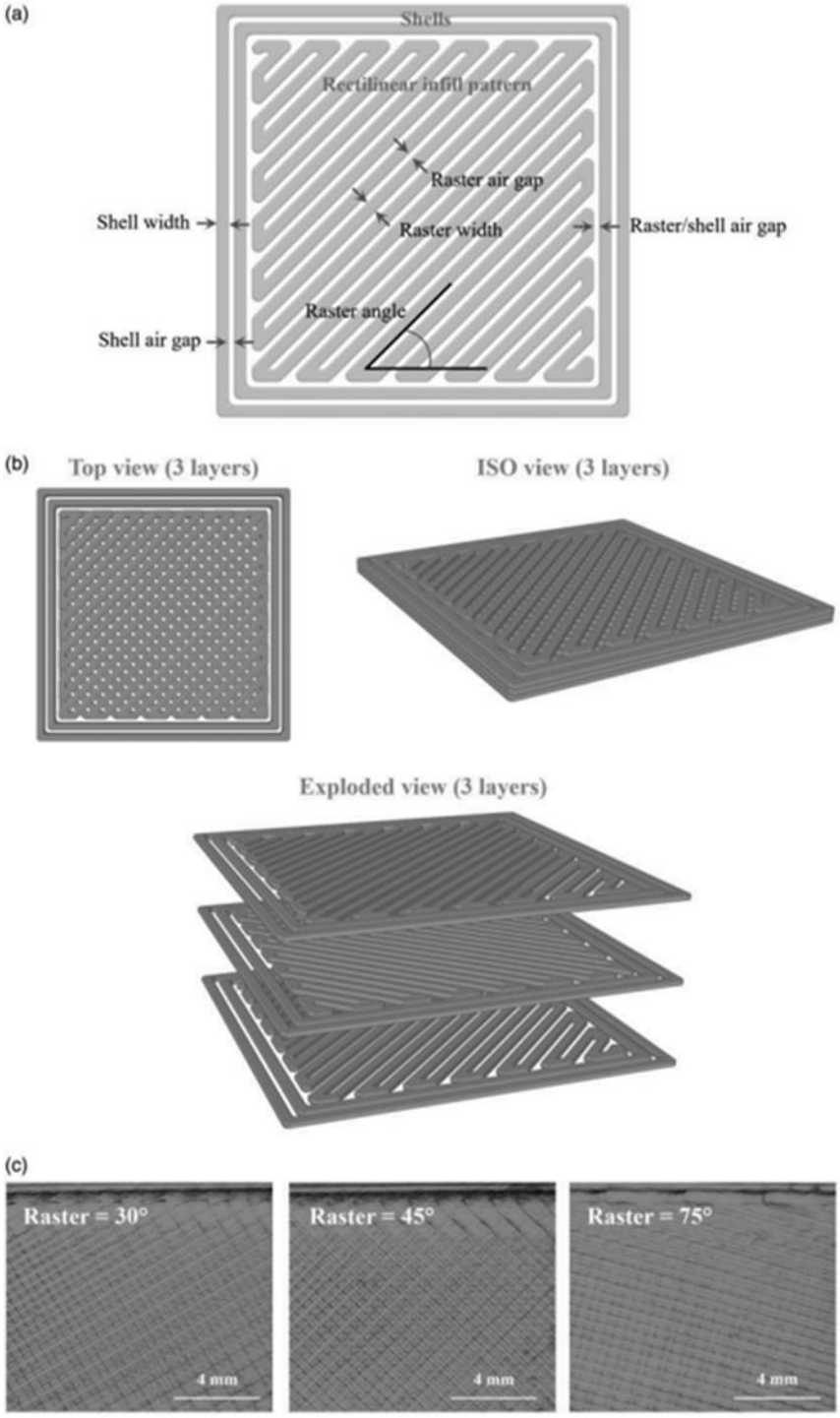

Figure 33 (a) Rectilinear layer structure, (b) configuration of several layers for FDM materials, and (c) manufactured examples (using transparent PLA with light behind) [19].

CHAPTER IV

METHODOLOGY

4.1 Materials

The chemicals and raw materials for the experiment are summarized in Table 3.

Table 3 List of chemicals and raw materials used in the experiments.

Name of Chemicals	Grade	Supplier
Black liquor	pH ≈ 12	Siam Kraft Industry Co., Ltd, Thailand
Acetic acid (glacial) (CH_3COOH)	100%, AR grade	Q RëC™
Sulfuric acid (H_2SO_4)	98%, AR grade	Q RëC™
Maleic anhydride ($C_4H_2O_3$)	≥ 99.0% (NT)	Sigma-Aldrich
Ethylene glycol (EG)	99.5%, AR grade	Q RëC™
N, N-Dimethyl formamide (DMF)	≥ 99.9%, AR grade	RCI Labscan Limited
Ethyl Alcohol (C_2H_6O)	99.9%, AR grade	Q RëC™
Poly(lactic acid) (PLA)	Ingeo™ Grade 2003D, Density 1.24 g cm^{-3}	NatureWorks LLC
Distilled water	-	-

4.2 Apparatus

The list of apparatus for this experiment is summarized in Table 4.

Table 4 List of apparatus utilized in the experiments.

Apparatus	Supplier/Trademark
Hot plate with Stirrer,	IKA^{R}C-MAG HS7, IKATRON^{R}ETS-D5
Heating Mantle with Stirrer, Volume 500 ml	MS-Series Model MS-ES-303, Made in Korea
Burette, 50 ml	DURAN®
Round bottom flask, 500 ml	DURAN®
Glass condenser	Glassco
Circulating Water Vacuum Pump	-
Chemistry laboratory glassware	DURAN®
CT Internal Mixer (Cam Type)	CHAREON TUT CO., LTD.
Compression Molding Machine	-
Extrusion Lines	Labtech Engineering Co., Ltd.
3D Printer	Delta X200 3D printer
Universal Testing Machine (UTM)	Shimadzu, EZ Test, EZ-LX/EZ-SX Series
Field Emission Scanning electron microscope (FE-SEM)	TESCAN MIRA3
Fourier-transform infrared spectrometer (FTIR)	BRUKER (ALPHA II)
Proton Nuclear Magnetic Resonance Spectroscopy (^{1}H-NMR)	AV-500, Bruker Biospin
X-Ray diffraction (XRD)	Bruker AXS Model D8 Advance
Thermogravimetric Analysis (TGA)	SDT Q600, TA Instruments, UK

4.3 Experiments

Part I: Preparation of lignin from black liquor by Acidification process

4.3.1 Extraction process

The extraction of lignin from black liquor was conducted by acidification. The process of adjusting the pH value is divided into two parts. The first method adjusts the pH value with acetic acid (CH_3COOH), an organic acid. The second method adjusted the pH value with sulfuric acid (H_2SO_4), an inorganic acid. The experiments were divided into steps according to the specified pH range to adjust the pH value, as summarized in Figure 34.

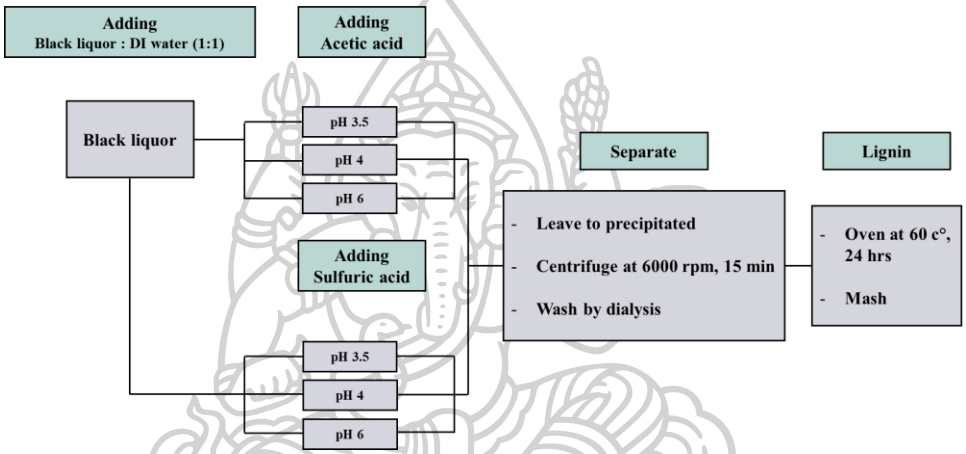

Figure 34 Overview of the extraction process of lignin from black liquor by acidification.

Figure 34 describes the preparation of black liquor with distilled water in a 1:1 ratio, then placed in a magnetic stirrer and heated at 60 °C. The pH value was adjusted with acid until the desired pH value was obtained. The pH values were adjusted at 3.5, 4, and 6. The experiment is divided into 2 parts: 1) Use acetic acid (CH_3COOH) and 2) Use sulfuric acid (H_2SO_4). Once the pH-alkaline value had been adjusted, the pH-adjusted black liquor sample was left to precipitate and then placed in a centrifuge at 6000 rpm for 15 min per cycle to separate solid and liquid particles, including contaminants with DI water. The solid fraction was separated after the centrifuge was washed by a dialysis process and dried at 60 °C for 24 h in the oven to remove moisture.

4.3.2 Characterization of lignin from black liquor by acidification

The morphology and chemical structure of the resulting lignin extraction were examined as follows:

4.3.2.1 Field emission scanning emission microscopy (FE-SEM)

FE-SEM images taken from a scanning electron microscope were used to examine the lignin's surface morphology and size. The samples were prepared by stabbing them with carbon tape and coating them with gold ions for conductivity enhancement. The condition of FE-SEM (TESCAN MIRA3) was used at 500X, 1000X, 2000X, and a voltage of 2 kV.

4.3.2.2 Fourier-transform infrared (FTIR) spectroscopy

The chemical structures and components of the lignin were investigated by an FTIR spectrometer, BRUKER (ALPHA II). The spectra were collected in an attenuated total reflection (ATR) mode and transmittance mode (TR). The spectra were recorded using 64 scans at a 4 cm^{-1} resolution.

4.3.2.3 Thermal properties

TGA analysis with SDT Q600 (TA Instruments, UK) characterized the thermal degradation of sample. The powder (10-20 mg) was measured in a nitrogen atmosphere from 50-800˚C at a heating rate of 10˚C/min

Part II: Preparation of alcoholyzed PLA (A-PLA)

4.3.3 Preparation

A-PLA is synthesized by alcoholysis of PLA using poly(lactic acid) (PLA), ethylene glycol (EG), and glycerol as reactants. This reaction was carried out using a conventional reflux reactor (as shown in Figure 35) at a temperature of 190-200 °C for 12 hours (collecting samples every 2 hours) according to different weight ratios of PLA: EG and PLA: Glycerol for comparison, as summarized in Table 5. The sample was then volatilized in a vacuum oven at 60 °C for 24 h.

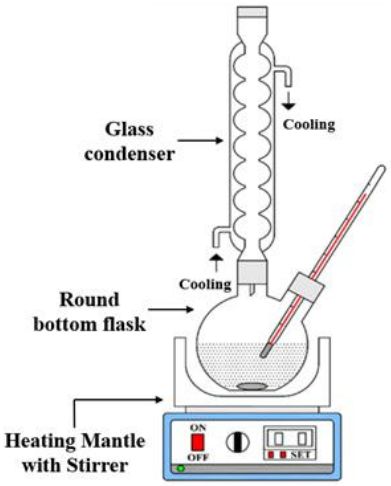

Figure 35 Diagram of a conventional reflux reactor for alcoholysis of PLA.

Table 5 Alcoholysis condition of PLA with a conventional reflux reactor.

No.	PLA: EG	PLA: Glycerol	Temperature (°C)
1	3:1	3:1	≈190
2	6:1	6:1	≈190
3	9:1	9:1	≈190

4.3.4 Characterization of alcoholyzed PLA (A-PLA) products

The chemical structures of the alcoholyzed PLA (A-PLA) products were examined using the same procedures described in section 4.3.2.2. Additionally, the chemical compositions of the samples were examined as follows:

4.3.4.1 Proton Nuclear Magnetic Resonance Spectroscopy (^{1}H-NMR)

^{1}H-NMR Spectroscopy investigated the chemical structure and components of the A-PLA. AV-500, Bruker Biospin, collected the spectra. Samples were prepared in NMR tubes using 3-5 mg dissolved in solution Chloroform-d, for NMR, 99.8 atom% D, stabilized with silver foil.

Part III: Preparation of lignin/maleic anhydride/alcoholysis PLA

4.3.5 Preparation

The chemical modification of lignin and preparation of lignin/maleic anhydride/alcoholysis PLA is divided into 4 methods. First method, the conventional reflux reactor is chemically modified through the PLA alcoholysis reaction. The second method, the use of solvent solutions for reactions,

is chemically modified. The third method, the conventional heating, is employed to chemically modify by separating the reaction steps. Fourth method, an internal mixer was used to modify through shear force by thermal processing chemically. The chemical structures, compositions, and properties of the products from the 4 preparation methods are compared.

4.3.5.1 Chemically modified in the conventional reflux reactor through A-PLA (Method 1)

The pre-treatment was prepared by adding lignin and maleic anhydride into alcoholyzed PLA (at 4 h reaction time) at a ratio of 4:1 (A-PLA: lignin), with the MA concentration set at 10 wt%, during the alcoholysis reaction in a simple reflux reactor, as shown in Figure 4.2. The process was continued at 190 ºC for an additional 2 h after the alcoholyzed PLA preparation. The method and steps are illustrated in Figure 36.

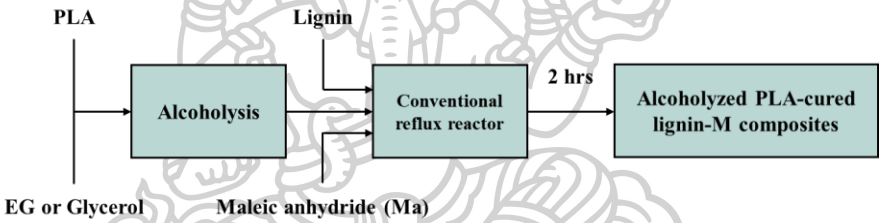

Figure 36 Diagram of the chemical modification in a conventional reflux reactor (Method 1).

4.3.5.2 Chemical modification by conventional heating (Method 2)

The pre-treatment preparation differs from Method 1 in that the step is separated from the alcoholysis of PLA. The obtained alcoholyzed PLA was melted at 120 ºC, followed by the addition of lignin and maleic anhydride at a ratio of 4:1 (A-PLA: lignin), with the MA concentration set at 10 wt%, for 2 h. The method and steps are illustrated in Figure 37.

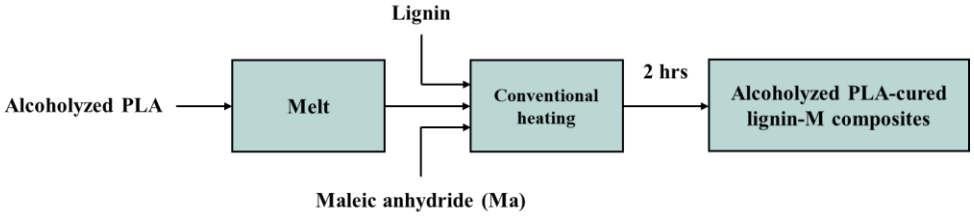

Figure 37 Diagram of the chemical modification using conventional heating (Method 2).

4.3.5.3 Chemical modification in solution (Method 3)

The lignin was dispersed into N,N-Dimethyl formamide (DMF) solution and stirred until homogeneous, then alcoholyzed PLA and maleic anhydride were added to the solution aand heated at 120°C fot 6h. The method and steps are summarized in Figure 38.

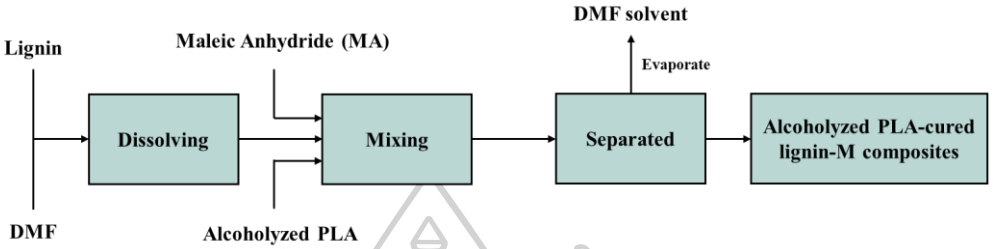

Figure 38 Diagram of the chemical modification in solution (Method 3).

4.3.5.4 Chemically modified in an internal mixer through thermal processing (Method 4)

This preparation step differs from the other methods in that no pre-treatment was performed. Instead, thermal processing was carried out by simultaneously adding alcoholyzed PLA, lignin, and maleic anhydride into the internal mixer together with the PLA matrix at proportions of 1, 3, and 5 wt%. The additives were introduced at a ratio of 4:1 (A-PLA: lignin), with the MA concentration set at 10 wt%,at 170°C, rotor speed 50 rpm for 20 min. The method and steps are illustrated in Figure 39.

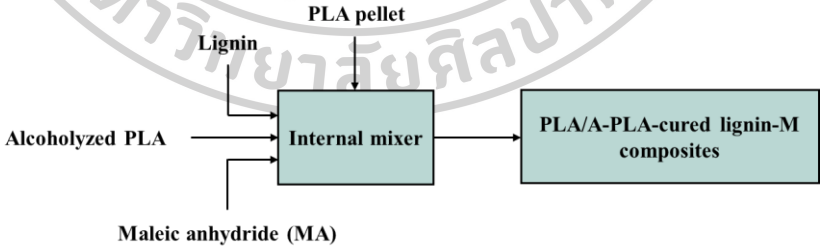

Figure 39 Diagram of the chemical modification in an internal mixer (Method 4).

4.3.6 Characterization of alcoholyzed PLA-cured lignin-M composites

The chemical structure was examined using the same procedures described in sections 4.3.2.2.

Part IV: Blend of neat PLA resin with alcoholyzed PLA-cured lignin-M composites

4.3.7 Preparation

The commercial PLA pellets were melted at 170 ºC until the torque value was constant in an internal mixer. Alcoholyzed PLA-cured lignin-M composites from 4.3.5.1 (Method 1), 4.3.5.2 (Method 2), and 4.3.5.3 (Method 3) were added, and the mixture was further blended for 20 min with a rotor speed of 50 rpm. The A-PLA-cured lignin-M composites contents were varied at 1, 3, and 5 weight%. Then, molded by compression molding, polymer composites were dried in an oven at 80 °C for 1 h to evaporate moisture. The samples were fabricated into dumbbell, bar, and film shapes for appropriate analyses at 170 °C, 4000 psi in 10 min, as summarized in Figure 40.

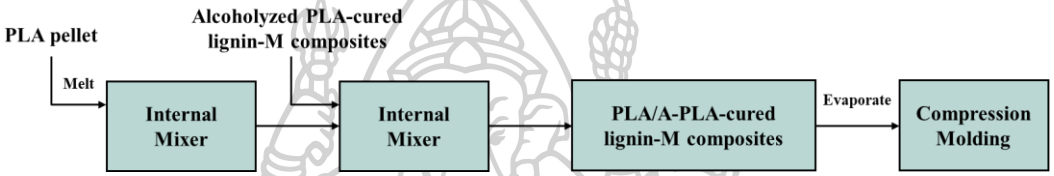

Figure 40 Diagram of preparation of PLA/A-PLA-cured lignin-M composites.

4.3.8 Characterization of PLA/A-PLA-cured lignin-M composites

The mechanical of the resulting PLA/A-PLA-cured lignin-M composites were examined as follows:

4.3.8.1 Mechanical properties

The tensile tests were performed according to ASTM D 638 using a universal test machine by Shimadzu, EZ Test, EZ-LX/EZ-SX Series. Tensile tests were obtained at room temperature with a 50 mm/min crosshead speed. The dumbbell-shaped specimens of all the blending samples were stretched continuously speed until they failed. Each value obtained represented the average of the results of twelve samples.

Part V: Optimization of filament fabrication and Printing performance and properties of the printed specimens

4.3.9 Preparation

PLA pellets and PLA/Lignin were made into monofilament with an extrusion speed of 50 rpm using a counter-rotating twin-screw extruder in the temperature range of 160-190 °C. PLA/A-PLA-cured lignin-M composites samples at the optimum ratio were then ground. Small particles with a cutting mill utilize 3 essential parameters: the V rotor (Speed: 1500 rpm), the 0.5 mm sieves, and the

cyclone-suction unit under liquid N_2. The reduced samples are used as raw material to produce 3D-printed filaments. The monofilament with different extrusion speeds, such as 35 and 50 rpm (referring to PGE35 and PGE50, respectively), was fabricated as described above, as shown in Figure 41.

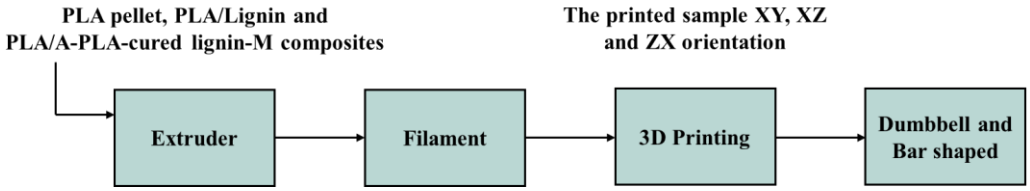

Figure 41 Diagram of preparation of Optimization of filament fabrication and Printing performance and properties of the printed specimens.

The filaments are used as starting materials for 3D printed parts by extruding the sample into filaments. The specimens were designed and exported in STL file format by the Free CAD software and then sliced in G-code format by the Ultimaker Cura (version 4.8.0). Then, the created specimens were printed by a Delta X200 3D printer to investigate the printing performance and prepare the Izod impact specimens. The tensile test was compared to commercial PLA filaments, and printed in XY (Flat), XZ (Horizontal or On edge), and ZX (Vertical or Up-right), as shown in Figure 42.

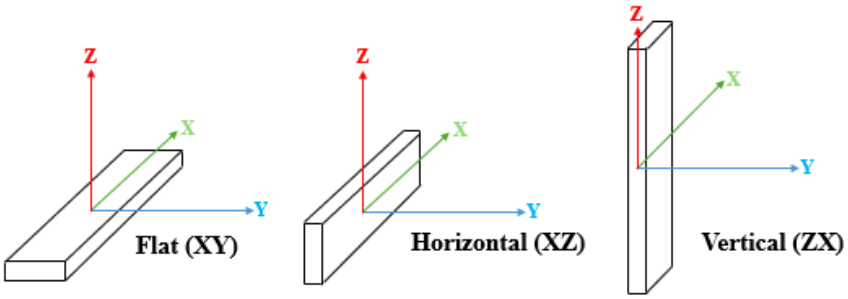

Figure 42 Diagram of the designed samples in XY (Flat), XZ (On edge), and ZX (Up-right) printing orientations.

4.3.10 Characterization of printed tensile test specimens

Dumbbell-shaped specimen conforming to ASTM D638 Type IV for tensile testing methods. It was designed and printed in XY (Flat), XZ (On Edge), and ZX (Top Right) printing using a Delta X200 3D printer. The mechanical properties were examined using the procedures described in section 4.3.8.1.

CHAPTER V

RESULTS AND DISCUSSION

Part I Characterization of lignin from black liquor by acidification

The morphology, chemical compositions, and chemical structures of lignin extracted from black liquor by acidification with different types of acids and pH conditions were characterized.

5.1 Lignin from black liquor by acidification

5.1.1 Morphology

The morphology of the lignin product extracted from black liquor was examined. The acidification process is done by comparing two different acids, organic and inorganic acids, and by examining the morphological structure with SEM, as shown in Figure 43. Under low-acidic conditions (pH 6), the particles are predominantly in the form of crystalline tetragonal dipyramids, with an average size of approximately 5 µm. When the pH was further reduced to 4 and 3.5, a reduction in crystalline particles was observed, accompanied by the appearance of non-porous solid flakes, which are indicative of the amorphous nature of lignin [11, 64].

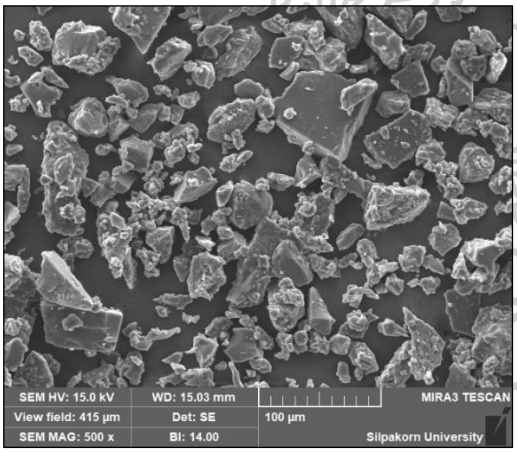

(a)

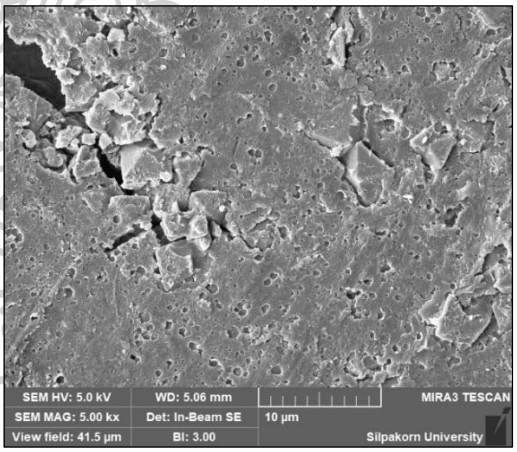

(b)

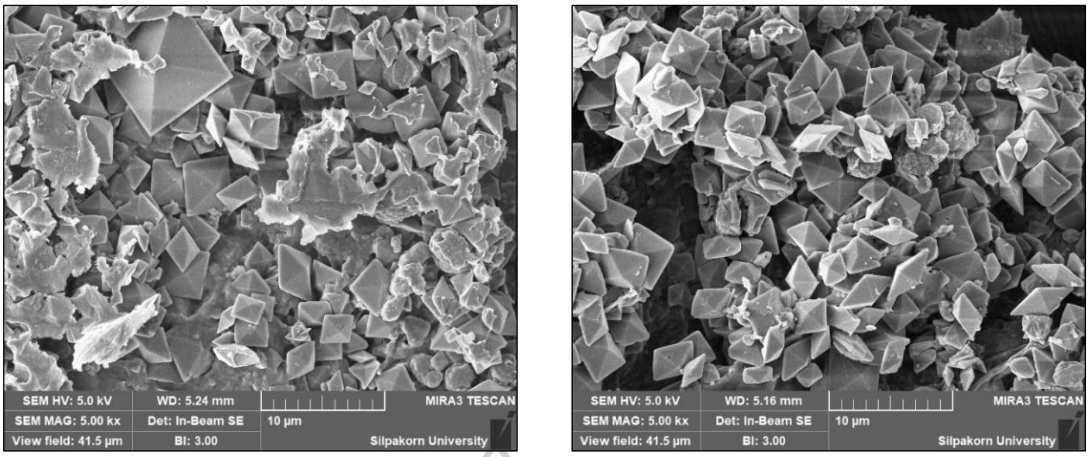

(c) (d)

Figure 43 SEM micrographs of (a) black liquor, and the extracted lignin from black liquor by acidification at various pHs: (b) 3.5, (c) 4, and (d) 6.

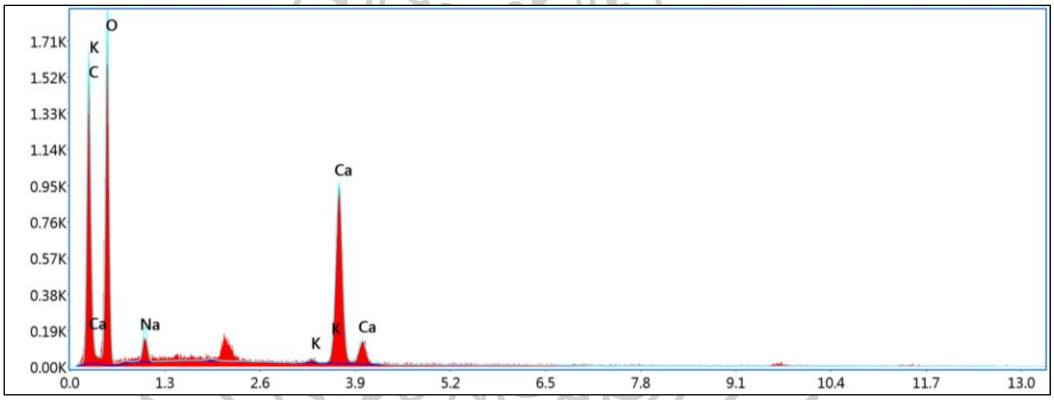

Figure 44 SEM-EDS spectrum of the crystalline fraction of the extracted products obtained at pH 6.

The SEM-EDS analysis indicated that these crystals contained Ca, C, and O, as summarized in Figure 44. This suggests that these crystals are likely $Ca(OH)_2$ and $CaCO_3$ residues from the pulping process during the chemical recovery stage [64, 65]. This reduces the solubility of lignin in black liquor solution, and it begins to precipitate at pH 6. The major source of Ca^{2+} in black liquor explains this partly because lime (CaO) is used in the chemical recovery step to recover NaOH for use within the system [66]. As the acidity decreased, the crystal content also decreased, while an amorphous fraction, indicating the amorphous nature of lignin, was observed. The increase in lignin fraction compared to the decreased Ca^{2+} crystals is consistent with the product yield as shown in Table 6, which was caused by acidification to reduce the solubility of lignin in black liquor solution to cause precipitation [64].

The results from acidification with different types of acids and different pH ranges showed that the pH value affected the precipitation of lignin in the synthesis from black liquor, as summarized in Table 6. The acidification reduces the solubility of lignin by neutralizing its negative charges, resulting in increased lignin precipitation. The lower the solubility of lignin, the % Yield increases, even at the same acidity condition. This is because the chemical structures of the two types of acids are different, and their ability to break down is different [51].

Table 6 The effects of acid types and pH range on the product yields of lignin extraction.

Acid Type and pH		Amount of acid used (mL)	%Yield
Organic acid (Acetic acid)	pH 3.5	35.2	40.15
	pH 4	19.2	15.03
	pH 6	7.4	1.62
Inorganic acid (Sulfuric acid)	pH 3.5	10.8	43.97
	pH 4	7.4	23.29
	pH 6	4.2	13.97

5.1.2 Crystallinity

The crystalline structure and crystalline content of Ca compounds relative to the recovered lignin at different acidification pH levels of 3.5, 4, and 6 were examined by XRD, as shown in Figure 45-46. The signals at 22, 24, 28, 37, 40, 42, and 47° represent the $Ca(OH)_2$ and $CaCO_3$ phases [65, 67]. This confirms that in the chemical recovery process in the paper industry, substances like $Ca(OH)_2$ react with Na_2CO_3 to separate NaOH and $CaCO_3$ from each other. However, if the separation or filtration is incomplete, some compounds remain in the black liquor solution [66, 68]. The relative intensities of these signals decreased with the pH of the acidification, reflecting the lower relative content of the Ca compounds compared to lignin. This agrees with SEM and SEM-EDS results. It is noted that the peaks at 32, 20, and 14° may be due to contamination by cellulose.

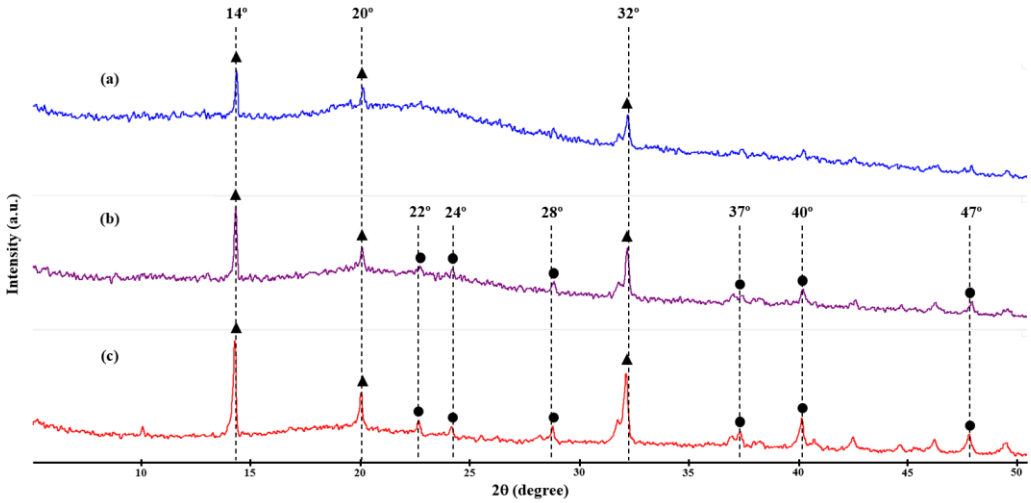

Figure 45 XRD traces of the extracted lignin from black liquor by CH_3COOH acid at various pHs: (a) 3.5, (b) 4, and (c) 6.

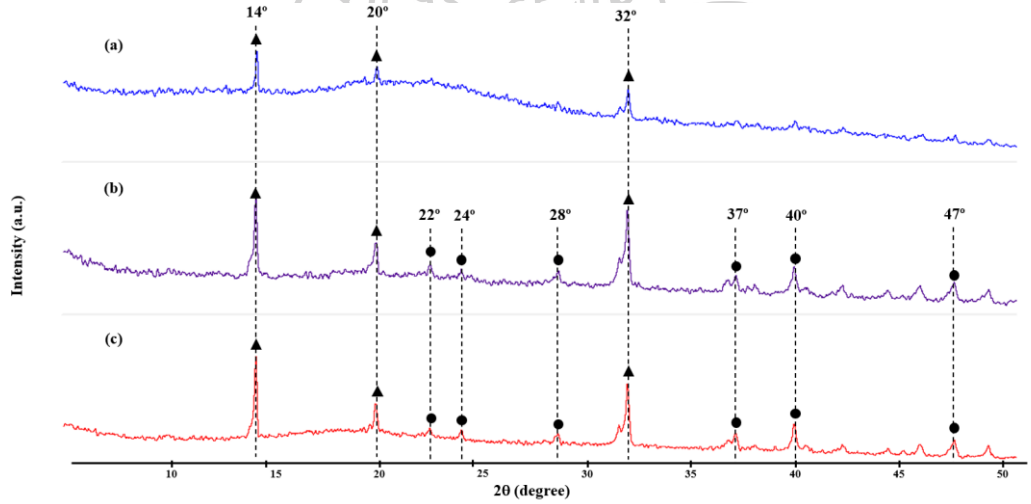

Figure 46 XRD traces of the extracted lignin from black liquor by H_2SO_4 at various pHs: (a) 3.5, (b) 4, and (c) 6.

5.1.3 Chemical structures

The chemical structures of the lignin products extracted from black liquor with organic and inorganic acids at different pH conditions were characterized. The FTIR spectra of the dried black liquor were compared with the extracted products in Figures 47-48. The characteristic bands of the functional groups in the lignin structure, i.e., phenolic and carbonyl, were examined. Lignin is typically composed of three alcohols: paracoumaryl alcohol, coniferyl alcohol, and sinapyl alcohol. These are further subdivided into three phenyl propanols: p-hydroxyphenyl (H), guaiacyl unit (G), and syringyl unit (S) [52]. The C=O stretching band at 1708 cm^{-1} corresponds to the carbonyl group,

while bands 1638 and 1642 cm^{-1} correspond to hemicellulose [12, 69]. The weak band at approximately 1591 cm^{-1} is associated with the C=C stretching mode of aromatic rings. The C=O stretching band of carboxylate (COO) was observed at 1570 cm^{-1}, indicating the ability of lignin to dissolve in the black liquor. The band at 1324 cm^{-1} is attributed to the C-O stretching mode of (S), while the band at 1266 cm^{-1} is attributed to the characteristic of (G) [70, 71], and the bands at approximately 1112 and 1032 cm^{-1} are associated with the vibration of the C-H in the aromatic of the (S) and (G) rings, respectively [11, 69, 71].

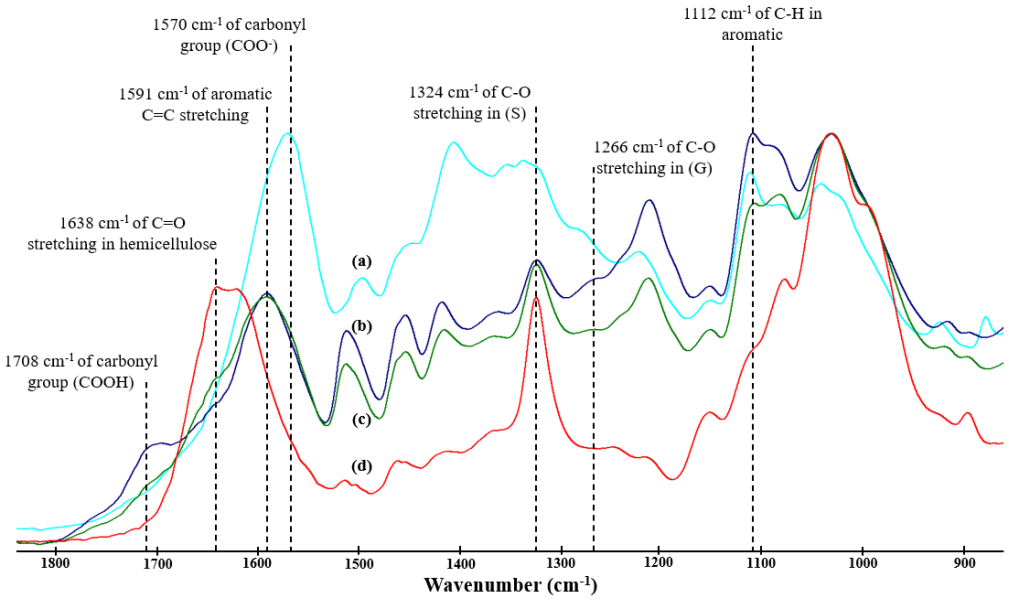

Figure 47 FTIR spectra of lignin synthesis from black liquor by acidification with various acids: (a) Black Liquor, (b) Lignin synthesis by CH_3COOH pH 3.5, (c) Lignin synthesis by CH_3COOH pH 4, and (d) Lignin synthesis by CH_3COOH pH 6.

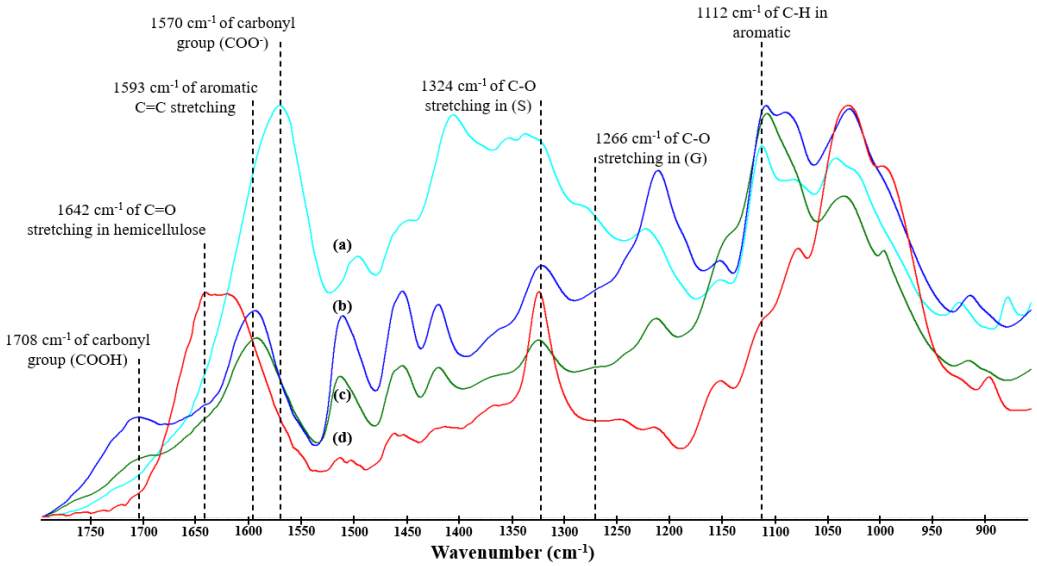

Figure 48 FTIR spectra of lignin synthesis from black liquor by acidification with various pHs: (a) Black Liquor, (b) Lignin synthesis by H_2SO_4 pH 3.5, (c) Lignin synthesis by H_2SO_4 pH 4, and (d) Lignin synthesis by H_2SO_4 pH 6.

The product yield obtained from acidification at different pH conditions is different. Since acidification affects the solubility of lignin in black liquor solution, which may be due to protonation of COO^- to COOH, causing lignin in solution to precipitate [72, 73], a decrease in the intensity of $-COO^-$ was observed at the peak position of 1570 cm^{-1} or a negative band at the frequency in the difference FTIR spectra, as shown in Figures 49-50. The C=O stretching mode of -COOH groups was also observed at 1708 cm^{-1}. The intensity of the positive difference band at 1708 cm^{-1} increased with decreasing pH conditions, while the opposite trend was observed for the negative difference band at 1570 cm^{-1}, which is consistent with the obtained product yield.

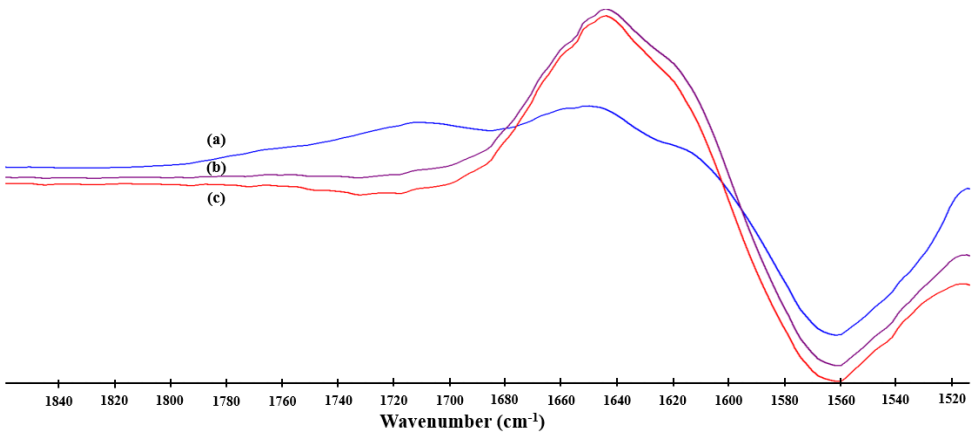

Figure 49 Difference FTIR spectra generated by subtracting the dried black liquor sample from the extracted lignin products at different acidification by CH_3COOH conditions: (a) pH 3.5, (b) pH 4, and (c) pH 6.

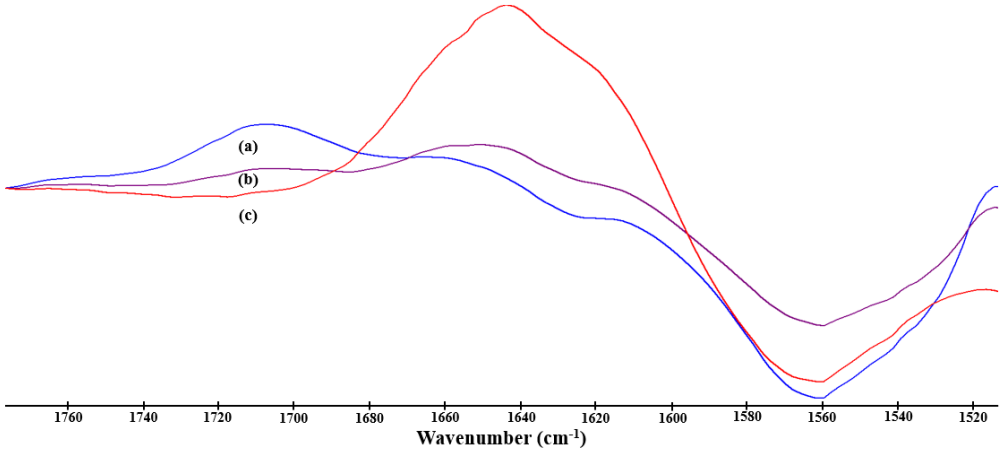

Figure 50 Difference FTIR spectra generated by subtracting the dried black liquor sample from the extracted lignin products at different acidification by H_2SO_4 conditions: (a) pH 3.5, (b) pH 4, and (c) pH 6.

5.1.4 Thermal properties

Thermal gravimetric analysis (TGA) was used to determine the thermal stability and composition of the products, as shown in Figure 51, by comparing with the dried product from black liquor. The results showed that most of the degradation steps occurred in the temperature range of 250-400°C [64, 74]. This is consistent with the covalent bond degradation, such as the cleavage of C-C and C-O-C bonds of the aromatic network. However, this difference was observed in the samples obtained at high pH values. This degradation was higher than normal temperatures in the range of 250-450°C. The degradation of $Ca(OH_2)$ compounds was observed in the temperature range of 350-450°C, whereas that in the temperature range of 600-700°C is due to the degradation of $CaCO_3$ compounds [75-77]. This is due to the presence of inorganic substances that precipitated together with lignin during the acidification process. The results indicate that there are inorganic constituents present in the recovered lignin, and this directly affects the thermal degradation behavior of the products from this process [78, 79].

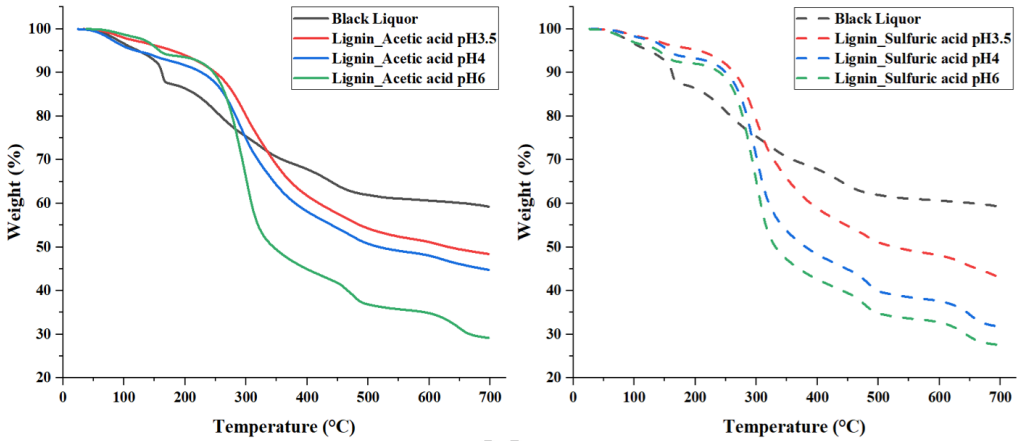

Figure 51 Thermal degradation behavior of precipitated products obtained from acetic and sulfuric acid extraction at different pH values.

The results of the total amount of lignin and Ca compounds in each sample, calculated from the yield TGA results, are summarized in Figure 52. It was found that the type of acid and the acidity condition had an apparent effect on the composition of the products separated from black liquor, with sulfuric acid having a better acidification efficiency than acetic acid [79, 80]. The results reflect that the use of sulfuric acid provides higher product purity and lower Ca contamination compared to the use of acetic acid. This is also consistent with the TGA results which showed higher decomposition peaks of $Ca(OH_2)$ and $CaCO_3$, which is supporting evidence that the products from acetic acid use contain more inorganic contaminants when compared to the proportion of compounds in the products, where the proportion calculated from weight residue (%) or weight loss (%) can be calculated using equation (1).

Mass (g) = % (as fraction) x initial mass (g) (1)

*initial mass = 8.7592 g (black liquor)

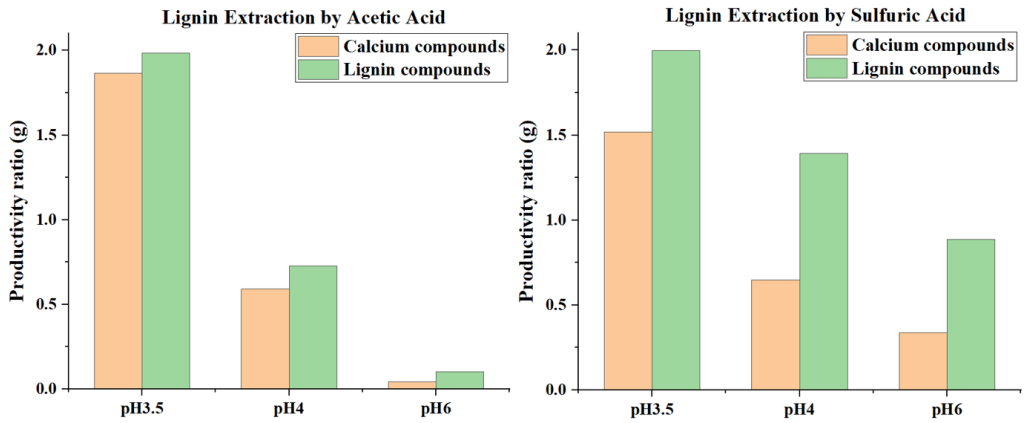

Figure 52 Productivity ratios of lignin and calcium compounds obtained from products precipitation using acetic acid and sulfuric acid at different pH levels.

Part II Characterization of Alcoholyzed PLA (A-PLA)

The effects of primary and secondary alcohols on the alcoholysis of PLA were investigated. Chemical structures and compositions of the products (A-PLA) and the impact of the alcoholysis condition are discussed below.

5.2 Alcoholysis of PLA

5.2.1 Alcoholysis of PLA Product by Primary Alcohols

The effect of the number of hydroxyls in the polyols on the reaction activity was studied using ethylene glycol (EG) and glycerol. The physical characteristics of alcoholyzed PLA (A-PLA) products at ratios of 3:1, 6:1, and 9:1 are shown in Figure 53. The alcoholysis of PLA with EG yielded solid-liquid or gel-like products, each with a yellow color and gradually darker shades, with the color of these products changing from yellow to light brown to dark brown as the PLA: EG feed ratio increased to 9:1 wt/wt. In contrast, the alcoholized PLA products with glycerol were golden yellow and changed to light brown to dark brown according to the reaction rate of all three ratios and had a gel-like physical appearance at 3:1 and solid-liquid ratios at 6:1 and 9:1 wt/wt.

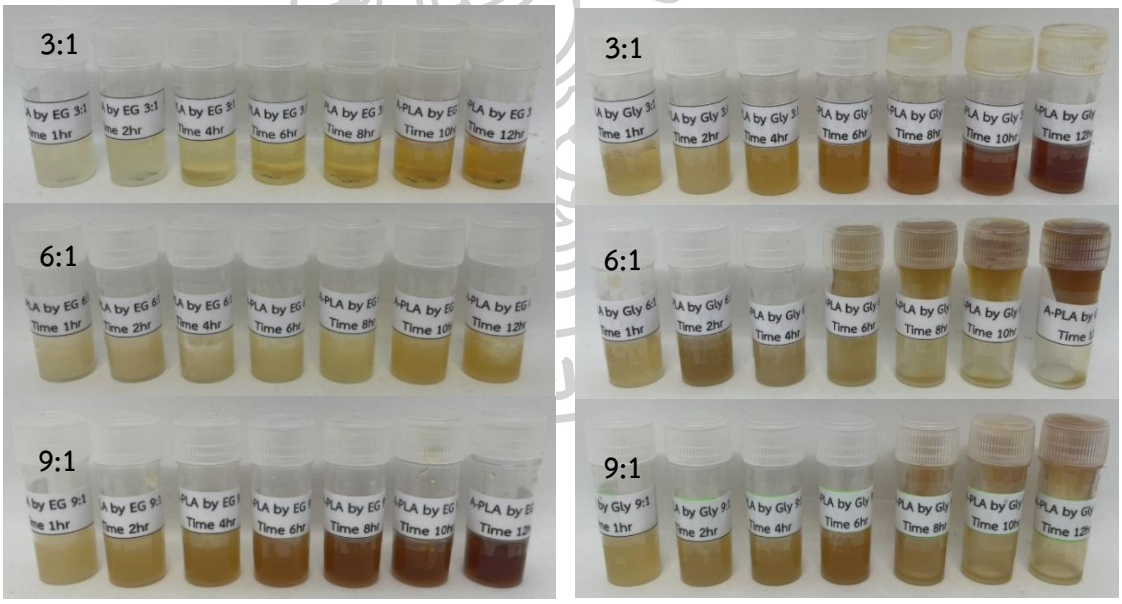

Alcoholyzed PLA by ethylene glycol Alcoholyzed PLA by glycerol

Figure 53 Appearance of alcoholyzed PLA products: A-PLA-EG and A-PLA-Gly samples obtained from PLA: diol ratios of 3:1, 6:1, and 9:1 wt/wt.

5.2.2 Chemical Structure by FTIR spectroscopy

The alcohols containing different hydroxyl groups in both primary and secondary alcohols, namely ethylene glycol (EG) and glycerol, are used as reactants in the alcoholysis of PLA. The alcohols are first characterized by FTIR spectroscopy, as shown in Figure 54. The hydroxyl group (OH) vibration mode of EG is located at 3293 cm^{-1}, while the asymmetric stretching of the methylene group (CH_2) is at 2944 cm^{-1}, and the methylene (CH_2) with the methine (CH) band at 2878 cm^{-1}. The important bands used to confirm the reaction of ester cleaving are the -COO- asymmetric, -COO- symmetric, and C-C vibration located at 1089, 1040, and 885 cm^{-1}, respectively [54, 55, 81]. The FTIR spectrum of glycerol is shown in Figure 5.10. The hydroxyl group (OH) at 3271 cm^{-1}, as methylene group (CH_2) at 2939 cm^{-1}, and methylene (CH_2) with methine (CH) stretch at 2882 cm^{-1}, while the -COO- asymmetric, -COO- symmetric, and OH vibration modes are observed at 1115, 1040, and 992 cm^{-1}, respectively [82].

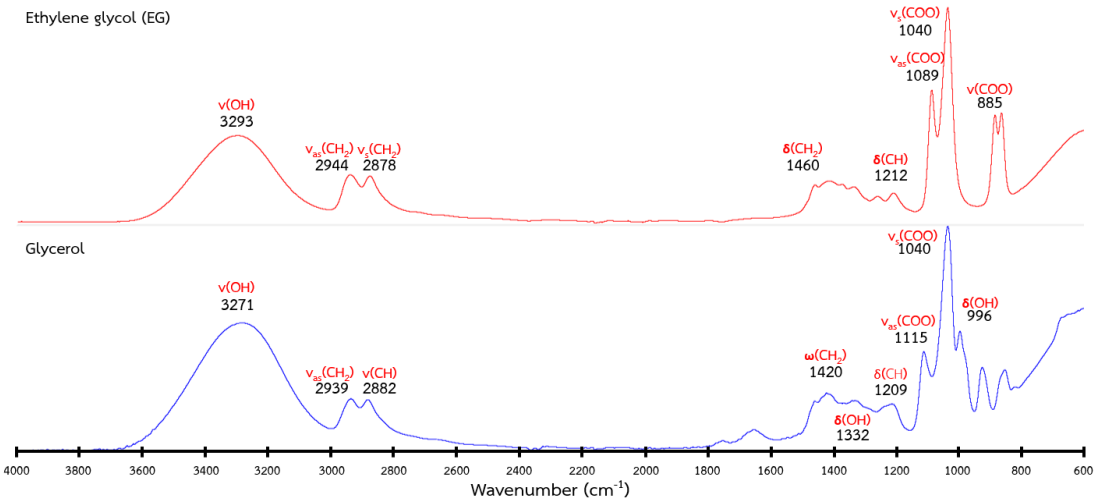

Figure 54 FTIR spectra of ethylene glycol (EG) and glycerol.

FTIR spectra of alcoholyzed PLA (A-PLA) products from the alcoholysis by EG are illustrated in Figure 55. The hydroxyl group (OH) is observed as a broad peak at 3293-3530 cm^{-1} with higher intensity than EG intensity and shifted position [83]. This indicates a decrease in hydrogen bonding between -OH and -OH groups and an increase in hydrogen bonding between -OH and C=O caused by the decreasing amount of -OH groups when the ratio of PLA to EG increases from 3:1, 6:1, and 9:1 respectively, The band shifts to higher frequency are due to the interaction between hydrogen bonds of -OH groups and the carboxylic acid of the C=O stretching, with a shift at approximately 1746-1739 cm^{-1} [55]. The shift in the position of the peak depends on the increasing ratio of diols,

resulting in a higher hydrogen bonding of -OH to -C=O-. The FTIR analysis results are used as a quantitative analysis in which the mechanism of the alcoholysis reaction is investigated. The ester groups of C-O stretching at 1127 cm^{-1}, C-O-C stretching at 1080 cm^{-1} and C-O bending at 1040 cm^{-1} are important characteristics that reflect the transesterification degree, generating products with different structures and compositions [9, 82]. The intensity of C-O-C at 1080 cm^{-1} decreased with increasing proportion of diols until reaching equilibrium, indicating the change of product structure or chain-cleaving ability of ethylene glycol (EG) toward PLA structure.

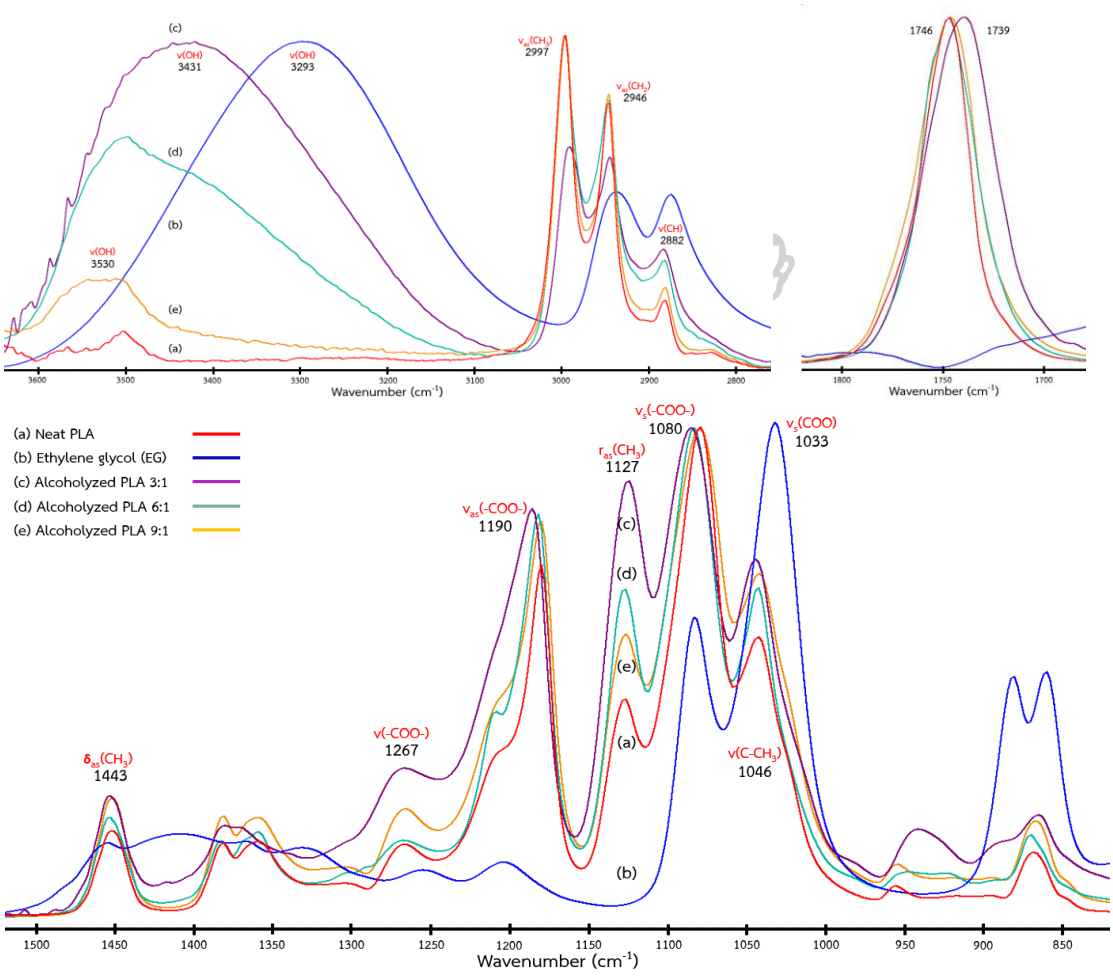

Figure 55 FTIR spectra of (a) neat PLA, (b) ethylene glycol (EG), and (c)-(e) alcoholyzed PLA products from alcoholysis with ethylene glycol (reaction time of 4 hr): 3:1, 6:1, and 9:1 wt/wt.

Similarly, FTIR spectra of alcoholyzed PLA (A-PLA) products by glycerol also showed the hydroxyl groups (OH) located at 3271-3504 cm^{-1}. This also exhibited OH shift characteristics and a broad peak similar to alcoholysis with EG, as shown in Figure 56. When the ratio of PLA to glycerol

increased from 3:1, 6:1, and 9:1 wt/wt, respectively, the product obtained from the 3:1 wt/wt ratio with more glycerol has a lower molecular weight or higher -OH chain ends according to the reaction rate. It has stronger hydrogen bonds with carbonyl groups, resulting in a lower shift of the C=O peak (1739 cm^{-1}) [9, 55]. This contrasts with the 9:1 wt/wt shift to 1745 cm^{-1} ratio, which gives similar results to alcoholysis by EG in the formation of hydrogen bonding interactions between hydroxyl groups and affects the carboxylic acid of the C=O stretching depending on the amount of diols added.

To explain the transesterification mechanisms of the products, the characteristic changes of -OH and C-O-C with decreasing intensity can be observed after the reaction [55]. The C-O-C stretching characteristic of the ester bond at 1080 cm^{-1} was observed as an important characteristic for detecting the transesterification reaction interaction of the alcoholized products, similar to alcoholization with EG. The intensity of C-O-C stretching decreased with increasing proportion of diols with increasing reaction rate, indicating the change of product structure after alcoholization.

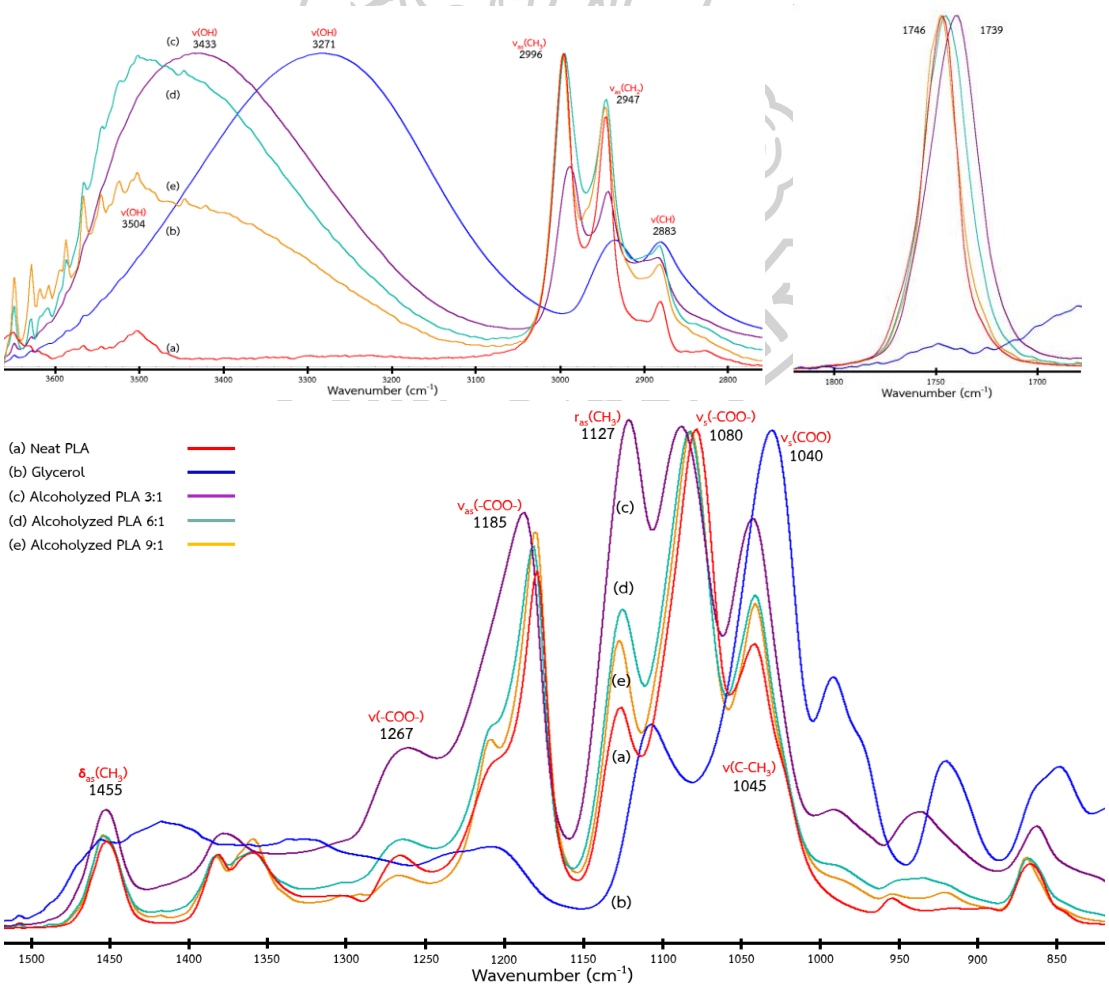

Figure 56 FTIR spectra of (a) neat PLA, (b) ethylene glycol (EG), and (c)-(e) alcoholyzed PLA products from alcoholysis with glycerol (reaction time of 4 hr): 3:1, 6:1, and 9:1 wt/wt.

5.2.3 Quantitative Analysis by FTIR spectroscopy

The quantitative analysis results can be used to study the alcoholysis reaction for complete reactions or to adjust the reaction conditions as appropriate for the application to obtain products with specific chemical structures and compositions. The carboxylic acid (C=O) changes are examined by using data on normalized peak area, as shown in Figure 57, and then comparing the product data during alcoholysis with ethylene glycol (EG) and glycerol. The peak area of the carboxylic acid (COOH) chain ended at 1720 cm^{-1} and C=O stretching at 1747 cm^{-1}, normalized by that of the reference methyl (CH_3) asymmetric at 1450 cm^{-1}. The data are summarized in Figure 58 (a) and (c). The shift of the peak position to low frequencies may be due to the formation of strong hydrogen bonds between the -OH groups of alcohols, increasing the amount of carboxylic acid at the chain ends in proportion to EG and glycerol, as well as an increase in the reaction rate [82, 83].

The quantitative analysis technique using FTIR spectroscopy was also applied to the characteristic bands to describe the changes in the transesterification reaction upon alcoholysis of PLA with EG and glycerol. In the transesterification reaction of PLA alcoholysis with EG and glycerol, the changes in the amount of ester bonds (-CO-O-) were observed, as shown in Figures 55 and 56. The procedures and methods used are examined by using data on the normalized peak area of C-O stretching at 1127 cm^{-1} is normalized by that of the reference C-O-C stretching at 1080 cm^{-1} [9, 55], and the data are summarized in Figure 58 (b) and (d). It was found that the amount of ester bonds decreased with increasing reaction rate as the reaction rate increased, including the proportion of EG and glycerol.

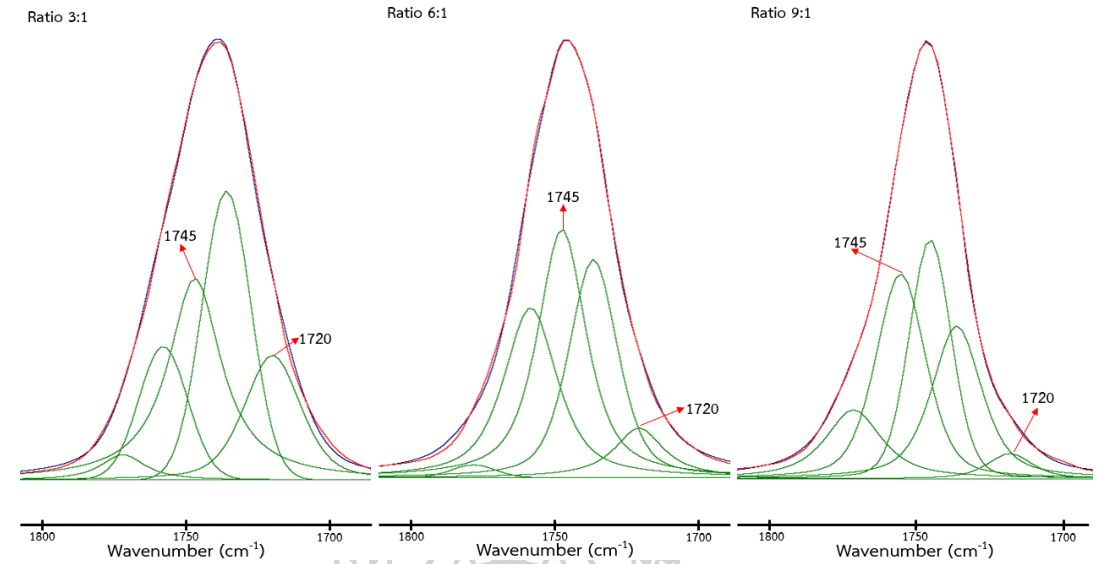

Alcoholyzed PLA by Ethylene glycol (EG)

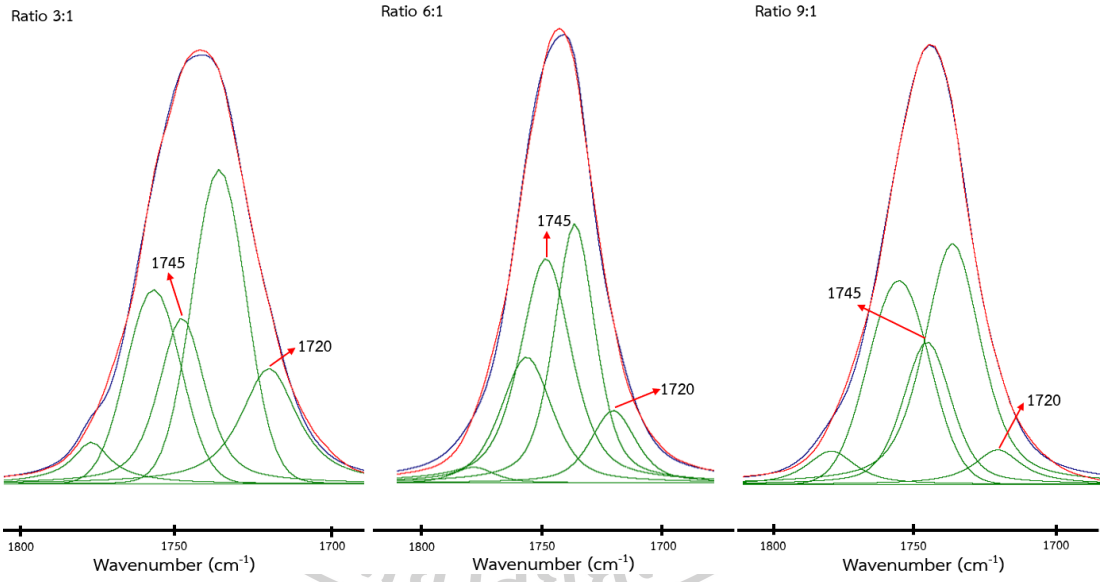

Alcoholyzed PLA by Glycerol

Figure 57 FTIR curve fitting procedures of alcoholyzed PLA products (reaction rate at 4 hr) in the regions of carboxylic acid (-COOH).

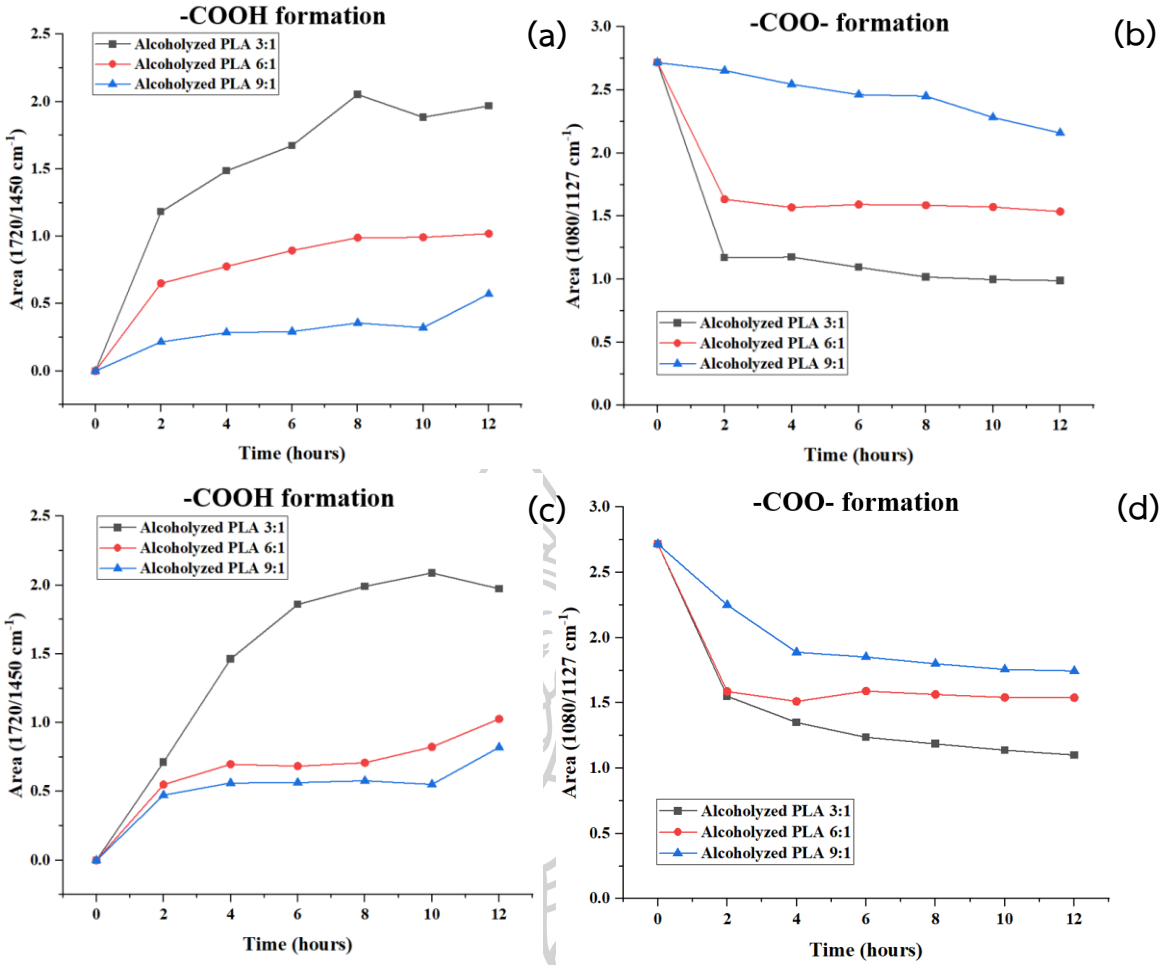

Figure 58 FTIR curve fitting result on carboxylic acid (-COOH) and ester group (-COO-) from alcoholyzed PLA by ethylene glycol (EG); (a-b) with glycerol; (c-d) by dividing to reference peak of 1450 and 1127 cm^{-1}.

5.2.4 Chemical compositions by ^{1}H-NMR spectroscopy

Since the alcoholysis reaction produces a mixture of PLA products with different molecular weights and chemical structures, detailed structural analysis using 1H-NMR spectroscopy is required. From the FTIR spectra results in Figure 5.14, it can be seen that alcoholysis with EG is more efficient than glycerol due to several factors, such as steric hindrance, which has a different structure due to EG having a smaller molecular size and straight chain arrangement [84]. In contrast, glycerol has a branched chain arrangement, creating a greater structural barrier, making it difficult for PLA to access ester bonds for reactivity [10]. In addition, glycerol has a higher viscosity, resulting in slower diffusion than EG, which has a lower viscosity, resulting in better mass transfer because molecular

movement significantly affects reaction kinetics [54, 85]. Therefore, alcoholysis of PLA with ethylene glycol (EG) is suitable for this application.

The chemical composition of alcoholzed PLA (A-PLA) products, indicated that A-PLA consists of two possible structures when the single primary hydroxyl groups (OH) of EG react via transesterification, will be in the form (A), while the structure (B) will be in the form where the primary hydroxyl groups (OH) at both ends of the chain react with PLA. The ethylene glycol poly-lactate has signals of methyl groups (b ~ 1.57 and d ~ 1.49 ppm) and methine groups (a ~ 5.17 and c ~ 4.36 ppm) [82, 86]. As excess ethylene glycol feed compositions are employed, structure (A) is a major product. This is reflected by the absence of the characteristic signals of structure (B), associated with methylene (e" ~ 4.33 ppm) protons [82, 87]. The unique signals of structure (A) are observed; methylene signals (e' and e^o ~ 3.81 ppm). The unreacted hydroxyls in ethylene glycol units are reflected by the methylene (e_1 ~ 3.65 ppm) and singlet hydroxyl groups (e_2 ~ 5.65 ppm). The dilactate exhibits methyl signals (L' ~ 1.79 ppm) and methine groups (L ~ 4.92 ppm) [55, 82, 86]. In addition, the mechanism of the alcoholysis reaction of PLA via the transesterification process and the chemical structure of the A-PLA product are shown in Figure 59.

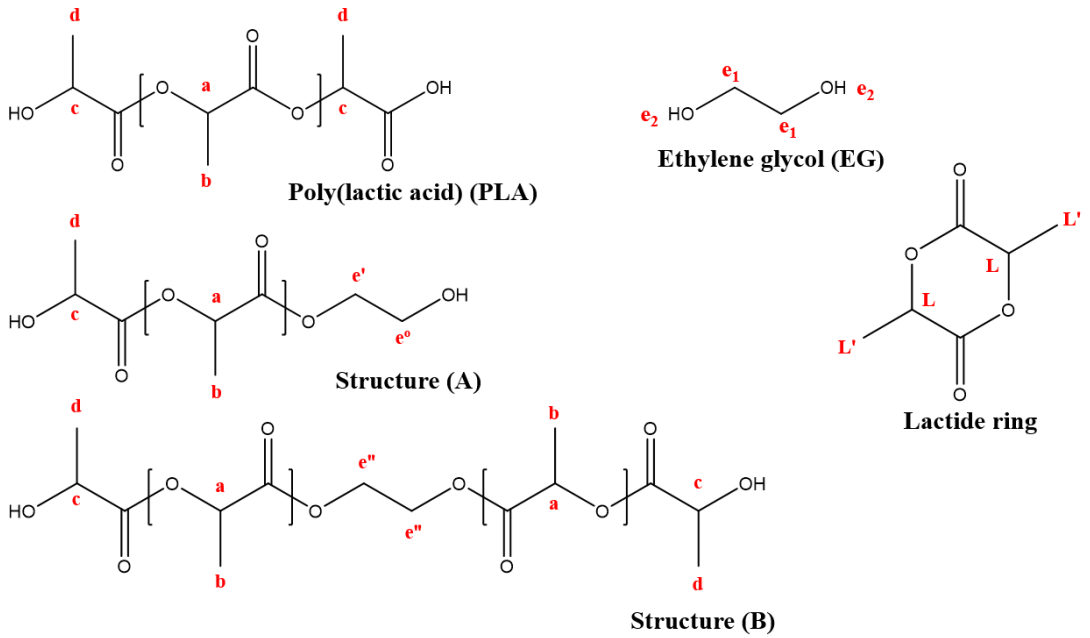

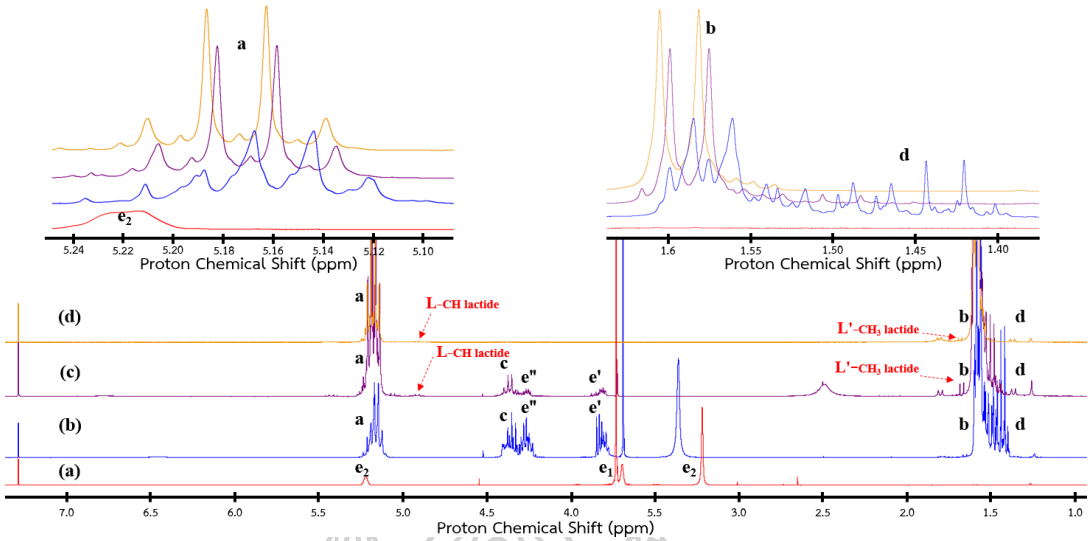

Figure 59 ^{1}H-NMR spectra of (a) ethylene glycol (EG), (b) alcoholyzed PLA at 9:1, (c) alcoholyzed PLA at 3:1, and (d) neat PLA.

5.2.5 Quantitative Analysis by ^{1}H-NMR spectroscopy

The chemical structure of A-PLA with EG is shown in Figure 60. The amount of chemical conformation can be calculated by integrating the methylene group bands of conformation (A) or (B) (e' and e^{o} ~ 3.81 ppm, and e" ~ 4.33 ppm) divided by the combined methylene group values of both conformation (A) and (B) (e', e^{o}, and e") [10, 87]. The amount of conformation formed can be calculated from the methylene signals of each conformation, with the results summarized in Figure 5.16. From the 1H-NMR results, the degree of polymerization (DP) change can be calculated using equation (1). The results of this calculation are summarized in Table 7.

$$\text{Degree of Polymerization (DP)} = \frac{\text{intensity of methine (CH) repeating unit}}{\text{Intensity of methyl } (CH_3) \text{ chain ended}} \quad (1)$$

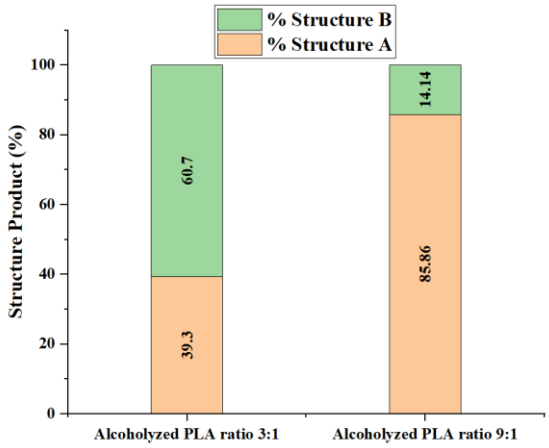

Figure 60 The compositions of products obtained from alcoholysis of PLA by different diol contents.

The calculated results of alcoholyzed PLA (A-PLA) products processed with different alcoholysis ratios in Table 7 show a reduction in the chain length of the A-PLA products compared to commercial PLA (Mn ~ 84,000 g/mol^{-1}) [87]. The FTIR analysis results showed a similar trend as shown in Figure 5.14, indicating that the PLA chains were degraded by the transesterification reaction with ethylene glycol (EG) in increasing proportion.

Table 7 Summary of structure compositions of alcoholyzed product as a feed different ratio, calculated from ^{1}H-NMR spectra.

PLA:EG feed ratio (wt/wt)	Structural compositions
	DP
3:1	0.81
9:1	8.91

Part III Characterization of chemical modification lignin/maleic anhydride/alcoholysis PLA reaction

The products obtained from the lignin extraction process and the alcohol-treated PLA are used as raw materials for chemical modification using various pre-treatment and non-pre-treatment methods to select them for their performance.

5.3 Chemical modification lignin/maleic anhydride/alcoholysis PLA reaction

The chemical modification experiments are summarized in Table 8, comparing both pre-treatment and non-pre-treatment methods of lignin/maleic anhydride/alcoholysis PLA reaction, which differ in terms of reaction systems and application suitability, resulting in different product properties and usability. The pre-treatment method 1 is similar to the pre-treatment method 2, but the reaction proceeds in a continuous manner from the alcoholyzed PLA, requiring constant temperature and system control. This method is suitable for research that requires consistent control of the mechanism and structure of the product, but in a similar way to method 2, the alcoholyzed PLA step is separated, and then a lower heat is applied to the alcoholysis of PLA reaction to initiate the reaction [88]. This process reduces the complexity of the system compared to conventional reflux reactor systems and is therefore suitable for laboratory or semi-industrial sample preparation where simplicity of scalability is emphasized over accuracy. And in the third pre-treatment method, a solvent, DMF, is used to help disperse lignin and enable alcoholyzed PLA and maleic anhydride (MA) to disperse evenly [14, 89]. The solvent acts to help the movement of molecules and promotes the reaction to occur more thoroughly. However, the presence of residues from preparation will affect the mechanical properties of the product. Although this method helps to disperse well, it has the limitation of solvents. And for the last form, the non-pre-treatment method 4 is thermal processing is the use of shear force and heat within the internal mixer, the main mechanism of this form is physical mixing. This is a simple process that does not take long and can be scaled up to the industrial level. Therefore, this method is suitable for large-scale production applications and has process efficiency. Although the use of solvents helps in good dispersion, there are side effects of solvents on the product, while thermal processing is more convenient and gives better results. However, for chemical methods, pre-treatments 1 and 2 are suitable for controlling the reaction and adjusting the product structure.

Table 8 Comparison of preparation methods and their suitability for lignin/maleic anhydride/alcoholysis PLA reaction.

Method	Process	Applicability
Pre-Treatment 1 (Conventional reflux reactor)	The continuous chemical modification with alcoholysis reaction of PLA.	Suitable for applications requiring control of reactions and chemical structures.
Pre-Treatment 2 (Conventional heating)	The separation of the chemical modification process from the alcoholysis of PLA.	Suitable for scale-up in laboratory or semi-industrial applications and reaction control.
Pre-Treatment 3 (Solution)	The chemical modified using a solution.	It has good dispersibility but has problems for solvent residue.
Non Pre-Treatment 4 (Thermal Processing)	the use of thermal processing through the use of shear force and heat.	It is the most scalable method, but additives should be used to improve compatibility.

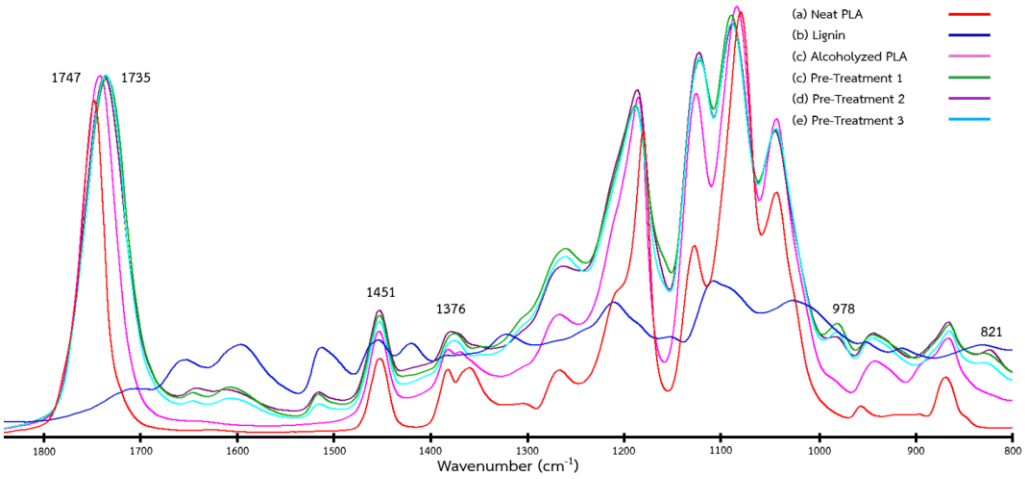

Figure 61 FTIR spectra indicating chemical interaction and grafting formation in lignin/maleic anhydride/alcoholysis PLA reaction prepared by different methods.

From the analysis of FTIR spectra, it was found that the samples prepared by various methods as shown in Figure 61 showed changes indicating the occurrence of chemical modification reactions. Indicating the occurrence of chemical modification reaction, the carbonyl groups (C=O) band at approximately 1750-1735 cm^{-1} has a shift pattern indicating the formation of ester bonds from grafting between anhydride groups and hydroxyl groups of lignin or chain ended of alcoholyzed PLA, and there is also a broad peak with shoulder at approximately 1710 cm^{-1} [90-92]. This is related to the formation of carboxylic acids upon chain cleavage. In addition, the shift of peaks at 1383 and

1366 cm^{-1} was observed upon pre-treatment, showing the peak at 1376 cm^{-1}, indicating the presence of methyl groups (CH_3) within the structure due to the enhanced interphase interaction [93]. While the shift of the band around 978 cm^{-1}, which is related to the vibration of C-C/C-O-C bonds of the chain arrangement pattern and crystal structure of PLA, and the band at 821 cm^{-1}, represents the vibration of the aromatic ring (C-C) of lignin, indicate the interaction in this system [93, 94].

Part IV Characterization of PLA resin with alcoholyzed PLA-cured lignin-M composites

The products obtained from chemical modification processes using various methods, both pre-treatment and non-pre-treatment, are selected to be efficient materials. This research will study the effects on the melted behavior of polymers and the mechanical properties of the materials.

5.4 PLA resin with alcoholyzed PLA-cured lignin-M composites

5.4.1 Mixing behavior of polymer composites

From the analysis of mixing torque curves as shown in Figure 62 from the mixing of polymers in the internal mixer, it was found that the changes can clearly explain the mixing behavior and melt viscosity of the polymer system. From the preparation of additives in different forms by pre-treatment methods 1, 2 and 3, it shows lower torque values than other systems. This may be due to the continuous alcoholysis process of PLA causing chain scission of the polymer and reducing the average molecular mass [95, 96]. This results in a decrease in the viscosity of the liquid and a decrease in the rotational resistance of the mixture. It acts as a plasticizer or lubricant of the system, improving mixing [97]. Due to the low torque value, it indicates a reduced melting resistance and from the sample image which is mixed in a homogeneous manner as shown in Figure 62.

On the other hand, the system of non pre-treatment method 4 (Thermal processing), which relies on shear force and heat without chemical modification before mixing. The torque values were close to those of neat PLA, indicating that no chemical changes or intermolecular interactions occurred during the thermal mixing process. The system was only physical mixing, resulting in limited interphase bonding and poor compatibility between PLA and lignin [98].

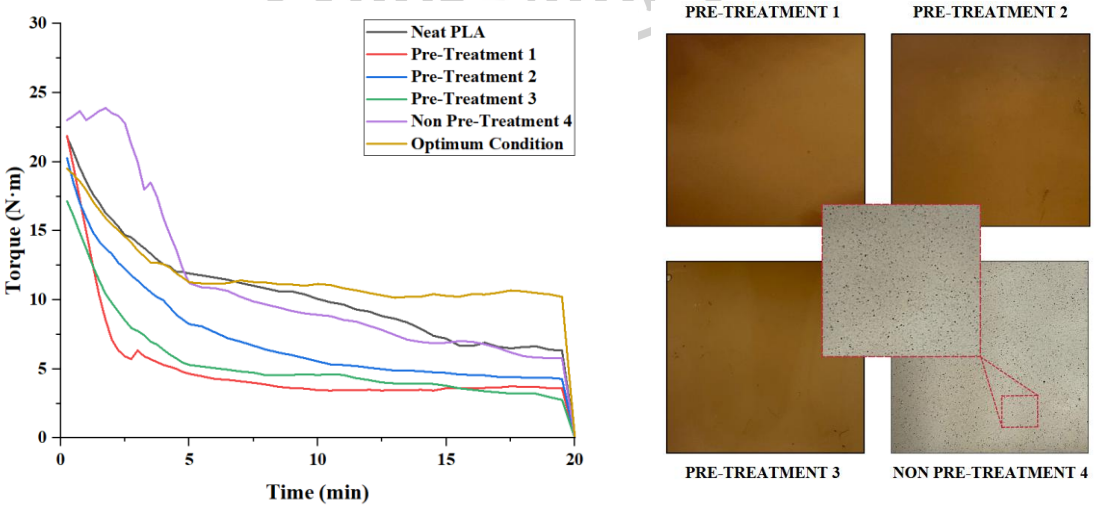

Figure 62 The mixing torque curve obtained from the internal mixer was used to analyze the mixing behavior and melt viscosity evolution of the polymer composites.

5.4.2 Mechanical properties

While the pre-treatment in method 2, adjusting the ratio of alcoholyzed PLA to 9:1 (optimum condition), it was found that the torque value increased as shown in Figure 62, indicating the interaction between molecules in the system. The increase in torque in such cases can be explained by the interaction between the anhydride groups of MA and the hydroxyl groups of lignin and alcoholyzed PLA product, causing covalent grafting and hydrogen bonding within the system, which enhances the compatibility between the phases. [89, 99]

The mechanical properties testing of PLA resin/A-PLA-cured lignin-M composites from different preparations as shown in Figure 63, it was found that the preparation by method 2 gave the highest tensile strength and Young's modulus values, with average values of approximately 60-70 MPa and 2700-2800 MPa, respectively. This is higher than the preparation by methods 1, 3 and 4 by an average of about 10-15%. This result indicates the better distribution of lignin and the interaction between the phases, [14, 100] as shown in Figure 62. In addition, the elongation at break was found to be slightly reduced compared to neat PLA at approximately 1.5-2%, which is consistent with the increased rigidity in Young's modulus, unlike method 3 which incorporates DMF solvent in the preparation process, which causes problems of solvent retention and polymer chain degradation [101]. This resulted in very brittle materials and could not be tested mechanically in samples with increased volumes of 3 and 5 wt%, due to degradation of the PLA matrix and internal void formation. This is consistent with the diagram in Figure 64, which describes the brittle composites mechanism due to solvent residues and short filler molecules from continuous alcoholysis of PLA [102]. While the material prepared by method 4 showed strength values close to neat PLA and decreased with increasing filler content, reflecting the absence of phase interaction, only physical mixing, the preparation by method 2 was therefore the most suitable method. Due to the good balance between interphase bonding reaction and the structural stability of the polymer matrix, the researchers chose to use method 2 for further study by adjusting the ratio of alcoholyzed PLA from 3:1 to 9:1 to increase the chain length and the number of functional groups that can bond with lignin to help enhance the interphase bonding and reduce the brittleness of the composite material at the molecular level [102].

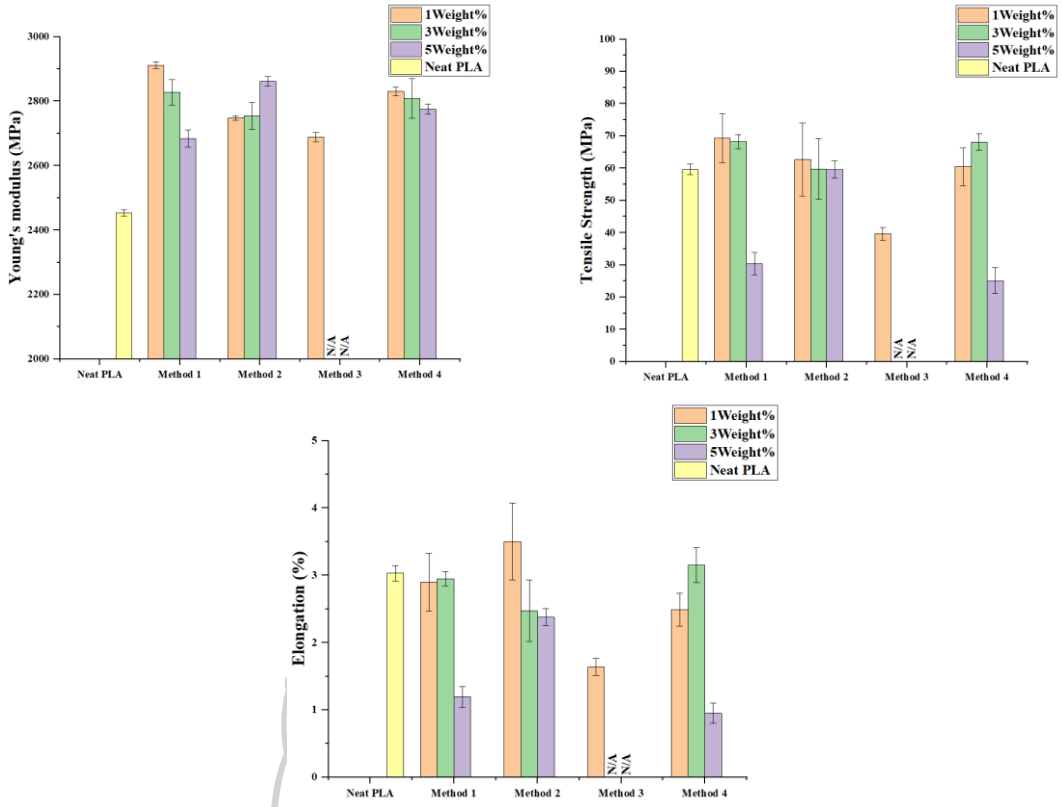

Figure 63 Mechanical properties of PLA resin/A-PLA-cured lignin-M composites, prepared from different methods and content.

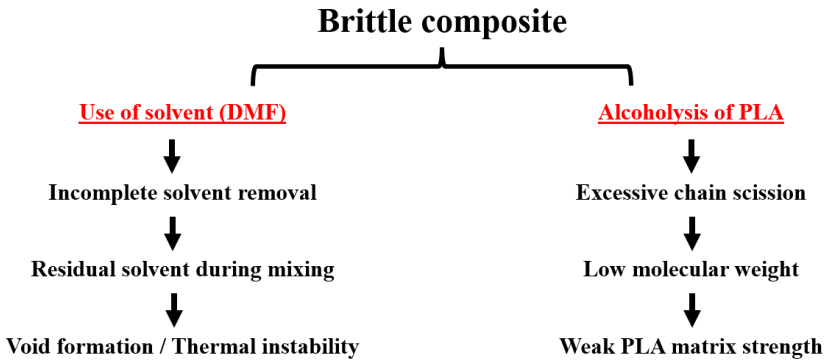

Figure 64 Cause-effect diagram of polymer pre-treatment 3 forming.

Mechanical properties testing of PLA resin/A-PLA-cured lignin M shown in Figure 65 showed that adjusting the preparation ratio in Method 2 from the original 3:1 alcoholyzed PLA to 9:1 gave significantly improved mechanical properties compared to the original, with the material strength increasing by approximately 10-15% and the flexibility increasing by approximately 30-35%, while the rigidity of the material decreased slightly from Young's modulus by approximately 5-10%,

reflecting the balance between strength and toughness of the material in the appropriate direction. Increasing the proportion of alcoholyzed PLA with higher molecular weight results in increased interphase force transfer within the material and reduced stress concentration within the polymer material. [103] This is consistent with the mixing behavior shown in Figure 62, where the increased torque values indicate a stronger melt viscosity due to the stronger interphase interaction. The increased torque values also explain the stronger interphase adhesion. Although the material stability is slightly decreased in Young's modulus, the overall structure is not affected by the increase in mechanical strength and toughness. Therefore, adjusting the ratio of alcoholyzed PLA to 9:1 is considered the most suitable ratio (optimum condition) for further applications as it can create a good balance between strength, toughness and interphase adhesion, both mechanically and structurally. [100] From the study of the amount of additives added, it was found that 1 Weight% is the appropriate proportion. Although the strength values of the materials of each proportion are not different, at 1 Weight%, it tends to give a more constant and stable value with low fluctuation. [104, 105]

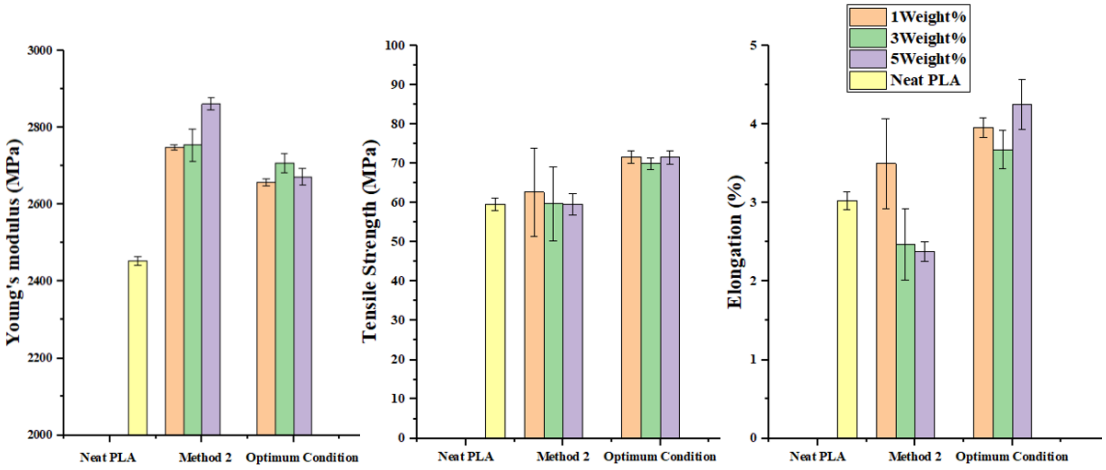

Figure 65 Mechanical properties of PLA resin/A-PLA-cured lignin-M composites from method 2 and optimum condition different content.

Part V Characterization of optimization of filament fabrication and Printing performance and properties of the printed specimens

5.1 Filament fabrication for 3D printing

The optimum condition mixture is PLA resin/A-PLA-cured lignin-M prepared by method 2 at a ratio of 1 wt% and used as a raw material for filament production for 3D printing using a counter-rotating twin-screw extruder with a 1.75-mm die. The monofilament of PLA resin and optimum condition of PLA/A-PLA-cured lignin-M composites with an extrusion speed of 35 rpm were successfully produced using a 1.75 mm extruder die, an extrusion temperature of 165-200ºC, and a filament drawing speed of approximately 3 ± 1 m/min. The diameter of the produced filaments is in the range of 1.25-1.65 mm (in Figure 67 (b)), which is smaller than the standard 3D filament of 1.75 mm (in Figure 67 (a)). The uneven diameter of the filaments is caused by the coarse scaling and unstable control during the filament extrusion process.

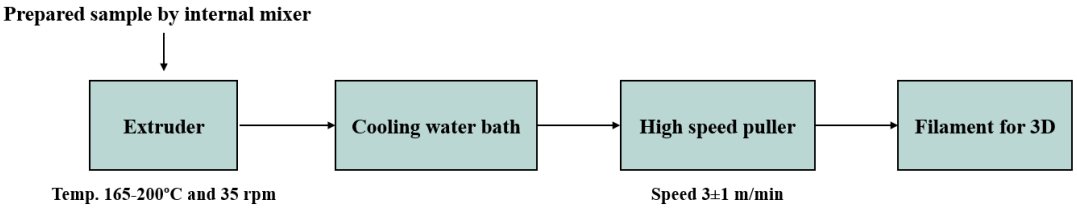

Figure 66 Overall filament fabrication for 3D printing.

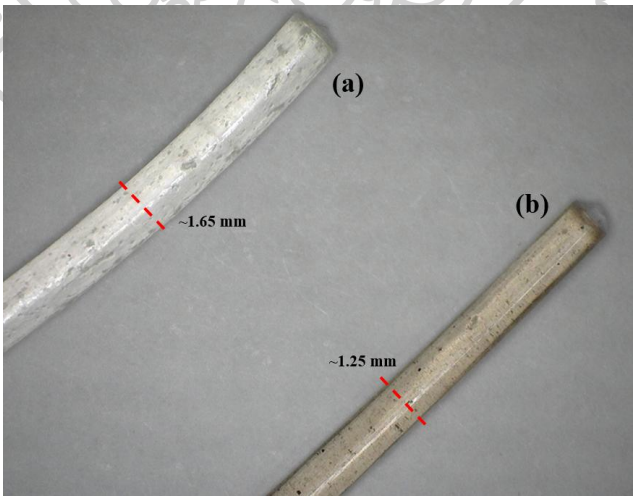

Figure 67 The final filament specimens of (a) PLA commercial and (b) PLA resin/A-PLA-cured lignin-M composites.

5.2 3D printing performance

The printing performance was verified by printing tensile test samples using a Delta X200 3D printer with the printing parameters specified in Table 9. The dumbbell-shaped was printed for each filament in 3 orientations as XY(Falt), XZ(Horizontal), and ZX(Vertical) orientations. A support structure called a brim is cut from the sample after the printing process. The printing time for each type of specimen, namely XY(Falt), XZ(Horizontal), and ZX(Vertical) orientations were 50, 120, and 150 min, respectively, as shown in Figure 68, showing the dumbbell-shaped specimen according to ASTM 638 Type IV standard for tensile testing. The printing time varies depending on the number of printing layers. The printing tests showed that the PLA/A-PLA-cured lignin-M composites filament samples could be printed in all printing directions, but in the XZ(Horizontal) direction, a distortion of approximately 5-10% of the sample base was observed during printing. Since the XZ printing method prints two sample bases and welds them together, the joints of the samples may not be well bonded [106]. The mechanical properties of the PLA/A-PLA-cured lignin-M composites printed tensile test show the average force transfer from the test. Printing in the XY(Falt) direction has better overall average Young's modulus, tensile strength, and elongation at break. Because printing along the XY axis has better fiber adhesion along the applied force direction than printing along the XZ and ZX axes [107], because printing along this axis has a high number of layers from printing, resulting in a large number of workpiece joints, when subjected to force, the adhesion force between layers will decrease and the resistance capability will be low [108, 109]. Therefore, the number of layers in printing has a direct effect on the adhesion force between layers, including the contact surface area of each layer of the workpiece [110]. A larger number of layers in a print allows each layer to cool quickly from the melt and has less time for polymer chain diffusion between layers, resulting in less complete fusion. Conversely, printing with fewer layers allows for better fusion and adhesion between layers [14, 111].

Table 9 The printing parameter of neat PLA and PLA resin/A-PLA-cured lignin-M composites tensile specimen.

Printing Parameters	Conditions
Layer height (mm)	0.2
Shell wall thickness (mm)	1
Shell top or bottom thickness (mm)	0.80
Infill density (%)	100
Infill pattern	Longitudinal

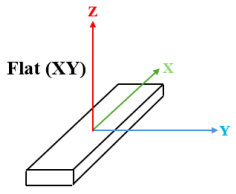

Infill line direction	0/90º
Infill overlap percentage (%)	10
Infill layer thickness (mm)	0.15
Filament dimeter (mm)	1.25-1.75
Nozzle dimeter (mm)	0.4
Filament flow (%)	100
Raster orientation	0/90º
Printing orientation	XY(Flat), XZ(Horizontal), and ZX(Vertical)
Printing speed (mm/s)	60
Travel speed (mm/s)	120
Enable print (mm/s)	Yes
Brim width (mm)	3
Plate temperature (ºC)	60-70
Nozzle temperature (ºC)	190-210
Nozzle diameter (mm)	0.4

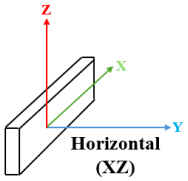

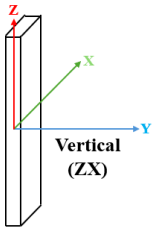

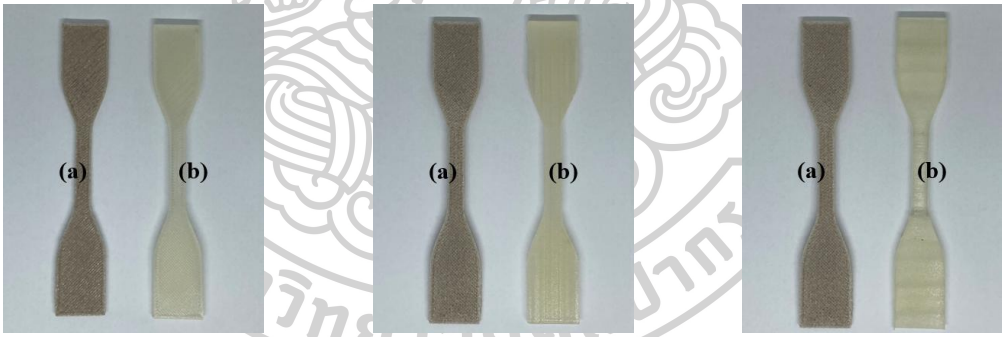

XY (Falt) XZ (Horizontal) ZX (Vertical)

Figure 68 The final printed dumbbell-shaped for tensile test of (a) PLA commercial and (b) PLA resin/A-PLA-cured lignin-M composites.

The results of the mechanical property tests of the 3D printed parts are shown in Figure 69. It was found that printing in the XY (Flat) direction gave tensile strength and elongation at break values of 66 MPa and 4.79%, respectively, which were higher than printing in the XZ (Horizontal) and ZX (Vertical) directions. However, the rigidity values were similar because in printing in the XY direction, the fiber alignment is parallel to the direction of the applied force, allowing for force transfer directly through the fiber structure with high efficiency. As a result, the material's strength and toughness are better than printing in other directions. [107, 109] While printing in the XZ and ZX

directions has a higher number of interlayers passes and the applied tensile force is perpendicular to the structural interface, the interlayer interface area has lower interlayer polymer chain diffusion, resulting in lower interlayer adhesion and easier brittle fracture. Therefore, printing in the XY direction, with good interlayer bonding and fiber alignment in the same direction as the applied force, as well as printing with a higher surface area, has superior properties. [14]

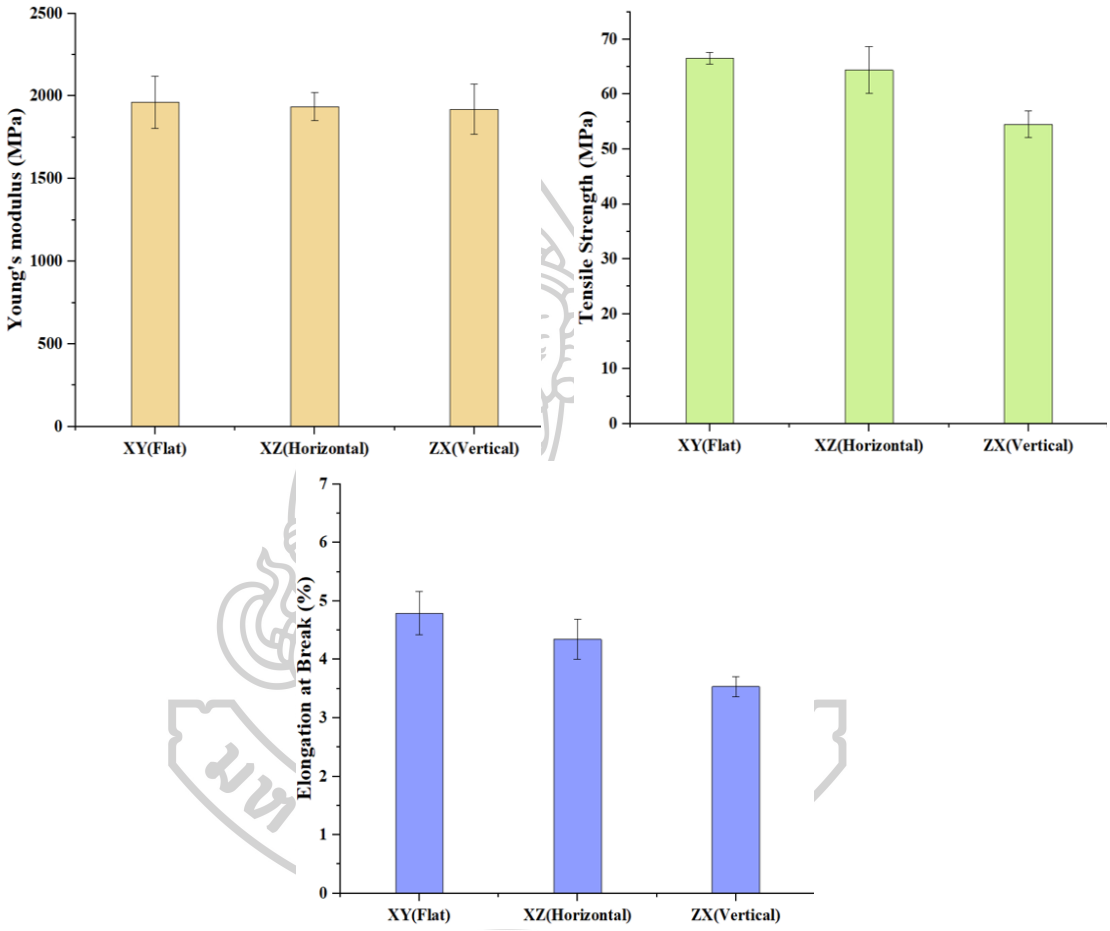

Figure 69 Mechanical properties of 3D-printed specimens at different printing orientations (XY, XZ, and ZX).

From the morphology of the fiber arrangement in different directions, as shown in figure 70 and 71. It was found that the structure of the workpiece printed in the XY direction has the fiber orientation arranged continuously in both the same direction as the force and alternating diagonal orientations, allowing the force to be transferred directly through the fiber direction and down along the slanted free line, resulting in the material receiving two-step tensile force and good force sharing between each layer of fibers [109]. This results in a ductile fracture pattern with a rough fracture surface, showing the elongation and movement of the polymer chains before fracture. And for

printing in the XZ direction, the filament is oriented in line with the tensile force direction, causing the force to be transferred along the filament. Cracks begin to appear as separation of individual fibers at some points, consistent with moderate mechanical values. Conversely, printing in the ZX direction creates a seam between layers perpendicular to the tensile force, especially in the ZX direction when the material is subjected to force. Force is transferred directly to the structural joints. When stress builds up, the joints will fracture. This results in brittle fractures, a smoother surface and more visible layering. [107, 109]

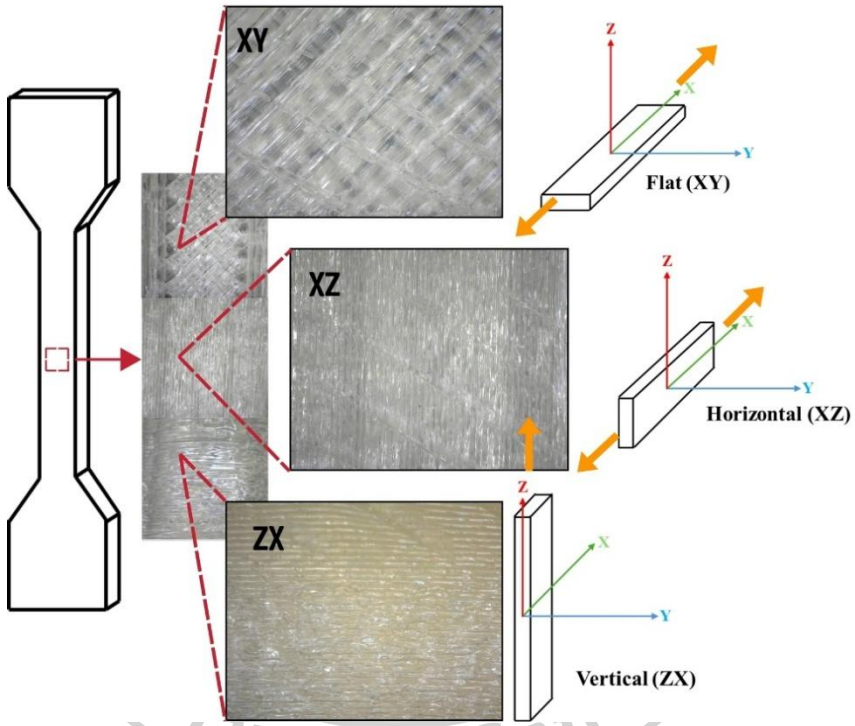

Figure 70 Microstructural morphology of 3D-printed specimens at different printing orientations (XY, XZ, and ZX).

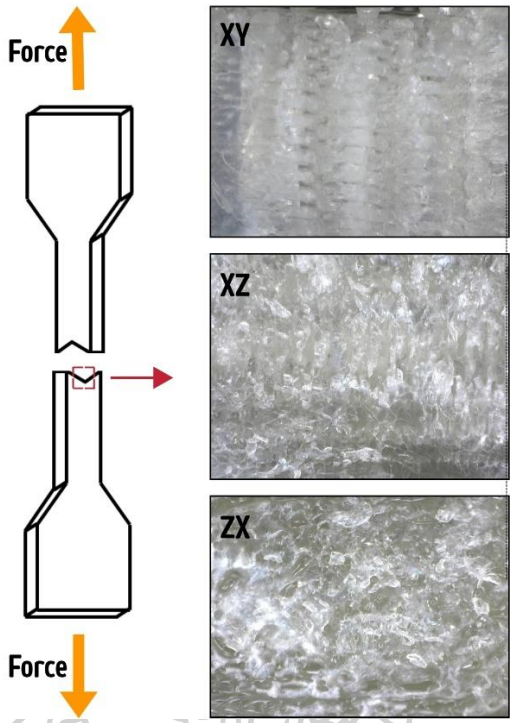

Figure 71 Fracture surface morphology of 3D-printed specimens at different printing orientations (XY, XZ, and ZX).

Printing in the XY (Flat) direction was the most efficient option, with the fiber orientation parallel to the tensile direction. The PLA/A-PLA-cured lignin-M composites were found to have improved mechanical properties compared to neat PLA, with the Young's modulus and tensile strength values indicating improved force transfer between the polymer structures. This improvement in mechanical properties was attributed to the covalent and hydrogen bonding between the anhydride groups of MA and the hydroxyl groups of lignin and at the chain ends of alcoholyzed PLA, which enhanced the interphase adhesion [9, 14, 89]. This results in a structure with better lignin distribution and reduces the occurrence of segregation within the material. Although the elongation is slightly reduced, it reflects an increase in material strength, which is typical of materials with stronger interphase adhesion [88, 110]. Thus, PLA/A-PLA-cured lignin-M composites demonstrate an optimal balance between strength and structural stability and are suitable for efficient application as filament materials for 3D printing.

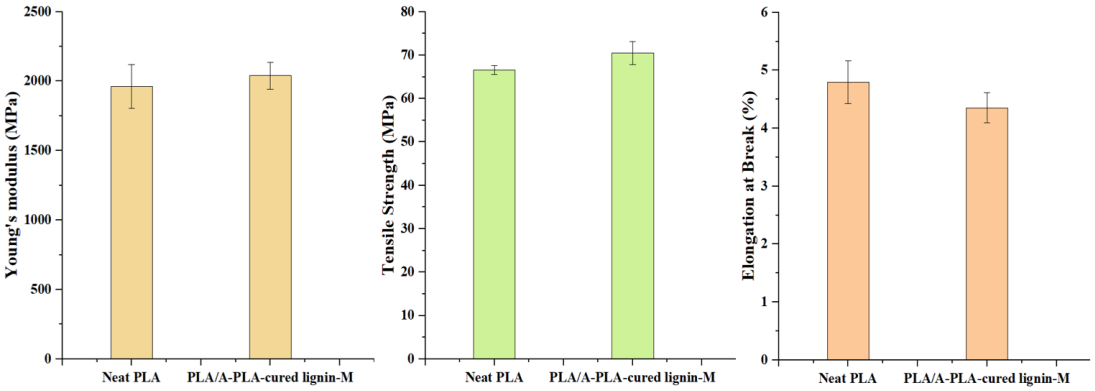

Figure 72 Mechanical properties of 3D-printed specimens in the XY printing orientation, comparing neat PLA and PLA resin/A-PLA-cured lignin-M composites.

CHAPTER VI

CONCLUSIONS

6.1 Conclusions

The lignin extracted from black liquor by acidification process. The study found that inorganic acid (H_2SO_4) gave higher precipitation efficiency than organic acid (CH_3COOH), with a yield of 43.97% at pH 3.5, which was related to the reduction of $Ca(OH)_2$ and $CaCO_3$ crystals and amorphous morphology according to SEM-EDS and XRD results. FTIR analysis confirmed the protonation of COO- to COOH as the main mechanism of precipitation, thus the use of inorganic acid under acid-base conditions at pH 3.5 is most suitable for the extraction of high yield and purity lignin. To be used as raw materials in the chemical modification process and further applications.

Study of alcoholysis of PLA with different diols revealed that ethylene glycol (EG) provides better transesterification reaction efficiency than glycerol due to its lower molecular size and viscosity, which allows for faster molecular diffusion. The FTIR analysis results revealed a shift of C=O peak at 1746 cm^{-1} to the position of 1739 cm^{-1} and a change of C-O-C intensity at 1080 cm^{-1}, indicating the formation of new ester bonds and the reduction of the PLA base structure, while the ^{1}H-NMR results confirmed that the alcoholyzed PLA products obtained from ethylene glycol (EG) were mostly mono-terminated and had significantly lower degree of polymerization (DP), with a PLA:EG ratio of 9:1 gave the most suitable alcoholysis value, EG is therefore the most suitable reagent and has a controllable structure for further application as a raw material.

The chemical modification of lignin/maleic anhydride/alcoholyzed PLA reaction system showed that the preparation method with pre-treatment 2 (Conventional heating) gave the highest efficiency. Due to the good controllability of the reaction mechanism, as confirmed by the shift of the C=O peak at 1750-1735 cm^{-1} in the FTIR spectra indicating the formation of new ester bonds, the PLA resin/A-PLA-cured lignin-M composites prepared by this method had tensile strength and Young's modulus values of approximately 60-70 MPa and 2700-2800 MPa, respectively. When the A-PLA ratio was adjusted from 3:1 to 9:1, it was found that the material could maintain a balance between strength and elasticity by approximately 30-35%, and the mixing-torque of the samples also showed higher torque values reflecting the increase in interphase bonding force and melt viscosity. Therefore, it can be concluded that the pre-treatment method using the second method and the A-PLA ratio of 9:1 is the most suitable condition for preparing PLA resin/A-PLA-cured lignin-M

composites with good interphase adhesion, high mechanical properties, and can be further developed for 3D printing filaments or engineering biomaterials.

3D printing filaments from PLA resin/A-PLA-cured lignin-M composites prepared using a pre-treatment method 2 and an additive content of 1 wt% were successfully formed into filaments using a counter-rotating twin-screw extruder, yielding filaments with an average diameter of 1.25-1.65 mm, which is suitable for 3D printing. The printing test results show that the material can be printed in all directions, but there is a slight distortion in the XZ direction due to the imperfect bond between layers. Mechanical properties testing of the parts revealed that printing in the XY (Flat) direction gave the highest tensile strength and modulus values due to the better interlayer adhesion and the fiber orientation along the applied force direction, indicating that the number of printing layers and the interlayer melting influence the material strength. Therefore, composite materials prepared under these optimal conditions have high potential for use as bio-filament materials for 3D printing, offering a balance between strength and flexibility, as well as effective adhesion between layers of the workpiece.

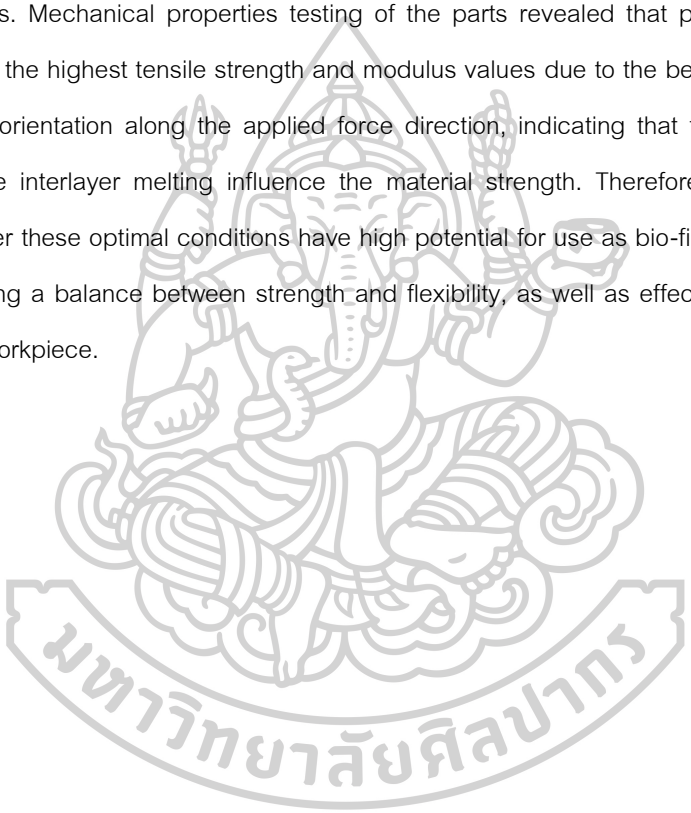

REFERENCES

[1] J. G. Derraik, "The pollution of the marine environment by plastic debris: a review," *Marine pollution bulletin,* vol. 44, no. 9, pp. 842-852, 2002.

[2] R. E. Engler, "The complex interaction between marine debris and toxic chemicals in the ocean," *Environmental science & technology,* vol. 46, no. 22, pp. 12302-12315, 2012.

[3] E. L. Teuten *et al*., "Transport and release of chemicals from plastics to the environment and to wildlife," *Philosophical transactions of the royal society B: biological sciences,* vol. 364, no. 1526, pp. 2027-2045, 2009.

[4] K. Hamad, M. Kaseem, M. Ayyoob, J. Joo, and F. Deri, "Polylactic acid blends: The future of green, light and tough," *Progress in Polymer Science,* vol. 85, pp. 83-127, 2018.

[5] A. Demirbas, "Biodegradable plastics from renewable resources," *Energy Sources, Part A,* vol. 29, no. 5, pp. 419-424, 2007.

[6] N. Mostafa, A. A. Farag, H. M. Abo-dief, and A. M. Tayeb, "Production of biodegradable plastic from agricultural wastes," *Arabian journal of chemistry,* vol. 11, no. 4, pp. 546-553, 2018.

[7] M. Flury and R. Narayan, "Biodegradable plastic as an integral part of the solution to plastic waste pollution of the environment," *Current Opinion in Green and Sustainable Chemistry,* vol. 30, p. 100490, 2021.

[8] O. Torpanyacharn, P. Sukpuang, A. Petchsuk, P. Opaprakasit, and M. Opaprakasit, "Curable precursors derived from chemical recycling of poly (ethylene terephthalate) and polylactic acid and physical properties of their thermosetting (co) polyesters," *Polymer Bulletin,* vol. 75, pp. 395-414, 2018.

[9] B. Nim and P. Opaprakasit, "Quantitative analyses of products from chemical recycling of polylactide (PLA) by alcoholysis with various alcohols and their applications as healable lactide-based polyurethanes," *Spectrochimica Acta Part A: Molecular and Biomolecular Spectroscopy,* vol. 255, p. 119684, 2021.

[10] J. Tounthai, A. Petchsuk, P. Opaprakasit, and M. Opaprakasit, "Curable polyester precursors from polylactic acid glycolyzed products," *Polymer bulletin,* vol. 70, pp. 2223-2238, 2013.

[11] N. D. Luong *et al*., "An eco-friendly and efficient route of lignin extraction from black liquor and a lignin-based copolyester synthesis," *Polymer bulletin,* vol. 68, pp. 879-890, 2012.

[12] S. H. F. da Silva, O. Gordobil, and J. Labidi, "Organic acids as a greener alternative for the precipitation of hardwood kraft lignins from the industrial black liquor," *International journal of biological macromolecules,* vol. 142, pp. 583-591, 2020.

[13] H. K. Hemanathan Kumar, R. Alen, and G. S. Gokarneswar Sahoo, "Characterization of hardwood soda-AQ lignins precipitated from black liquor through selective acidification," 2016.

[14] S.-H. Hong, J. H. Park, O. Y. Kim, and S.-H. Hwang, "Preparation of chemically modified lignin-reinforced PLA biocomposites and their 3D printing performance," *Polymers,* vol. 13, no. 4, p. 667, 2021.

[15] M. A. Taher, X. Wang, K. Faridul Hasan, M. R. Miah, J. Zhu, and J. Chen, "Lignin Modification for Enhanced Performance of Polymer Composites," *ACS Applied Bio Materials,* vol. 6, no. 12, pp. 5169-5192, 2023.

[16] L. Musa *et al*., "A review on the potential of polylactic acid based thermoplastic elastomer as filament material for fused deposition modelling," *journal of materials research and technology,* vol. 20, pp. 2841-2858, 2022.

[17] D. Mitsouras and A. A. Giannopoulos, "The Technical Basics of Cardiac 3D Printing," *3-Dimensional Modeling in Cardiovascular Disease,* pp. 17-42, 2020.

[18] A. Van Wijk and I. van Wijk, *3D printing with biomaterials: Towards a sustainable and circular economy*. IOS press, 2015.

[19] A. E. Patterson, T. R. Pereira, J. T. Allison, and S. L. Messimer, "IZOD impact properties of full-density fused deposition modeling polymer materials with respect to raster angle and print orientation," *Proceedings of the Institution of Mechanical Engineers, Part C: Journal of Mechanical Engineering Science,* vol. 235, no. 10, pp. 1891-1908, 2021.

[20] J. Ahmed and S. K. Varshney, "Polylactides—chemistry, properties and green packaging technology: a review," *International journal of food properties,* vol. 14, no. 1, pp. 37-58, 2011.

[21] L. Soderhjelm, "Factors affecting the viscosity of strong black liquor," *Appita journal,* vol. 41, no. 5, 1988.

[22] M. Cardoso, E. Oliveira, and M. Passos, "Kraft black liquor of eucalyptus from Brazilian mills: chemical and physical characteristics and its processing in the recovery unit," *O papel,* vol. 67, no. 7, pp. 71-83, 2006.

[23] C. Xu and F. Ferdosian, *Conversion of lignin into bio-based chemicals and materials*. Springer, 2017.

[24] T. A. Khan, J.-H. Lee, and H.-J. Kim, "Lignin-based adhesives and coatings," in *Lignocellulose for future bioeconomy*: Elsevier, 2019, pp. 153-206.

[25] G. W. Huber, S. Iborra, and A. Corma, "Synthesis of transportation fuels from biomass: chemistry, catalysts, and engineering," *Chemical reviews,* vol. 106, no. 9, pp. 4044-4098, 2006.

[26] H. Hatakeyama and T. Hatakeyama, "Lignin structure, properties, and applications,"

Biopolymers: lignin, proteins, bioactive nanocomposites, pp. 1-63, 2010.

[27] U. Schuchardt, R. Sercheli, and R. M. Vargas, "Transesterification of vegetable oils: a review," *Journal of the Brazilian Chemical Society,* vol. 9, pp. 199-210, 1998.

[28] J. Otera, "Transesterification," *Chemical reviews,* vol. 93, no. 4, pp. 1449-1470, 1993.

[29] K. Weissermel and H.-J. Arpe, *Industrial organic chemistry*. John Wiley & Sons, 2008.

[30] Z. Khan *et al.*, "Current developments in esterification reaction: A review on process and parameters," *Journal of Industrial and Engineering Chemistry,* vol. 103, pp. 80-101, 2021.

[31] R. C. Larock and R. Rozhkov, "Inverconversion of Nitriles, Carboxylic Acids, and Derivatives," *Comprehensive Organic Transformations: A Guide to Functional Group Preparations,* pp. 1-81, 2018.

[32] J. G. Drobny, "Processing methods applicable to thermoplastic elastomers," *Handbook of Thermoplastic Elastomers,* pp. 33-173, 2014.

[33] J. L. White, A. Y. Coran, and A. Moet, *Polymer mixing: technology and engineering*. Hanser Verlag, 2001.

[34] M. Stevens and J. A. Covas, *Extruder principles and operation*. Springer Science & Business Media, 2012.

[35] J. Gopinathan and I. Noh, "Recent trends in bioinks for 3D printing," *Biomaterials research,* vol. 22, no. 1, p. 11, 2018.

[36] T. D. Ngo, A. Kashani, G. Imbalzano, K. T. Nguyen, and D. Hui, "Additive manufacturing (3D printing): A review of materials, methods, applications and challenges," *Composites Part B: Engineering,* vol. 143, pp. 172-196, 2018.

[37] R. B. Kristiawan, F. Imaduddin, D. Ariawan, Ubaidillah, and Z. Arifin, "A review on the fused deposition modeling (FDM) 3D printing: Filament processing, materials, and printing parameters," *Open Engineering,* vol. 11, no. 1, pp. 639-649, 2021.

[38] J. M. Chacón, M. A. Caminero, E. García-Plaza, and P. J. Núnez, "Additive manufacturing of PLA structures using fused deposition modelling: Effect of process parameters on mechanical properties and their optimal selection," *Materials & Design,* vol. 124, pp. 143-157, 2017.

[39] M. Milosevic, D. Stoof, and K. L. Pickering, "Characterizing the mechanical properties of fused deposition modelling natural fiber recycled polypropylene composites," *Journal of Composites Science,* vol. 1, no. 1, p. 7, 2017.

[40] J. M. Franco Alves and C. M. Medina Rivero, "Extrusora de plásticos para fabricación de filamento de impresora 3D," 2015.

[41] V. Mirón, S. Ferràndiz, D. Juàrez, and A. Mengual, "Manufacturing and characterization of 3D printer filament using tailoring materials," *Procedia Manufacturing,* vol. 13, pp. 888-894, 2017.

[42] S. Kasala, "Recycled technical plastics as raw material for plastics and composite products," 2018.

[43] J. R. Davis, *Tensile testing*. ASM international, 2004.

[44] M. Kannan, "Scanning electron microscopy: Principle, components and applications," *A textbook on fundamentals and applications of nanotechnology,* pp. 81-92, 2018.

[45] J. Mathias. "How Does FTIR Analysis Work?" https://www.innovatechlabs.com/newsroom/672/stuff-works-ftir-analysis/ (accessed.

[46] B. H. Stuart, *Infrared spectroscopy: fundamentals and applications*. John Wiley & Sons, 2004.

[47] S. K. Bharti and R. Roy, "Quantitative 1H NMR spectroscopy," *TrAC Trends in Analytical Chemistry,* vol. 35, pp. 5-26, 2012.

[48] P. F. Fewster, "A new theory for X-ray diffraction," *Acta Crystallographica Section A: Foundations and Advances,* vol. 70, no. 3, pp. 257-282, 2014.

[49] Ratchadaphon Pantharos., "Thermogravimetric Analysis (TGA) machine," 2021. [Online]. Available: https://erp.mju.ac.th/acticleDetail.aspx?qid=1229.

[50] L. Dessbesell, M. Paleologou, M. Leitch, R. Pulkki, and C. C. Xu, "Global lignin supply overview and kraft lignin potential as an alternative for petroleum-based polymers," *Renewable and Sustainable Energy Reviews,* vol. 123, p. 109768, 2020.

[51] A. S. Klett, "Purification, fractionation, and characterization of lignin from Kraft black liquor for use as a renewable biomaterial," 2017.

[52] C. G. Boeriu, D. Bravo, R. J. Gosselink, and J. E. van Dam, "Characterisation of structure-dependent functional properties of lignin with infrared spectroscopy," *Industrial crops and products,* vol. 20, no. 2, pp. 205-218, 2004.

[53] T. Rashid, C. F. Kait, and T. Murugesan, "A "Fourier transformed infrared" compound study of lignin recovered from a formic acid process," *Procedia engineering,* vol. 148, pp. 1312-1319, 2016.

[54] N. D. Pingale, V. S. Palekar, and S. Shukla, "Glycolysis of postconsumer polyethylene terephthalate waste," *Journal of Applied Polymer Science,* vol. 115, no. 1, pp. 249-254, 2010.

[55] B. Nim, M. Opaprakasit, A. Petchsuk, and P. Opaprakasit, "Microwave-assisted chemical recycling of polylactide (PLA) by alcoholysis with various diols," *Polymer Degradation and Stability,* vol. 181, p. 109363, 2020.

[56] I. Vieitez *et al.*, "Continuous catalyst-free methanolysis and ethanolysis of soybean oil under supercritical alcohol/water mixtures," *Renewable Energy,* vol. 35, no. 9, pp. 1976-1981, 2010.

[57] A. Kamimura and S. Yamamoto, "An efficient method to depolymerize polyamide plastics: A

new use of ionic liquids," *Organic Letters,* vol. 9, no. 13, pp. 2533-2535, 2007.

[58] J. Chen *et al.*, "Alcoholysis of PET to produce dioctyl terephthalate by isooctyl alcohol with ionic liquid as cosolvent," *Polymer degradation and stability,* vol. 107, pp. 178-183, 2014.

[59] A. Naseem, S. Tabasum, K. M. Zia, M. Zuber, M. Ali, and A. Noreen, "Lignin-derivatives based polymers, blends and composites: A review," *International journal of biological macromolecules,* vol. 93, pp. 296-313, 2016.

[60] M. D. Cannatelli and A. J. Ragauskas, "Conversion of lignin into value-added materials and chemicals via laccase-assisted copolymerization," *Applied microbiology and biotechnology,* vol. 100, pp. 8685-8691, 2016.

[61] V. K. Thakur, M. K. Thakur, P. Raghavan, and M. R. Kessler, "Progress in green polymer composites from lignin for multifunctional applications: a review," *ACS Sustainable Chemistry & Engineering,* vol. 2, no. 5, pp. 1072-1092, 2014.

[62] P. Sukpuang, M. Opaprakasit, A. Petchsuk, P. Tangboriboonrat, P. Sojikul, and P. Opaprakasit, "Polylactic acid glycolysate as a cross-linker for epoxidized natural rubber: effect of cross-linker molecular weight," *Journal of Elastomers & Plastics,* vol. 48, no. 2, pp. 105-121, 2016.

[63] W. Liu, J. Zhou, Y. Ma, J. Wang, and J. Xu, "Fabrication of PLA filaments and its printable performance," in *IOP Conference Series: Materials Science and Engineering*, 2017, vol. 275, no. 1: IOP Publishing, p. 012033.

[64] N. H. Do *et al.*, "The novel method to reduce the silica content in lignin recovered from black liquor originating from rice straw," *Scientific reports,* vol. 10, no. 1, p. 21263, 2020.

[65] J.-H. Huh, Y.-H. Choi, C. Ramakrishna, S. H. Cheong, and J. W. Ahn, "Use of calcined oyster shell powders as CO 2 adsorbents in algae-containing water," *Journal of the Korean Ceramic Society,* vol. 53, no. 4, pp. 429-434, 2016.

[66] R. Pöykiö and H. Nurmesniemi, "Calcium carbonate waste from an integrated pulp and paper mill as a potential liming agent," *Environmental Chemistry Letters,* vol. 6, no. 1, pp. 47-51, 2008.

[67] V. K. Vadivel, H. Cikurel, and H. Mamane, "Removal of indigo dye by CaCO3/Ca (OH) 2 composites and resource recovery," *Industrial & Engineering Chemistry Research,* vol. 60, no. 28, pp. 10312-10318, 2021.

[68] T. Richards, C. Pavletic, and J. Pettersson, "Efficiencies of NaOH production methods in a Kraft pulp mill," *International journal of energy research,* vol. 33, no. 15, pp. 1341-1351, 2009.

[69] L. El Fels, M. Zamama, and M. Hafidi, "Advantages and limitations of using FTIR spectroscopy for assessing the maturity of sewage sludge and olive oil waste co-composts," *Biodegradation and Bioremediation of Polluted Systems-New Advances and Technologies,* pp. 127-144,

2015.

[70] N. M. Stark, D. J. Yelle, and U. P. Agarwal, "Techniques for Characterizing Lignin," in *Lignin in Polymer Composites*, ed: Elsevier, 2016, pp. 49-66.

[71] W. Teeka, K. Srisujaritpanich, P. Somnuake, and S. Wacharawichanant, "Development of Biodegradable Poly (Lactic Acid)/Lignin Treated Alkyl Ketene Dimer Properties for Packaging Applications," *Advances in Science and Technology,* vol. 150, pp. 11-20, 2024.

[72] J. Cañavate, P. Pages, J. Saurina, X. Colom, and F. Carrasco, "Determination of small interactions in polymer composites by means of FTIR and DSC," *Polymer Bulletin,* vol. 44, no. 3, pp. 293-300, 2000.

[73] P. Kolhe and R. M. Kannan, "Improvement in ductility of chitosan through blending and copolymerization with PEG: FTIR investigation of molecular interactions," *Biomacromolecules,* vol. 4, no. 1, pp. 173-180, 2003.

[74] A. Xiang, J. R. Ebdon, A. R. Horrocks, and B. K. Kandola, "On the utility of thermogravimetric analysis for exploring the kinetics of thermal degradation of lignins," *Bioresource Technology Reports,* vol. 20, p. 101214, 2022/12/01/ 2022, doi: https://doi.org/10.1016/j.biteb.2022.101214.

[75] S. Niu, K. Han, F. Zhou, and C. Lu, "Thermogravimetric analysis of the decomposition characteristics of two kinds of calcium based organic compounds," *Powder Technology,* vol. 209, no. 1, pp. 46-52, 2011/05/15/ 2011, doi: https://doi.org/10.1016/j.powtec.2011.02.002.

[76] Y. Feng, X. Li, H. Wu, C. Li, M. Zhang, and H. Yang, "Critical Review of Ca(OH)2/CaO Thermochemical Energy Storage Materials," *Energies*, vol. 16, no. 7, doi: 10.3390/en16073019.

[77] A. Gupta, P. D. Armatis, P. Sabharwall, B. M. Fronk, and V. Utgikar, "Kinetics of Ca (OH) 2 decomposition in pure Ca (OH) 2 and Ca (OH) 2-CaTiO3 composite pellets for application in thermochemical energy storage system," *Chemical Engineering Science,* vol. 246, p. 116986, 2021.

[78] I.-Y. Eom *et al.*, "Effect of essential inorganic metals on primary thermal degradation of lignocellulosic biomass," *Bioresource Technology,* vol. 104, pp. 687-694, 2012/01/01/ 2012, doi: https://doi.org/10.1016/j.biortech.2011.10.035.

[79] Y. Li, T. Zhu, H. Yang, and G. Nong, "Characteristics of calcium lignin from pulping waste liquor and application for the treatment middle-stage wastewater of paper making," *Environmental Technology,* vol. 44, no. 5, pp. 695-707, 2023/02/23 2023, doi: 10.1080/09593330.2021.1982021.

[80] T. Mouthier, M. M. Appeldoorn, H. Pel, H. A. Schols, H. Gruppen, and M. A. Kabel, "Corn stover

lignin is modified differently by acetic acid compared to sulfuric acid," *Industrial Crops and Products,* vol. 121, pp. 160-168, 2018/10/01/ 2018, doi: https://doi.org/10.1016/j.indcrop.2018.05.008.

[81] B. Shojaei, M. Abtahi, and M. Najafi, "Chemical recycling of PET: A stepping‐stone toward sustainability," *Polymers for Advanced Technologies,* vol. 31, no. 12, pp. 2912-2938, 2020.

[82] C. Eang, B. Nim, P. Sreearunothai, A. Petchsuk, and P. Opaprakasit, "Chemical upcycling of polylactide (PLA) and its use in fabricating PLA-based super-hydrophobic and oleophilic electrospun nanofibers for oil absorption and oil/water separation," *New Journal of Chemistry,* vol. 46, no. 31, pp. 14933-14943, 2022.

[83] B. Nim *et al.*, "Sizing down and functionalizing polylactide (PLA) resin for synthesis of PLA-based polyurethanes for use in biomedical applications," *Scientific reports,* vol. 13, no. 1, p. 2284, 2023.

[84] A. C. Sánchez and S. R. Collinson, "The selective recycling of mixed plastic waste of polylactic acid and polyethylene terephthalate by control of process conditions," *European Polymer Journal,* vol. 47, no. 10, pp. 1970-1976, 2011.

[85] F. Lamberti, "Studies on the Chemical recycling of Poly (lactic acid) via Alcoholysis," University of Birmingham, 2023.

[86] J. Espartero, I. Rashkov, S. Li, N. Manolova, and M. Vert, "NMR analysis of low molecular weight poly (lactic acid) s," *Macromolecules,* vol. 29, no. 10, pp. 3535-3539, 1996.

[87] T. Sripho, P. Opaprakasit, and A. Petchsuk, "Efficiency enhancement of chemical recycling process of degradable polylactic acid by employing microwave and magnetic nanoparticle catalyst," Thammasat University, 2015.

[88] J. Du, Y. Wang, X. Xie, M. Xu, and Y. Song, "Styrene-assisted maleic anhydride grafted poly (lactic acid) as an effective compatibilizer for wood flour/poly (lactic acid) bio-composites," *Polymers,* vol. 9, no. 11, p. 623, 2017.

[89] S. Yu *et al.*, "Effect of maleic anhydride grafted poly (lactic acid) on rheological behaviors and mechanical performance of poly (lactic acid)/poly (ethylene glycol)(PLA/PEG) blends," *RSC advances,* vol. 12, no. 49, pp. 31629-31638, 2022.

[90] H. Jang, S. Kwon, S. J. Kim, and S.-i. Park, "Maleic anhydride-grafted PLA preparation and characteristics of compatibilized PLA/PBSeT blend films," *International Journal of Molecular Sciences,* vol. 23, no. 13, p. 7166, 2022.

[91] C. Moya-Lopez *et al.*, "Polylactide perspectives in biomedicine: from novel synthesis to the application performance," *Pharmaceutics,* vol. 14, no. 8, p. 1673, 2022.

[92] V. Goetjes, J.-C. Zarges, and H.-P. Heim, "Differentiation between hydrolytic and thermo-

oxidative degradation of poly (lactic acid) and poly (lactic acid)/starch composites in warm and humid environments," *Materials,* vol. 17, no. 15, p. 3683, 2024.

[93] K. Yuniarto, Y. A. Purwanto, S. Purwanto, B. A. Welt, H. K. Purwadaria, and T. C. Sunarti, "Infrared and Raman studies on polylactide acid and polyethylene glycol-400 blend," in *AIP conference proceedings*, 2016, vol. 1725, no. 1: AIP Publishing LLC, p. 020101.

[94] R. J. Sammons, D. P. Harper, N. Labbé, J. J. Bozell, T. Elder, and T. G. Rials, "Characterization of organosolv lignins using thermal and FT-IR spectroscopic analysis," *BioResources 8 (2): 2752-2767,* vol. 8, no. 2, pp. 2752-2767, 2013.

[95] M. C. Montoya‐Ospina, H. Verhoogt, and T. A. Osswald, "Processing and rheological behavior of cross‐linked polyethylene containing disulfide bonds," *Spe Polymers,* vol. 3, no. 1, pp. 25-40, 2022.

[96] R. Ho, A. Su, C. Wu, and S. Chen, "Functionalization of polypropylene via melt mixing," *Polymer,* vol. 34, no. 15, pp. 3264-3269, 1993.

[97] M. Alotaibi, J. Shah, A. Sadani, and C. F. Barry, "Effect of Continuous Mixer Design and Parameters on the Degradation of Polylactic Acid," *Polymers,* vol. 17, no. 11, p. 1568, 2025.

[98] J. Campanelli, C. Gurer, T. Rose, and J. Varner, "Dispersion, temperature and torque models for an internal mixer," *Polymer Engineering & Science,* vol. 44, no. 7, pp. 1247-1257, 2004.

[99] P. Cassagnau and F. Fenouillot, "Rheological study of mixing in molten polymers: 1-mixing of low viscous additives," *Polymer,* vol. 45, no. 23, pp. 8019-8030, 2004.

[100] K. Shi, G. Liu, H. Sun, and Y. Weng, "Polylactic acid/lignin composites: A review," *Polymers,* vol. 15, no. 13, p. 2807, 2023.

[101] Z. Sun, L. Zhang, D. Liang, W. Xiao, and J. Lin, "Mechanical and thermal properties of PLA biocomposites reinforced by coir fibers," *International Journal of Polymer Science,* vol. 2017, 2017.

[102] I. Velghe, B. Buffel, V. Vandeginste, W. Thielemans, and F. Desplentere, "Review on the Degradation of Poly (lactic acid) during Melt Processing," *Polymers,* vol. 15, no. 9, p. 2047, 2023.

[103] A. Shakoor Shar, N. Wang, T. Chen, X. Zhao, and Y. Weng, "Development of PLA/Lignin Bio-Composites Compatibilized by Ethylene Glycol Diglycidyl Ether and Poly (ethylene glycol) Diglycidyl Ether," (in eng), *Polymers (Basel),* vol. 15, no. 20, Oct 11 2023, doi: 10.3390/polym15204049.

[104] S. P. Makri *et al*., "Lignin Particle Size Affects the Properties of PLA Composites Prepared by In Situ Ring-Opening Polymerization," *Polymers,* vol. 16, no. 24, p. 3542, 2024.

[105] S. Alshammari and A. Ameli, "Improved Performance of Polylactic Acid Biocomposites at High Lignin Loadings through Glycidyl Methacrylate Grafting of Melt-Flowable Organosolv Lignin," *ACS omega,* vol. 9, no. 33, pp. 35937-35949, 2024.

[106] T. Kuncius, M. Rimašauskas, and R. Rimašauskienė, "Interlayer adhesion analysis of 3d-printed continuous carbon fibre-reinforced composites," *Polymers,* vol. 13, no. 10, p. 1653, 2021.

[107] C. McIlroy and P. Olmsted, "Disentanglement effects on welding behaviour of polymer melts during the fused-filament-fabrication method for additive manufacturing," *Polymer,* vol. 123, pp. 376-391, 2017.

[108] J. R. Stojković *et al*., "An experimental study on the impact of layer height and annealing parameters on the tensile strength and dimensional accuracy of FDM 3D printed parts," *Materials,* vol. 16, no. 13, p. 4574, 2023.

[109] X. Gao, S. Qi, X. Kuang, Y. Su, J. Li, and D. Wang, "Fused filament fabrication of polymer materials: A review of interlayer bond," *Additive Manufacturing,* vol. 37, p. 101658, 2021.

[110] N. A. Nguyen, C. C. Bowland, and A. K. Naskar, "A general method to improve 3D-printability and inter-layer adhesion in lignin-based composites," *Applied Materials Today,* vol. 12, pp. 138-152, 2018.

[111] C.-Y. Liaw, J. W. Tolbert, L. W. Chow, and M. Guvendiren, "Interlayer bonding strength of 3D printed PEEK specimens," *Soft matter,* vol. 17, no. 18, pp. 4775-4789, 2021.

มหาวิทยาลัยศิลปากร

VITA

NAME	Wikoramet Teeka
INSTITUTIONS ATTENDED	Silpakorn University